Nanoparticles formed from the interaction between chitosan and proteins for encapsulation and delivery of hydrophobic molecules

ムハマド アリフ ラズィ

Nanoparticles formed from the interaction between chitosan and proteins for encapsulation and delivery of hydrophobic molecules

Muhamad Alif Razi

Faculty of Engineering
Department of Chemical Systems & Engineering
Kyushu University
2018 June

TABLE OF CONTENTS

CHAPTER 1 GENERAL INTRODUCTION

1.1 Nanoparticles (NPs) for encapsulation and drug delivery systems

1.1.1 Advantages of NPs

NPs have emerged as a promising platform for encapsulation and delivery of therapeutic compounds. NPs are submicron particles ranging from 10-1000 nm in diameter [1]. Their relatively small size provides them a number of advantages, including enhanced surface area to volume ratio and improved physicochemical properties compared with the larger counterpart or bulk material [1,2]. These properties allow NPs to be used for encapsulating or carrying a variety of compounds, such as drugs, biomolecules, and proteins. Moreover, the physical and chemical properties of NPs can be easily engineered to make them capable of controlling the release profiles of a payload and targeting a specific entity, which is of great importance for application as nanomedicine in the pharmaceutical and medical research [1,2]. NPs can also be utilized for enhancing the solubility of free therapeutic compounds that are poorly soluble in water. The enhanced solubility of hydrophobic compounds through encapsulation in NPs is important because many beneficial compounds such as anti-cancer drugs or nutraceuticals are poorly water soluble, which prevents them from being directly utilized for practical applications [1,2]. The poor solubility of drugs also leads to the low bioavailability, lowering the efficacy of drugs. As a consequence, the amount of drug administered to the body needs to be increased to achieve therapeutic effects. However, a higher dose can result in increased toxicity [3,4]. Therefore, development of NPs for such purposes is increasingly being explored in the pharmaceutical industry. Indeed, Abraxane®, which is an albumin-bound paclitaxel (PTX) has been exemplary NPs reaching translation into the clinic for cancer therapy [5]. In addition, NPs are also useful to improve chemical stability of therapeutic compounds that undergo rapid degradation in the solution, such as wortmannin and curcumin [6,7].

Another important benefit of utilizing NPs for drug delivery systems (DDS) is that NPs can prevent drugs from enzymatic degradation and thus affects the pharmacokinetic profiles [1,3]. Besides, the biodistribution of drugs can be improved by NPs for achieving more efficient and effective cancer therapy via active or passive targeting to the cancerous or damaged cells. Passive targeting can be inherently achieved by NPs due to their nanoscale size. This is possible due to the pathophysiology of tumors. Some tumors exhibit leaky and disordered tumor vasculatures, allowing particles from 10-500 nm in diameter to pass through and accumulate in the tumor interstitium. This phenomenon has been well-recognized as the enhanced permeability and retention (EPR) effect of NPs, which sets a dogma in the DDS related-research [2–4,8]. In addition, active targeting has been pursued due to the fact that tumor heterogeneity exists and most of NPs circulating in the blood will be cleared by mononuclear phagocytes, leading to the accumulation in the reticuloendothelial organs such as liver and spleen. Thus, active targeting where NPs are designed such that they have certain ability to reach tumor sites favorably over normal tissues, which may alleviate side-effect. Active targeting can be achieved by surface modification of NPs with a ligand that binds to a specific receptor or biomarker presented in targeted cells [3,4]. The targeting ligands can be proteins, peptides, small molecules, polysaccharides, or aptamer [9]. Some examples of the ligands are folic acid [10], hyaluronic acid [11], transferrin (Tf) [12], antigens [13], and antibodies include cetuximab [14], to target folate (FR), CD44, Tf, and epidermal growth factor receptor (EGFR), respectively. The schematic illustration of advantages of NPs through passive and active targeting is presented in **Fig. 1-1**.

The properties of NPs are comfortably tunable. “Smart” NPs can be fabricated where encapsulated drugs can be released in response to intrinsic and extrinsic stimuli aside from

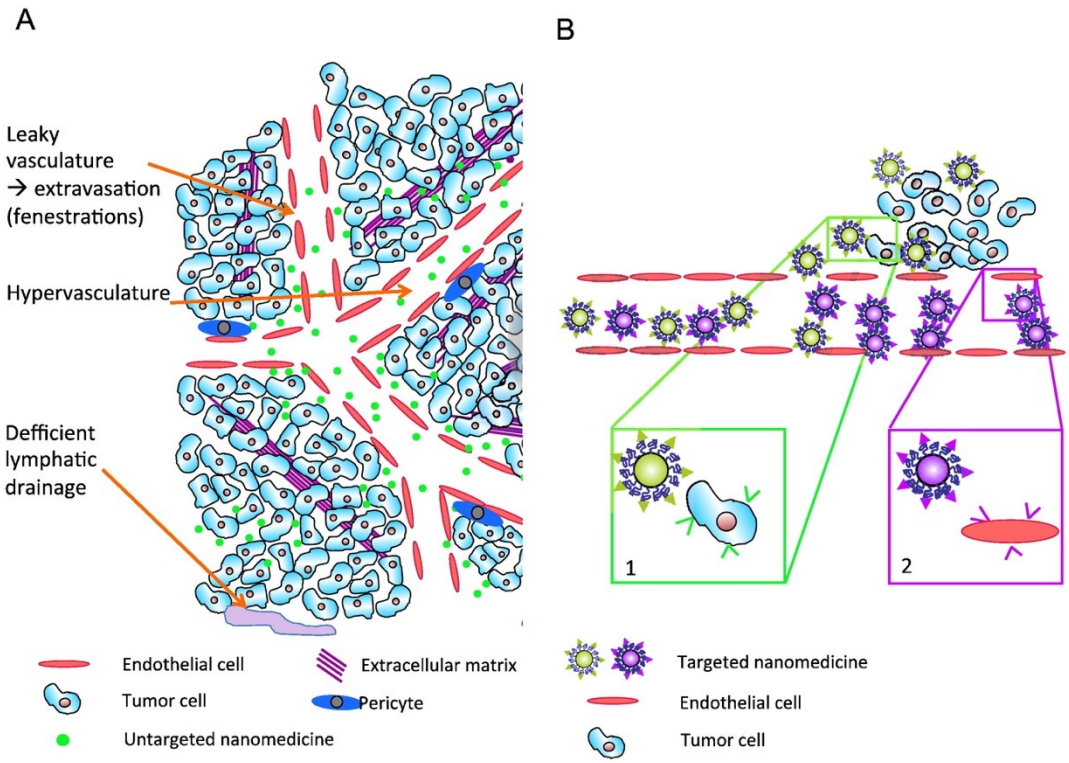

Fig. 1-1 Schematic illustration of advantages of NPs via passive (A) and active (B) targeting. Reprint from ref. 8 with permission.

their possible controlled release of drugs in a sustained manner for a longer period of time [9]. Intrinsic stimuli refer to stimuli present in the target tissues. Damaged or cancerous tissues undergo several changes in their pathology, such as elevated temperature, lower pH, increased specific enzymes production or greater redox potential compared with the normal tissues. At elevated temperature of around 40-45 $^{\circ}$C (hyperthermia), a greater blood flow and an improved vasculature permeability occur in the damaged tissues [9,15]. The extracellular pH of the tumor is acidic due to the lack of nutrients and oxygen, increasing the production of lactic acid via glycolysis pathway [16]. The increased expression of proteases such as the matrix metalloproteinases (MMPs) is associated with the growth and proliferation of the tumor [17]. Finally, the intracellular condition of cells is considered more reducing due to the presence of the glutathione (GSH) in the cytosol at 2-10 mM compared with the extracellular counterpart (2-20μM). Moreover, the concentration of GSH in the tumor cytosol is higher than that in the

normal counterpart [18]. These circumstances can be exploited for fabricating smart NPs for more effective cancer therapy. On the other hand, extrinsic stimuli refer to stimuli applied from the outside of the tissues [9]. The extrinsic stimuli include external heat from laser, ultramagnetic, or ultrasound, magnetic field, light (UV, visible, or near infrared (NIR)), and electric fields. Local hyperthermia can be induced by applying those external heat sources while light can penetrate the tissues to trigger the release of drugs through breaking down the structure's integrity of NPs [9,19]. Meanwhile magnetic forces can be used to guide the NPs to certain location and release the payload through elevated temperature [20]. Clearly, the advantage of using stimuli-triggered NPs is that systemic exposure can be minimized because drugs are released in the cancerous or targeted tissues where the trigger is presented, reducing the side-effect of drugs. In addition, smart NPs may enable the development of a new combination therapy such as theranostics, *i.e.*, therapy and diagnostic by taking advantage of tunability of NPs. Indeed, there are many excellent examples of stimuli-responsive NPs published in the literature with great promise to overcome some limitations in the current cancer therapy or other diseases.

1.1.2 Fabrication and type of NPs

Fabricating nanoscale DDS requires several manufacturing techniques that mainly involve the use of advanced equipment. Although in some cases, they can be simply created using a straightforward and convenient method. In general, NPs can be fabricated by a bottom-up and top-down approach by using a wide variety of materials. The top-down approach involves a reduction in the particle size through physical processes, such as milling and homogenization, whereas the bottom-up approach relies on the ability of the molecules to form nanoscale structures via generally supramolecular chemistry [21]. Several types of NPs have been developed ranging from inorganic-based NPs (hard NPs), such as gold, silica, and silver to their organic-based counterparts (soft NPs), such as lipid, polymer, proteins [22]. Selection

of suitable building materials for the fabrication of NPs is extremely important for applications in the food, pharmaceutical, and medical industry because there is a concern about the safety of NPs due to enhanced reactivity with the biological system, associated with their nanoscale size [3,4]. In addition to improving the efficacy of NPs formulation, ensuring selected building materials are safe and biodegradable is a key step in achieving successful utilization of NPs in the clinical practice. Moreover, the manufacturing method and technology for the production of NPs should be amenable for large-scale production and commercialization and be standardized to avoid heterogeneity in the quality of NPs produced [23]. It is not surprising that hard NPs such as gold or other metals NPs face extreme difficulties to reach the clinical stage although many promising results are shown in the literature and in the preclinical stage. This may be due to unknown biodegradability and toxicological profiles of hard or inorganic NPs in relation to the human body. Only iron oxide-based NPs such as Feridex®, Feraheme®, and NanoTherm® have entered the clinical stage for diagnostics, iron deficiency treatment, and local heat-triggered cancer therapy, respectively [5]. Thus, soft NPs have been extensively exploited by many scientists and affiliated industries for development of new nanotherapeutics with valuable properties with the goal of achieving advancement in the healthcare system.

Doxil® is the first approved and commercialized soft NPs for cancer therapy and has been served as a model for many researchers to develop newly approved nanomedicine with improved performance [5,24,25]. It mainly comprises liposomes that are conjugated with polyethylene glycol (PEG). Liposomes are a nanoscale phospholipid vesicle, which is formed by the self-assembly of phospholipids with the help of added kinetic and/or thermal energy [25]. This liposomal NPs formulation encapsulates doxorubicin hydrochloride, a potent anti-cancer drug. Doxil® sets the gold standard for the NPs formulation with proven advantages over conventional liposomal formulation and other cancer therapy in terms of targeting ability to the tumors [25]. After approval of Doxil® in 1995, several liposomal-based formulations

have also been approved for other uses, such as AmBisome®, DaunoXome®, Myocet®, DepoDur®, and many others [5,24]. Another successful soft NPs platforms is protein-based NPs formulation, such as Abraxane®, which utilizes high-pressure homogenization of PTX with human serum albumin (HSA) to yield colloidal NPs with 130 nm in diameter [26]. This albumin-based NPs takes advantages of the EPR effect and albumin-receptor mediated pathway to enhance the efficacy and reduce the side-effect of PTX. Pegylated proteins and antibodies such as Adagen®, Cimzia® are also get approval by the US Food Drug Administration (FDA) to treat immunodeficiency and Crohn's diseases [27,28]. Polymer-based NPs have also shown promises in the pre- and clinical settings for treatment of cancer. Eligard® and Genexol® are the initial examples of polymeric NPs reaching to the clinic [29,30]. Eligard® is NPs composed of biodegradable poly (DL-lactide-co-glycolide) polymer for sustained release of leuprolide acetate, a synthetic analog of gonadotropin releasing hormone (GnRH or LH-RH), whereas Genexol® is polymeric micelles of poly (ethylene glycol)-poly (DL-lactide) with 20-50 nm in size for PTX delivery to treat metastatic breast and pancreatic cancer and is approved and marketed in South Korea. Some other polymer-based NPs are still in the development phase but show a great potential for approval and commercialization as nanotherapeutics with improved performance to treat various diseases. Indeed, the current trend is to develop novel soft NPs with unique properties and improved capabilities for use as a nanocarrier in the food, pharmaceutical, and medical industry.

1.2 NPs fabricated from the interaction between proteins and polysaccharides

1.2.1 Proteins and polysaccharides as promising soft materials

Proteins and polysaccharides are soft materials that play important roles in the biological systems due to their functional properties. Proteins are biomacromolecules consisting of polypeptide chains of a specific amino acid sequence linked together via peptide bonds and are required in the structure and regulation, energy production, and metabolism of

the living systems [31–33]. Proteins have long been extensively studied for a wide variety of applications due to their beneficial biological and chemical properties as well as potential health benefits [34]. One of important functional properties of proteins is emulsifying ability through reducing the interfacial tension between oil and water phase [33]. On the other hand, polysaccharides comprise chains of monosaccharides connected through condensation reactions and serve as a key component found abundantly in nature that can be utilized for various purposes due to their unique structures and valuable biological properties. For instance, polysaccharides may self-assembled to form three-dimensional structures, which can be used as viscosifying and gelling agents [1]. Both proteins and polysaccharides possess diverse structural characteristics (molecular weight, conformation, monomer arrangement, polarity, electricity, etc), which can be utilized for some specific purposes [32,35]. Proteins and polysaccharides can interact with each other in solution to form supramolecular structures such as complexes, which can be naturally found or artificially created. Some examples of naturally occurring interactions between the two biomolecules include the formation of complexes between the chondroitin sulfate proteoglycan aggrecan and hyaluronan, which is responsible for the mechanical strength of cartilage, and the binding of heparin to antithrombin protein for anti-coagulation of blood [36]. For artificially made, biologically relevant interactions, the electrostatic interaction between pectin of wine and proteins present in the saliva, which decreases astringency in wine, can be a practical application [36]. Indeed, there are more practical applications of the protein-polysaccharides complexes generally found in the food, cosmetics and pharmaceutical industry, such as microencapsulation of bioactive molecules or ingredients, and recently the development of novel nanocomplexes (NCs) and NPs from the interaction between proteins and polysaccharides and their evaluation as nano delivery systems is gaining much attention by many scientists [35,37,38].

1.2.2 Formation mechanism of proteins-polysaccharides complexation

Fabricating NPs with desired physicochemical properties requires understanding in the formation's mechanism, molecular characteristics of proteins and polysaccharides, and several other processing parameters. Understanding the events that may take place when mixing proteins and polysaccharides in the solution is important to design and create suitable NPs. In general, NPs can be fabricated by mixing of the biopolymers that undergo phase separation through segregative (repulsive) or associative (attractive) interactions (**Fig. 1-2**) [39,40]. In segregative system, shearing and extrusion of the phase-separated biopolymers are usually needed to form spheroid particles, followed by gelling of the biopolymers via heating, additions of ions, or cross-linking reaction to stabilize the particles [32,37]. In associative system, the biopolymers attract to each other to form aggregates or complexes. The state of complexation and particle size can be controlled by adjusting the initial biopolymer concentration, pH, ionic strength, mass ratio, and other parameters [32]. The association between proteins and polysaccharides involves various intermolecular forces, including electrostatic, hydrogen bonding, and hydrophobic interactions [35–39,41]. Indeed, the most utilized system to form NPs is through associative interactions that involve oppositely charged proteins and polysaccharides, *i.e.*, electrostatic complexation. Electrostatic complexation-based NPs can be formed by simply mixing cationic or anionic polysaccharides and proteins in the solution. Different types of complexation can occur by adjusting the pH of solution, and the isoelectric point (pI) of proteins and pK_a of polysaccharides play critical role in the formation of complexes or NPs [35,38].

There are four possible phenomena when proteins and polysaccharides are mixed, *i.e.*, no complexation, soluble complexes, insoluble complexes/coacervation, and precipitation [32]. 1) No complexation takes place when both proteins and polysaccharides have the same, sufficiently strong charge that prevents them from interacting to each other. This phenomenon

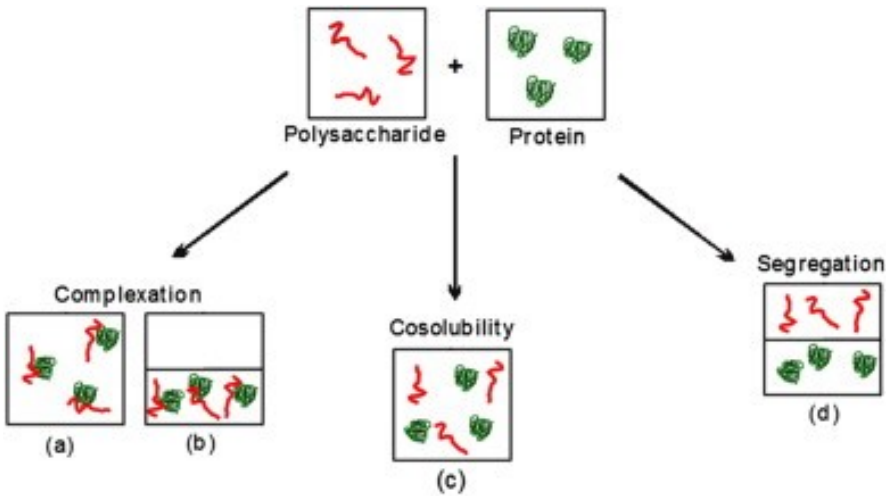

Fig. 1-2 Phase separation behaviour of mixtures of proteins and polysaccharides. (a) soluble complexes, (b) insoluble complexes, (c) co-solubility, (d) segregative phase. Reprinted from ref. 40 with permission.

is pH dependent. For instance, when the pH of the solution is below pI of proteins, both cationic polysaccharides and proteins are positively charged. 2) Soluble complexes can be formed when proteins and polysaccharides weakly associate to each other. This phenomenon usually occurs at below critical pH, where insoluble complexes exists. The characteristics of soluble complexes includes translucent or slightly turbid solution in the appearance due to their relatively small size and weak scattering, and reversible, highly dynamics structures due to the weak physical interactions between them, and highly charged entities [32,42]. The occurrence of soluble complexes can be determined using simultaneous use of light scattering technique and UV-vis spectrophotometer [41]. An increase in the intensity observed in the light scattering technique where no increase in the absorbance value from UV-vis spectrophotometer indicates the formation of soluble complexes [43]. 3) Insoluble complexes/coacervation are probably the most interesting, biologically and functionally relevant phenomenon when it comes to the electrostatic complexation between proteins and polysaccharides [35,38]. This phenomenon occurs when proteins and polysaccharides strongly associate to form relatively large complexes (100-10000 nm range). Thus, they tend to scatter light strongly, resulting in the turbid solution.

Another important characteristics is that their net charge is relatively low so that coalescence easily takes place, leading to phase separation into two different phases, *i.e.*, one phase is rich, dense, usually viscous solution that consists of the association of the proteins and polysaccharides, another phase is dilute solution that mainly consists of the solvents [44]. The driving force for the formation of insoluble complexes/coacervation is indeed the electrostatic interaction that comes from oppositely charged proteins and polysaccharides in the solution and the decrease of the free energy of the system through the gain of entropy by the release of counterions and water molecules and the decrease of electrostatic enthalpy contribution by the complex formation [36,39,44]. In addition, other weak, non-covalent interactions, such as hydrogen bonding, hydrophobic interactions can have a significant impact on the formation of insoluble complexes/coacervation [21]. It should be noted that for some researchers, the term "coacervation" is strictly defined to liquid-liquid phase separation where the formation of coacervates are confirmed by the presence of fused coacervate droplets with liquid-like or highly viscous properties by the use of centrifugation, light microscopy techniques, and interfacial tension measurement [45]. 4) Precipitation occurs when the electrostatic interactions are strong enough to expel more counterions and water such that tight packing and binding between the two biopolymers take place [32]. As a result, solid-like particles (precipitates) can be observed in the system through visual observation and microscopy technique. Precipitates tend to scatter light more strongly and sediment faster than does coacervates. In contrast to coacervates, precipitates are kinetically controlled and essentially irreversible [32]. Among these phenomena, soluble and insoluble complexes are widely used to fabricate NPs for encapsulation and delivery systems. To get complexes in the nanoscale level, one has to adjust several operating parameters, including total proteins/polysaccharides concentration, proteins-polysaccharides ratio, pH, ionic strength, and molecular characteristics (molecular weight, flexibility, charge density, conformation) [37]. In some cases, external forces and additional

elements, such as heat and ions are required to form NPs from soluble/insoluble complexes [46,47]. In addition, processing operation methods, such as spray and freeze drying, homogenizer, and microfluidics can be utilized to form small and stable NPs [32]. In general, the formation of NPs is carried out under dilute (the total biopolymers concentration is typically less than 0.5% (w/v)) and low ionic strength conditions [48]. NPs fabricated from the electrostatic complexation are typically reversible and highly dynamic. Therefore, they are likely to deform and destabilize when the pH and ionic strength are changed. The particle stability is of importance to ensure the practicality of the NPs for encapsulation and delivery systems as they will be encountered harsh and unfavorable environments, such as acidic pH, high salt concentration in the body.

1.2.3 Stability of NPs

Enhancing the stability of NPs can be done using physical, enzymatic, conjugation, and chemical methods. Physical enhancement utilizes non-covalent forces, such as hydrogen bonding, hydrophobic interactions, and ionic cross-linking, which can be obtained by employing heat and mineral ions [46]. Hydrophobic and hydrogen bonding-related associations tend to increase with increasing and decreasing temperature, respectively [44]. For instance, the stability of whey protein-pectin complexes in a wide range of pH was remarkably enhanced after heat treatment due to increased hydrophobic interactions among unfolded whey proteins [49]. Similarly, pH and salt-stable nanogels composed of soy proteins and soy polysaccharides could be fabricated after heat treatment [50]. Ionic cross-linking can be employed to form stable NPs by adding mineral ions such as calcium and potassium into NPs containing anionic polysaccharides. Pectins, alginates, and carrageenan may self-assemble into gel-like structure, which promotes the integrity of NPs [51–53]. Enzymes such as transglutaminase, tyrosinase, and laccase can be also used to enhance the stability of the protein-polysaccharide complex [54,55]. Likewise, conjugation of protein with polysaccharides can render the NPs stable

against agglomerations and high salt concentrations [56–58]. One convenient and effective approach is the use of chemical cross-linker to make the NPs stable under physiological conditions by forming covalent bonds among proteins/polysaccharides within the NPs. Some examples of cross-linkers that have been commonly used are glutaraldehyde, 1-ethyl-3-(3-dimethylaminopropyl) carbodiimide (EDC), diisocyanate, and sulfhydryl-reactive cross-linkers [48,59–61]. However, the utilization of amenable, non-toxic cross-linker has recently been encouraged. Genipin is a foremost natural cross-linker that attracts many researchers due to its safety and great biological activities [62].

1.2.4 NPs formed from the interaction between chitosan and proteins

Among other polysaccharides, chitosan (CH) is of great interest for fabricating NPs through complexation with proteins due to its inherent cationic properties, mild toxicity, biodegradability, diverse biological activities, mucoadhesiveness, and great abundance. CH is a linear homopolymer that can be obtained by partial deacetylation of chitin, the major components of crustaceans, some bacterial and fungal cell walls (**Fig. 1-3**) [63]. CH consists of β-(1,4)-linked *N*-acetyl-glucosamine chains. CH is positively charged in the solution and its charge density decreases as pH is increased from acidic to neutral/alkaline condition [47,63]. However, CH is poorly soluble in water and requires mild acid to solubilize it [47]. For this reason, derivatives of CH have been synthesized such as carboxymethyl CH and glycol CH (GC) [64,65]. Nevertheless, CH has still been extensively used in the various fields, including food, pharmaceuticals, and biomedical fields. NPs formed from the interaction between CH and proteins have been explored for encapsulation and delivery systems. Different types of proteins, including globular, linear, unstructured have been known to form nano-complexation with CH for encapsulation of hydrophilic or hydrophobic bioactive compounds. These include animal- and plant-based globular proteins such as β-lactoglobulin [66–68], β-conglycinin [69], soy proteins [70], zein [64,71]. Likewise, various albumins including those obtained from

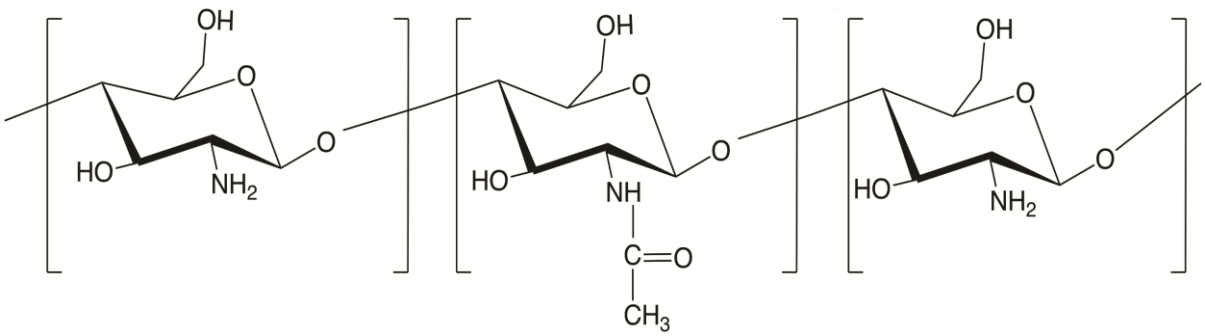

Fig. 1-3 Chemical structure of CH

plants (rice bran albumin) [72], bovine serum [73–76], milks (lactalbumin) [77,78], eggs (ovalbumin) [46,79,80], and human serum [81] have been explored for fabrication of NPs with CH. Linear and unstructured proteins such as gelatin [82], caseins [76,83,84] have also been reported to form nano-scale complexation with CH for encapsulation of therapeutic compounds. Recently, transport proteins such as ferritin [85,86] have also been studied for fabrication of NPs with CH. Moreover, therapeutic proteins such as insulin [87,88], peptides [48,62] have also been utilized for the formation of nano-scale complex. These NPs have shown promising abilities for controlled release, improved mucoadhesiveness and cellular interaction, enhanced stability and bioactivity of encapsulated compounds. However, these NPs are mainly studied for encapsulation of hydrophilic compounds.

1.3 Aim and outline of this thesis

The aim of this research is to get a better understanding on the capabilities of nano-complexation between CH and proteins as a nanocarrier for encapsulation and delivery of hydrophobic therapeutic compounds. In particular, the formation and properties of NPs from these complexations are investigated, and the cellular *in vitro* studies are carried out to evaluate their potential applications as a nanocarrier.

In **Chapter 2**, we focused on characterizing the nano-complexation between CH and unstructured protein, sodium caseinate (CS). The feasibility of these complexes to encapsulate

curcumin, a yellow medicinal compound from turmeric plants was investigated by evaluating their ability to enhance water dispersibility, thermal and storage stability, and antioxidant activity of curcumin.

In **Chapter 3**, we investigated the bioactivity of curcumin-loaded in the NPs described in the previous chapter. First, the stability of the NPs was enhanced by applying genipin cross-linker. Finally, the cytotoxicity *in vitro* and cellular uptake studies in cancer and normal cells were carried out to determine the capabilities of these NPs as delivery systems for curcumin.

In **Chapter 4**, we studied the formation of NPs between globular protein, bovine serum albumin (BSA) and glycol chitosan (GC). The formation mechanism and properties of these NPs were characterized in detail. We explored the ability of these NPs for PTX delivery by evaluating encapsulation efficiency, release profile, and cytotoxicity *in vitro* studies of PTX-loaded in these NPs.

Finally, in **Chapter 5**, we summarized the findings of this research and briefly discussed further research directions related to this research.

References

[1] T.A. Debele, S.L. Mekuria, H.C. Tsai. Polysaccharide Based Nanogels in the Drug Delivery System: Application as the Carrier of Pharmaceutical Agents. Mater. Sci. Eng. C, 68 (2016) 964–981.

[2] C.L. Ventola, D.J. Bharali, S.A. Mousa. The Nanomedicine Revolution: Part 1: Emerging Concepts. Pharmacy and Therapeutics. Pharmacol. Ther, 128 (2010) 512–525.

[3] A. Wicki, D. Witzigmann, V. Balasubramanian, J. Huwyler. Nanomedicine in Cancer Therapy: Challenges, Opportunities, and Clinical Applications. J. Control. Release, 200 (2015) 138–157.

[4] X. Xu, W. Ho, X. Zhang, N. Bertrand, O. Farokhzad. Cancer Nanomedicine: From Targeted Delivery to Combination Therapy. Trends Mol. Med, 21 (2015) 223–232.

[5] D. Bobo, K.J. Robinson, J. Islam, K.J. Thurecht, S.R. Corrie. Nanoparticle-based Medicines: A Review of FDA-approved Materials and Clinical Trials to Date. Pharm. Res, 33 (2016) 2373–2387.

[6] S. Karve, M.E. Werner, R. Sukumar, N.D. Cummings, J.A. Copp, E.C. Wang, C. Li, M. Sethi, R.C. Chen, M.E. Pacold, A.Z. Wang. Revival of the Abandoned Therapeutic Wortmannin by Nanoparticle Drug Delivery. Proc. Natl. Acad. Sci, 109 (2012) 8230–8235.

[7] K.K. Cheng, C.F. Yeung, S.W. Ho, S.F. Chow, A.H.L. Chow, L. Baum. Highly Stabilized Curcumin Nanoparticles Tested in an In Vitro Blood–brain Barrier Model and in Alzheimer's Disease Tg2576 Mice. AAPS J, 15 (2013) 324–336.

[8] F. Danhier. To Exploit the Tumor Microenvironment: Since the EPR Effect Fails In The Clinic, What is the Future of Nanomedicine?. J. Control. Release, 244 (2016) 108–121.

[9] A. Jhaveri, P. Deshpande, V. Torchilin Stimuli-sensitive Nanopreparations for Combination Cancer Therapy. J. Control. Release, 190 (2014) 352–370.

[10] Y. Chen, W. Cao, J. Zhou, B. Pidhatika, B. Xiong, L. Huang, Q. Tian, Y. Shu, W. Wen, I.M. Hsing, H. Wu. Poly(l-lysine)-graft-folic acid-coupled poly(2-methyl-2-oxazoline) (PLL-g-PMOXA-c-FA): A Bioactive Copolymer for Specific Targeting to Folate Receptor-Positive Cancer Cells. ACS Appl. Mater. Interfaces, 7 (2015) 2919–2930.

[11] Y. Zhong, J. Zhang, R. Cheng, C. Deng, F. Meng, F. Xie, Z. Zhong. Reversibly Crosslinked Hyaluronic Acid Nanoparticles for Active Targeting and Intelligent Delivery of Doxorubicin to Drug Resistant CD44 + Human Breast Tumor Xenografts. J. Control. Release, 205 (2015) 144–154.

[12] M.S. Muthu, R.V. Kutty, Z. Luo, J. Xie, S.S. Feng. Theranostic Vitamin E TPGS Micelles of Transferrin Conjugation for Targeted Co-delivery of Docetaxel and Ultra Bright Gold Nanoclusters. Biomaterials, 39 (2015) 234–248.

[13] H.Y. Chiu, W. Deng, H. Engelke, J. Helma, H. Leonhardt, T. Bein. Intracellular Chromobody Delivery by Mesoporous Silica Nanoparticles for Antigen Targeting and Visualization in Real Time. Sci. Rep, 6 (2016) 1–12.

[14] M. Kaluzova, A. Bouras, R. Machaidze, C.G. Hadjipanayis. Targeted Therapy of Glioblastoma Stem-like Cells and Tumor Non-stem Cells Using Cetuximab-conjugated Iron-oxide Nanoparticles. Oncotarget, 6 (2015) 8788–8806.

[15] L. Zhu, V.P. Torchilin. Stimulus-responsive Nanopreparations for Tumor Targeting. Integr. Biol, 5 (2013) 96–107.

[16] S. Ganta, H. Devalapally, A. Shahiwala, M. Amiji. A Review of Stimuli-responsive Nanocarriers for Drug and Gene Delivery. J. Control. Release, 126 (2008) 187–204.

[17] K. Kessenbrock, V. Plaks, Z. Werb. Matrix Metalloproteinases: Regulators of the Tumor Microenvironment. Cell, 141 (2010) 52–67.

[18] J. Li, M. Huo, J. Wang, J. Zhou, J.M. Mohammad, Y. Zhang, Q. Zhu, A.Y. Waddad, Q. Zhang. Redox-sensitive Micelles Self-assembled from Amphiphilic Hyaluronic Acid-deoxycholic Acid Conjugates for Targeted Intracellular Delivery of Paclitaxel. Biomaterials, 33 (2012) 2310–2320.

[19] E. Fleige, M.A. Quadir, R. Haag. Stimuli-responsive Polymeric Nanocarriers for the Controlled Transport of Active Compounds: Concepts and Applications. Adv. Drug Deliv. Rev, 64 (2012) 866–884.

[20] P.B. Santhosh, N.P. Ulrih. Multifunctional Superparamagnetic Iron Oxide Nanoparticles: Promising Tools in Cancer Theranostics. Cancer Lett, 336 (2013) 8–17.

[21] M.A. Rogers. Naturally Occurring Nanoparticles in Food. Curr. Opin. Food Sci, 7 (2016) 14–19.

[22] A. Sangtani, O.K. Nag, L.D. Field, J.C. Breger, J.B. Delehanty. Multifunctional Nanoparticle Composites: Progress in the Use of Soft and Hard Nanoparticles for Drug Delivery and Imaging. Wiley Interdiscip. Rev. Nanomedicine Nanobiotechnology, 9 (2017) 1–23.

[23] J.I. Hare, T. Lammers, M.B. Ashford, S. Puri, G. Storm, S.T. Barry. Challenges and Strategies in Anti-cancer Nanomedicine Development: An Industry Perspective. Adv. Drug Deliv. Rev, 108 (2017) 25–38.

[24] V. Weissig, T.K. Pettinger, N. Murdock. Nanopharmaceuticals (part 1): Products on the Market. Int. J. Nanomedicine, 9 (2014) 4357–4373.

[25] Y. Barenholz. Doxil® - The First FDA-approved Nano-drug: Lessons Learned. J. Control. Release, 160 (2012) 117–134.

[26] E. Miele, G.P. Spinelli, E. Miele, F. Tomao, S. Tomao. Albumin-bound Formulation of Paclitaxel (Abraxane ABI-007) in the Treatment of Breast Cancer. Int. J. Nanomedicine, 4 (2009) 99–105.

[27] M. Vellard. The Enzyme as Drug: Application of Enzymes as Pharmaceuticals. Curr. Opin. Biotechnol, 14 (2003) 444–450.

[28] L. Lang. FDA Approves Cimzia to Treat Crohn's Disease. Gastroenterology, 134 (2008) 1819.

[29] R. Berges. Eligard®: Pharmacokinetics, Effect on Testosterone and PSA Levels and Tolerability. Eur. Urol. Suppl, 4 (2005) 20–25.

[30] Z. Fan, C. Chen, X. Pang, Z. Yu, Y. Qi, X. Chen, H. Liang, X. Fang, X. Sha. Adding Vitamin E-TPGS to the Formulation of Genexol-PM: Specially Mixed Micelles Improve Drug-loading Ability and Cytotoxicity Against Multidrug-resistant Tumors

Significantly. PLoS One, 10 (2015) 1–17.

[31] A.O. Elzoghby, W.M. Samy, N.A. Elgindy. Protein-based Nanocarriers as Promising Drug and Gene Delivery Systems. J. Control. Release, 161 (2012) 38–49.

[32] O.G. Jones, D.J. McClements. Functional Biopolymer Particles: Design, Fabrication, and Applications. Compr. Rev. Food Sci. Food Saf, 9 (2010) 374–397.

[33] M. Tarhini, H. Greige-Gerges, A. Elaissari. Protein-based Nanoparticles: From Preparation to Encapsulation of Active Molecules. Int. J. Pharm, 522 (2017) 172–197.

[34] D.J. McClements. Encapsulation, Protection, and Delivery of Bioactive Proteins and Peptides Using Nanoparticle and Microparticle Systems: A Review. Adv. Colloid Interface Sci, 253 (2018) 1–22.

[35] J.P. Fuenzalida, F.M. Goycoolea. Polysaccharide-protein Nanoassemblies: Novel Soft Materials for Biomedical and Biotechnological Applications. Curr. Protein Pept. Sci, 16 (2015) 89–99.

[36] S.L. Turgeon, C. Schmitt, C. Sanchez. Protein-polysaccharide Complexes and Coacervates, Curr. Opin. Colloid Interface Sci, 12 (2007) 166–178.

[37] O.G. Jones, D.J. McClements. Recent Progress in Biopolymer Nanoparticle and Microparticle Formation by Heat-treating Electrostatic Protein-polysaccharide Complexes. Adv. Colloid Interface Sci, 167 (2011) 49–62.

[38] M. Semenova. Protein–polysaccharide Associative Interactions in the Design of Tailor-made Colloidal Particles. Curr. Opin. Colloid Interface Sci, 28 (2017) 15–21.

[39] C.G. De Kruif, R. Tuinier. Polysaccharide Protein Interactions. Food Hydrocoll, 15 (2001) 555–563.

[40] J.M. Rodriguez Patino, A.M.R. Pilosof. Protein-polysaccharide Interactions at Fluid Interfaces. Food Hydrocoll, 25 (2011) 1925–1937.

[41] C.L. Cooper, P.L. Dubin, A.B. Kayitmazer, S. Turksen. Polyelectrolyte-protein Complexes, Curr. Opin. Colloid Interface Sci, 10 (2005) 52–78.

[42] J. Pathak, E. Priyadarshini, K. Rawat, H.B. Bohidar. Complex Coacervation in Charge Complementary Biopolymers: Electrostatic Versus Surface Patch Binding. Adv. Colloid Interface Sci, 250 (2017) 40–53.

[43] G. Mekhloufi, C. Sanchez, D. Renard, S. Guillemin, J. Hardy. pH-induced Structural Transitions During Complexation and Coacervation of β-Lactoglobulin and Acacia Gum. Langmuir, 21 (2005) 386–394.

[44] T. Moschakis, C.G. Biliaderis. Biopolymer-based Coacervates: Structures,

Functionality and Applications in Food Products. Curr. Opin. Colloid Interface Sci, 28 (2017) 96–109.

[45] N.N. Deng, W.T.S. Huck. Microfluidic Formation of Monodisperse Coacervate Organelles in Liposomes. Angew. Chemie - Int. Ed, 56 (2017) 9736–9740.

[46] S. Yu, J. Hu, X. Pan, P. Yao, M. Jiang. Stable and pH-sensitive Nanogels Prepared by Self-assembly of Chitosan and Ovalbumin. Langmuir, 22 (2006) 2754–2759.

[47] Y.H. Hong, D.J. McClements. Formation of Hydrogel Particles by Thermal Treatment Of β-Lactoglobulin-chitosan Complexes. J. Agric. Food Chem, 55 (2007) 5653–5660.

[48] W. He, M. Parowatkin, V. Mailänder, M. Flechtner-Mors, R. Graf, A. Best, K. Koynov, K. Mohr, U. Ziener, K. Landfester, D. Crespy. Nanocarrier for Oral Peptide Delivery Produced by Polyelectrolyte Complexation in Nanoconfinement. Biomacromolecules, 16 (2015) 2282–2287.

[49] M.C. Gentés, D. St-Gelais, S.L. Turgeon. Stabilization of Whey Protein Isolate-pectin Complexes by Heat. J. Agric. Food Chem, 58 (2010) 7051–7058.

[50] X. Ding, P. Yao. Soy Protein/soy Polysaccharide Complex Nanogels: Folic Acid Loading, Protection, and Controlled Delivery. Langmuir, 29 (2013) 8636–8644.

[51] H. Jonassen, A. Treves, A.L. Kjøniksen, G. Smistad, M. Hiorth. Preparation of Ionically Cross-linked Pectin Nanoparticles in the Presence of Chlorides of Divalent and Monovalent Cations. Biomacromolecules, 14 (2013) 3523–3531.

[52] M. Gonzàlez Ferreiro, L. Tillman, G. Hardee, R. Bodmeier. Characterization of Alginate/Poly-l-Lysine Particles as Antisense Oligonucleotide Carriers. Int. J. Pharm, 239 (2002) 47–59.

[53] M.P. Gashti, M. Stir, J. Hulliger. Synthesis of Bone-like Micro-porous Calcium Phosphate/Iota-carrageenan Composites by Gel Diffusion. Colloids Surfaces B Biointerfaces, 110 (2013) 426–433.

[54] A.S. Prata, M.H.A. Zanin, M.I. Ré, C.R.F. Grosso. Release Properties of Chemical and Enzymatic Crosslinked Gelatin-gum Arabic Microparticles Containing A Fluorescent Probe Plus Vetiver Essential Oil. Colloids Surfaces B Biointerfaces, 67 (2008) 171–178.

[55] Q. Wang, Y. Ren, Y. Ding, M. Xu, B. Chen. The Influence of pH and Enzyme Cross-linking on Protein Delivery Properties of WPI-beet Pectin Complexes. Food Res. Int, 105 (2018) 678–685.

[56] J. Yi, Y. Fan, Y. Zhang, Z. Wen, L. Zhao, Y. Lu. Glycosylated α-Lactalbumin-based Nanocomplex for Curcumin: Physicochemical Stability and DPPH-scavenging Activity.

Food Hydrocoll, 61 (2016) 369–377.

[57] J. Feng, S. Wu, H. Wang, S. Liu. Improved Bioavailability of Curcumin in Ovalbumin-dextran Nanogels Prepared by Maillard Reaction. J. Funct. Foods, 27 (2016) 55–68.

[58] G. Davidov-Pardo, S. Pérez-Ciordia, M.R. Marín-Arroyo, D.J. McClements. Improving Resveratrol Bioaccessibility Using Biopolymer Nanoparticles and Complexes: Impact of Protein-carbohydrate Maillard Conjugation. J. Agric. Food Chem, 63 (2015) 3915–3923.

[59] R. Hedayati, M. Jahanshahi, H. Attar. Fabrication and Characterization of Albumin-acacia Nanoparticles Based on Complex Coacervation as Potent Nanocarrier. J. Chem. Technol. Biotechnol, 87 (2012) 1401–1408.

[60] F. Xing, G. Cheng, K. Yi, L. Ma. Nanoencapsulation of Capsaicin by Complex Coacervation of Gelatin, Acacia, and Tannins. J. Appl. Polym. Sci, 96 (2005) 2225–2229.

[61] C. Chang, T. Wang, Q. Hu, Y. Luo. Caseinate-zein-polysaccharide Complex Nanoparticles as Potential Oral Delivery Vehicles for Curcumin: Effect of Polysaccharide Type and Chemical Cross-linking. Food Hydrocoll, 72 (2017) 254–262.

[62] B. Hu, M. Xie, C. Zhang, X. Zeng. Genipin-structured Peptide - Polysaccharide Nanoparticles with Significantly Improved Resistance to Harsh Gastrointestinal Environments and Their Potential for Oral Delivery of Polyphenols. J. Agric. Food Chem, 62 (2014) 12443–12452.

[63] S. Yu, B. Sun, S. Gao, S. Guo, K. Zhao. Biomedical Applications of Chitosan and Its Derivatives Nanoparticles. Polymers, 10 (2018) 462.

[64] H. Zhang, Y. Fu, F. Niu, Z. Li, C. Ba, B. Jin, G. Chen, X. Li. Enhanced Antioxidant Activity and In Vitro Release of Propolis by Acid-induced Aggregation Using Heat-denatured Zein and Carboxymethyl Chitosan. Food Hydrocoll, 81 (2018) 104–112.

[65] A. Trapani, S. Di Gioia, N. Ditaranto, N. Cioffi, F.M. Goycoolea, A. Carbone, M. Garcia-Fuentes, M. Conese, M.J. Alonso. Systemic Heparin Delivery by the Pulmonary Route Using Chitosan and Glycol Chitosan Nanoparticles. Int. J. Pharm, 447 (2013) 115–123.

[66] C. Liu, Z. Liu, X. Sun, S. Zhang. Fabrication and Characterization of β-Lactoglobulin-Based Nanocomplexes Composed of Chitosan Oligosaccharides as Vehicles for Delivery of Astaxanthin, J. Agric. Food Chem (2018) *Accepted Manuscript*.

[67] L. Chen, M. Subirade. Chitosan/β-Lactoglobulin Core-shell Nanoparticles as Nutraceutical Carriers. Biomaterials, 26 (2005) 6041–6053.

[68] J. Liang, H. Yan, H.-J. Yang, H.W. Kim, X. Wan, J. Lee, S. Ko. Synthesis and Controlled-release Properties of Chitosan/β-Lactoglobulin Nanoparticles as Carriers for Oral Administration of Epigallocatechin Gallate. Food Sci. Biotechnol, 25 (2016) 1583–1590.

[69] Y. Liu, J. Liang, S. Wei, L. Liu, M. Liao. Nanoparticles Based on β-Conglycinin and Chitosan: Self-assembly, Characterization, and Drug Delivery. J. Appl. Polym. Sci, 132 (2015).

[70] Y. Yuan, Z.Y. Kong, Y.E. Sun, Q.Z. Zeng, X.Q. Yang. Complex Coacervation of Soy Protein With Chitosan: Constructing Antioxidant Microcapsule for Algal Oil Delivery. LWT - Food Sci. Technol, 75 (2017) 171–179.

[71] Y. Luo, B. Zhang, M. Whent, L.L. Yu, Q. Wang. Preparation and Characterization of Zein/Chitosan Complex for Encapsulation of α-Tocopherol, and Its In Vitro Controlled Release Study. Colloids Surfaces B Biointerfaces, 85 (2011) 145–152.

[72] H. Peng, Z. Gan, H. Xiong, M. Luo, N. Yu, T. Wen, R. Wang, Y. Li. Self-assembly of Protein Nanoparticles from Rice Bran Waste and Their Use as Delivery System for Curcumin. ACS Sustain. Chem. Eng, 5 (2017) 6605–6614.

[73] J. Qi, P. Yao, F. He, C. Yu, C. Huang. Nanoparticles with Dextran/Chitosan Shell and BSA/Chitosan Core-doxorubicin Loading and Delivery. Int. J. Pharm, 393 (2010) 177–185.

[74] Y. Wang, S. Xu, W. Xiong, Y. Pei, B. Li, Y. Chen. Nanogels Fabricated from Bovine Serum Albumin and Chitosan via Self-assembly for Delivery of Anticancer Drug, Colloids Surfaces B Biointerfaces. 146 (2016) 107–113.

[75] N. Varga, M. Benko, D. Sebok, I. Dékány. BSA/Polyelectrolyte Core-shell Nanoparticles for Controlled Release of Encapsulated Ibuprofen. Colloids Surfaces B Biointerfaces, 123 (2014) 616–622.

[76] D. Kurukji, I. Norton, F. Spyropoulos. Fabrication of Sub-micron Protein-chitosan Electrostatic Complexes for Encapsulation and pH-modulated Delivery of Model Hydrophilic Active Compounds. Food Hydrocoll, 53 (2016) 249–260.

[77] N. Particles, J. Du, Y. Cho, R. Murphy, O.G. Jones. Impact of Chitosan Molecular Weight and Attached Non-interactive Chains on the Formation of α-Lactalbumin Nanogel Particles. Gels, 3 (2017) 14.

[78] Q. Li, Z. Zhao, Characterization of the Structural and Colloidal Properties of α-Lactalbumin/Chitosan Complexes as a Function of Heating, J. Agric. Food Chem. 66

(2018) 972–978.

[79] S. Jana, S. Manna, A.K. Nayak, K.K. Sen, S.K. Basu. Carbopol Gel Containing Chitosan-egg Albumin Nanoparticles for Transdermal Aceclofenac Delivery. Colloids Surfaces B Biointerfaces, 114 (2014) 36–44.

[80] S. Jana, N. Maji, A.K. Nayak, K.K. Sen, S.K. Basu. Development of Chitosan-based Nanoparticles through Inter-polymeric Complexation for Oral Drug Delivery. Carbohydr. Polym, 98 (2013) 870–876.

[81] M. Esfandyari-Manesh, A. Mohammadi, F. Atyabi, S.M. Nabavi, S.M. Ebrahimi, E. Shahmoradi, B.S. Varnamkhasti, M.H. Ghahremani, R. Dinarvand. Specific Targeting Delivery to MUC1 Overexpressing Tumors by Albumin-chitosan Nanoparticles Conjugated to DNA Aptamer. Int. J. Pharm, 515 (2016) 607–615.

[82] M. Rajkumar, K. Kavitha, M. Prabhu, N. Meenakshisundaram, V. Rajendran. Nanohydroxyapatite-chitosan-gelatin Polyelectrolyte Complex with Enhanced Mechanical and Bioactivity. Mater. Sci. Eng. C, 33 (2013) 3237–3244.

[83] M. Razmi, A. Divsalar, A.A. Saboury, Z. Izadi, T. Haertlé, H. Mansuri-Torshizi. Beta-Casein and Its Complexes with Chitosan as Nanovehicles for Delivery of A Platinum Anticancer Drug. Colloids Surfaces B Biointerfaces, 112 (2013) 362–367.

[84] S.Y. Koo, I.K. Mok, C.H. Pan, S.M. Kim. Preparation of Fucoxanthin-loaded Nanoparticles Composed of Casein and Chitosan with Improved Fucoxanthin Bioavailability. J. Agric. Food Chem, 64 (2016) 9428–9435.

[85] R. Yang, Y. Liu, Y. Gao, Z. Yang, S. Zhao, Y. Wang, C. Blanchard, Z. Zhou. Nano-Encapsulation of Epigallocatechin Gallate in the Ferritin-chitosan Double Shells: Simulated Digestion and Absorption Evaluation. Food Res. Int, 108 (2018) 1–7.

[86] R. Yang, J. Tian, Y. Liu, D. Meng, C.L. Blanchard, Z. Zhou. One-step Fabrication of Phytoferritin-chitosan-epigallocatechin Shell-core Nanoparticles by Thermal Treatment. Food Hydrocoll, 80 (2018) 24–32.

[87] A.M. Elsayed, A.H. Khaled, M.M. Al Remawi, N.A. Qinna, H.A. Farsakh, A.A. Badwan. Low Molecular Weight Chitosan-insulin Complexes Solubilized in A Mixture of Self-assembled Labrosol and Plurol Oleaque and Their Glucose Reduction Activity in Rats. Mar. Drugs, 16 (2018).

[88] C.P. Silva, J.H. Martínez, K.D. Martínez, M.E. Farías, F.C. Leskow, O.E. Pérez. Proposed Molecular Model for Electrostatic Interactions between Insulin and Chitosan. Nano-complexation and Activity in Cultured Cells. Colloids Surfaces A Physicochem. Eng. Asp, 537 (2018) 425–434.

CHAPTER 2 FORMATION AND CHARACTERIZATION OF CASEINATE–CHITOSAN NANOCOMPLEXES FOR ENCAPSULATION OF CURCUMIN

2.1 Abstract

Curcumin holds promise as a therapeutic agent due to its capability of conferring several pharmacological activities. While curcumin shows efficacy in preclinical studies as an anti-cancer agent, its translation into the clinic as a drug has yet to be realized. One possible reason is its poor solubility and stability in water, which decreases the bioavailability. Here, we report the formation of biocompatible nanocomplexes (NCs) from caseinate (CS) and chitosan (CH) using an electrostatic interaction-based approach to stabilize and enhance water solubility of curcumin. The formation of CS–CH NCs (CCNCs) was studied as a function of CH concentration. We show that positively charged NCs, having size between approx. 250 nm with a narrow distribution was formed by adjusting CH concentration. CCNCs successfully entrapped curcumin with a high entrapment efficiency. Curcumin was possibly located in a hydrophobic region of CS as indicated by a blue-shift in the emission maxima of curcumin. Ultimately, the stability and water solubility of curcumin in CCNCs could be remarkably enhanced. These results suggest that CCNCs would be useful for increasing the potential of curcumin as a preventive or therapeutic agent.

2.2 Introduction

Curcumin [1,7-bis(4-hydroxy-3-methoxyphenyl)-1,6-heptadiene-3,5-dione; diferuloylmethane] (**Fig. 2-1**) is a polyphenolic compound associated with several beneficial health effects such as anti-cancer, anti-inflammatory, anti-diabetes, anti-microbial, and anti-Alzheimer [1]. Moreover, curcumin also shows hepato-and cardio-protective activity [2, 3] and has strong antioxidant properties, which are attributed to the phenolic groups and conjugated diene moiety [4]. Curcumin has relatively low toxicity. High doses of curcumin (12 g daily) resulted in only a minor side effect [5], suggesting its remarkable pharmacological safety. However, curcumin bioavailability is extremely low as evidenced by the little curcumin detected in plasma after oral or intravenous administration [5, 6]. In addition to the rapid metabolism and systemic elimination [7], one of the major reasons for the low curcumin bioavailability is the poor aqueous solubility, which is about 11 ng/ml [8]. Therefore, a strategy to overcome the low bioavailability for realizing curcumin potential as a preventive or therapeutic agent against various cancers and diseases needs to be devised.

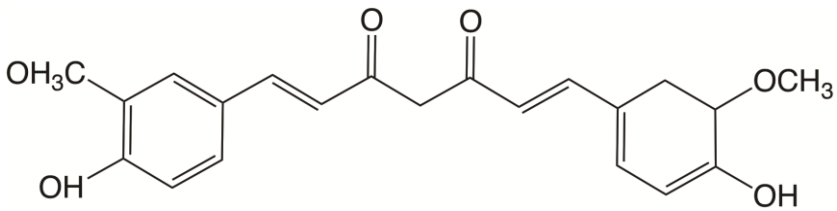

Fig. 2-1 The chemical structure of curcumin

Several strategies to improve solubilization and bioavailability of curcumin have been developed. The use of adjuvants such as piperine is able to improve curcumin bioavailability by inhibiting glucuronidation [9], which is responsible for curcumin metabolism in the body. The utilization of nano-sized carriers such as liposomes [10], self-assembling micelles [11], polymeric nanoparticles [12], nanoemulsion [13], and lipid-based nanocarriers [14] has shown a great promise in improving curcumin bioavailability and stability, enhancing curcumin

cellular uptake and facilitating controlled release and targeted delivery. Nevertheless, some of nanocarriers suffer from the complexity of the production method, the high cost of materials and equipment, and the frequent use of harmful organic solvents in the preparation of nanocarriers.

Recently, nanocomplexes (NCs) made from electrostatic interactions between proteins and polysaccharides have demonstrated excellent ability to enhance water solubility and bioavailability of bioactive molecules [15-17]. NCs can be easily formed by mixing proteins and polysaccharides having opposite charge in an aqueous solution, allowing simple, effective, and energy efficient manufacturing processes [18-19]. In addition, the use of a harmful organic solvent could be prevented, which is advantageous for the development of functional foods. While the main driving force of the formation of NCs is commonly believed to be a strong yet reversible electrostatic interaction, other forces, such as hydrogen bonding and hydrophobic interactions are also involved [19]. Improving aqueous solubility and bioavailability of curcumin by utilizing NCs from protein and polysaccharides is deemed a simple yet interesting approach.

Chitosan (CH), being a biopolymer bearing positive charge, has been extensively utilized to fabricate NCs [18, 19]. CH is a polysaccharide derived from crustacean shells and is composed of glucosamine and N-acetyl glucosamine groups linked by β-(1,4) glycosidic bond. It is well known for its excellent biocompatibility, biodegradability, mucoadhesiveness and non-toxic property (18-20]. Its potential use as a drug excipient or a bioactive compound in food [21], biomedical [22] and pharmaceutical [23] applications has been well demonstrated. Despite the fact that various kinds of nanocarriers employing CH have been developed, few studies are available investigating the capability of protein CH-based NCs for improving therapeutic effectiveness of curcumin.

Caseins, the major protein from bovine milk, are open-structured rheomorphic proteins, and consist of four casein phosphoproteins, αS_1-, αS_2-, β-, and κ-casein, with molecular weights between 19 and 25 kDa, and a calcium phosphate nanocluster [24]. Due to its biocompatibility and great surface-active characteristic, caseins have been widely used for developing delivery systems of hydrophobic molecules [16, 25], including curcumin. Curcumin encapsulated into caseins has shown improved chemical stability, enhanced water solubility and curcumin cellular uptake into cells [26, 27]. In the present work, caseinate (CS), which is an acid precipitation form of caseins, was used instead of native casein micelles for more practical application. A previous report demonstrated that NCs from CS and CH could be prepared by controlling the initial concentration and the mass ratio of two biopolymers and by adjusting pH of the solution [28]. However, no report is available to demonstrate the capability of these NCs to enhance aqueous solubility and stability of curcumin. So far, only one article investigating the delivery of a platinum-based anticancer drug by β-casein–chitosan NCs has been reported [29]. Therefore, the primary objective of this study was to get insight into the capability of CS–CH NCs (CCNCs) as a carrier for curcumin. In addition, the effect of CH concentration on the formation of CCNCs was investigated by monitoring their particle sizes, polydispersity index (PDI), derived count rate, zeta potential, and turbidity. The nature of the interaction between curcumin and CCNCs was confirmed by the fluorescence spectroscopy technique, and the enhanced water dispersibility and stability of curcumin loaded into CCNCs were shown.

2.3 Experimental

2.3.1 Materials and preparation of CH and CS solution

Low molecular weight CH (viscosity of 5-20 mPa.s and degree of deacetylation (DD) of 80.7%) was purchased from Tokyo Chemical Industry Co., Ltd (Tokyo, Japan) and was used as received. CS and potassium ferricyanide [$K_3Fe(CN)_6$] were purchased from Sigma-Aldrich,

USA. Curcumin, trichloroacetic acid, and ferric chloride ($FeCl_3$) were obtained from Wako Pure Chemical Industries (Osaka, Japan). CH solutions were prepared by dissolving CH in the powder form into 0.1 M acetic acid, and were then stirred until complete dissolution. Then, pH of the CH solution was adjusted to 5.5 by adding 1 M NaOH. CS solutions were prepared by dissolving them into Milli-Q water. Both CH and CS stock solutions were filtered against a 0.45 μm Millipore filter and were stored at 4°C overnight to ensure complete hydration before use.

2.3.2 CCNCs formation

CCNCs were fabricated based on electrostatic interaction between positively charged CH and negatively charged CS according to a previously published article [28]. Briefly, a CS solution was slowly added into the CH solution at the same volume ratio under slow agitation. NCs formation was indicated by the occurrence of a turbid or translucent solution. The final pH was adjusted to 5.5 by adding 0.1 M HCl or 0.1 M NaOH. In order to find optimum conditions for the formation of CCNCs, varying CH concentrations were prepared (0.25, 0.33, 0.5, 1, 2 mg/ml) at a final CS concentration of 1 mg/ml.

2.3.3 Curcumin-loaded CCNCs

Stock curcumin was prepared in an ethanolic solution (1 or 2 mg/ml) and was used for loading curcumin into CCNCs. Briefly, curcumin was loaded after NCs formation by adding the curcumin ethanolic stock solution to CCNCs under gentle stirring for 30 min. Preparation was done in the dark to avoid curcumin degradation. The final ethanol concentration used in the formulation was below 3%. The particle size, and PDI before and after curcumin addition were recorded. The entrapment efficiency (EE) of curcumin was determined based on the method reported previously [16] with a slight modification. CCNCs were centrifuged at 9,000 g for 30 min at 20°C. A small aliquot of supernatant was extracted with ethanol, then the mixture was subjected to a micro plate reader to quantify the amount of unloaded curcumin by

measuring the absorbance of supernatant at 425 nm. The standard curve of curcumin in ethanol was previously made (R^2 = 0.998). The entrapment efficiency (EE) (%) of curcumin in CCNCs was calculated using the following equation.

$$EE\ (\%)\ = \frac{Total\ curcumin\ added - curcumin\ in\ supernatant}{Total\ curcumin\ added} x\ 100\%$$

2.3.4 Fluorescence spectroscopy study

Fluorescence emission of CS and curcumin was measured using a LS 55 Perkin-Elmer fluorescence spectrometer. To observe fluorescence quenching of CS with the addition of increasing amount of curcumin (51-119 μM), CS (0.25 mg/ml) in the presence of CH (0.125 mg/ml) was used. The excitation wavelength was set at 295 nm, and the emission spectra were recorded from 310 to 450 nm with a slit width of 10 nm set for both excitation and emission. The inner filter effect was also considered. Fluorescence spectra of free curcumin in ethanol and curcumin loaded into CCNCs were recorded at the excitation wavelength of 420 nm, and the emission profiles from 450 to 700 nm were obtained.

2.3.5 Thermal stability and antioxidant activity of curcumin-loaded CCNCs

Free curcumin dissolved in 5 mM acetate buffer (pH 5.5) with a small amount of ethanol (2.6% v/v), curcumin-loaded CCNCs with CH concentrations of 0.5, 1, 2 mg/ml were heated at 80^{o}C for 2 h with light protection. At predetermined times (0, 0.5, 1, 1.5, and 2 h), aliquots of samples were taken and extracted with ethanol. The mixtures then were centrifuged at 9000 g at 20^{o}C for 5 min. The supernatant was taken and its absorbance at 425 nm was read as described in section 1.3. Curcumin retention (%) was defined as the amount of curcumin remaining after the thermal stability test.

The ferric reducing antioxidant power (FRAP) method [30] with a minor modification was used to estimate antioxidant activity of free curcumin and curcumin-loaded in CCNCs (at curcumin concentration of 50 μg/ml) with varying CH concentrations (0.5, 1, and 2 mg/ml).

Briefly, 0.4 ml of samples were mixed with 1 ml of sodium phosphate buffer pH 6 and 1 ml of 1% potassium ferricyanide [$K_3Fe(CN)_6$]. The mixtures then were incubated at 50°C for 20 min. One milliliter of 10% trichloroacetic acid was added to acidify the mixtures, followed by mixing and centrifugation at 3000 rpm for 10 min. Supernatant (0.5 ml) was taken out and mixed with 0.5 ml distilled water and 0.1 ml of 0.1% ferric chloride ($FeCl_3$). After incubation for 10 min at room temperature, the absorbance at 700 nm was read. Higher absorbance indicates higher antioxidant activity. Blanks were samples and all reagents without 1% potassium ferricyanide.

2.3.6 Water dispersibility and storage stability of freeze-dried curcumin-loaded CCNCs

Curcumin-loaded CCNCs were freeze-dried for 24 h in the presence of 5% trehalose to avoid aggregation. Milli-Q water was then added to the freeze-dried cake, and vortexed for 30 seconds to ensure complete dispersion. The physical properties of redispersed curcumin-loaded CCNCs were characterized. Free curcumin dissolved in Milli-Q water containing 5% trehalose was served as a control. A small amount of ethanol (2.6%) was used to help solubilization of free curcumin in Milli-Q. The amount of curcumin in redispersed CCNCs was determined by measuring absorbance at 425 nm. The storage stability of redispersed curcumin-loaded CCNCs was done at 25°C for one week. The changes in the particle size, PDI, and zeta potential were noted.

2.3.7 Characterization of CCNCs and curcumin-loaded CCNCs

Z-average particle size of CCNCs or curcumin-loaded CCNCs was determined by a dynamic light scattering (DLS) at scattering angle of 173° at 25°C with 10 runs each for 10 s (a Zetasizer Nano Series, Malvern Instrument). Zeta potential and derived count rate (10^3 kcps) were obtained using the same instrument. The derived count rate is defined as the theoretical count rate (signal strength) at maximum laser power without attenuation. It indicates the concentration of particles detected by DLS [31]. Turbidity was defined as optical density at

600 nm (OD 600) and was measured using a Jasco V-630 UV-Vis spectrophotometer. The absorbance profile of curcumin in ethanol and curcumin-loaded CCNCs were also determined using the same spectrophotometer. Attenuated total reflectance (ATR) FT-IR profiles of CH, CS and lyophilized CCNCs were conducted using a Perkin-Elmer FT-IR spectrometer with a resolution of 4 cm^{-1}.

2.4 Results and Discussion

NCs arising from the interaction of at least two oppositely charged polymers mainly involve strong electrostatic interactions [18]. In addition, hydrophobic interaction and hydrogen bonding participated in the formation of NCs. NCs could be instantaneously formed by simply mixing two oppositely charged molecules under a certain pH range and low ionic strength due to the entropy gain by the release of small counterions [18-19]. In this study, CH and CS were selected as positively and negatively charged entities, respectively. During the course of study, the initial pH of CH solution was adjusted to 5.5 to facilitate the formation of positively charged molecules, while CS was dissolved in Milli-Q water (pH 7) to ensure negatively charged CS molecules were obtained. CH is an amino-polysaccharide with a pKa value of ~6.5; therefore, in an acidic environment, the primary amino groups of CH undergo protonization, leading to a solubilization of chitosan chains with high density of positive charges. On the other hand, CS has an isoelectric point (pI) value of ~4.7. Above pI, CS is negatively charged. The final pH was fixed at 5.5 to ensure colloidal stability of CCNCs, as previously reported [28, 29]. Since the formation and physicochemical characteristics of electrostatic-based NCs are considerably affected by biopolymer concentrations [32], we studied the effect of CH concentration on the particle size, PDI, the number of particles, turbidity, and zeta potential to get a better understanding of the essential feature of CCNCs.

2.4.1 Effect of CH and total biopolymer concentration on the characteristics of CCNCs

CH concentration is one important parameter affecting the formation and the surface properties of NCs. CH is expected to endow CCNCs with positive surface charge, which could be beneficial for cellular uptake and mucoadhesiveness. In addition, CH should be in excess over CS in order to avoid the occurence of neutral particles, which can lead to precipitation or aggregation of NCs [18]. Therefore, the effect of CH concentration on the particle size, PDI, the number of particles, turbidity, and zeta potential of CCNCs were investigated. A varying CH concentration at a constant CS concentration of 1 mg/ml was evaluated. As shown in **Fig. 2-2A**, the particle size slightly decreased as CH concentration increased from 0.25 to 0.5 mg/ml, then increased as CH concentration increased from 0.5 to 2 mg/ml. The PDI decreased from 0.147 to 0.106 as CH concentration increased from 0.25 to 0.33 mg/ml, then increased linearly from 0.106 to 0.144 as increasing CH concentration. These results indicate that relatively small, homogeneous nanoparticles could be obtained within the CH concentrations studied. The derived count rate measured by a DLS could be used to estimate the stability and number of particles [33]. An increase in the derived count rate at CH concentrations of 0.5 and 1 mg/ml indicates effective NCs formation and more stable NCs. On the other hand, at CH concentration of 2 mg/ml, a slight decrease in the derived count rate indicates less NCs formation. At lower CH concentrations (0.25 and 0.33 mg/ml), NCs tend to settle down more quickly due to lower zeta potential (**Fig. 2-2B**), resulting in the lower derived count rate. The number of particles of CCNCs with CH concentrations of 0.5 and 1 mg/ml was comparable. The zeta potential of CCNCs almost increased linearly from +23.7 to +31.3 mV as CH concentration was increased. These results indicate that the composition of CS and CH in CCNCs has changed. It might be that less CS molecules interact with CH molecules to form NCs. Thus, the zeta potential becomes higher as a result of an excess positive charge. The zeta potential value of +30 mV is considered stable for colloidal particles that rely mostly on electrostatic interaction. It is worth mentioning that instant aggregation (data not shown), followed by precipitation of CCNCs with

CH concentration of 0.167 mg/ml was noticed, which is probably due to neutralization of the surface charge of CCNCs.

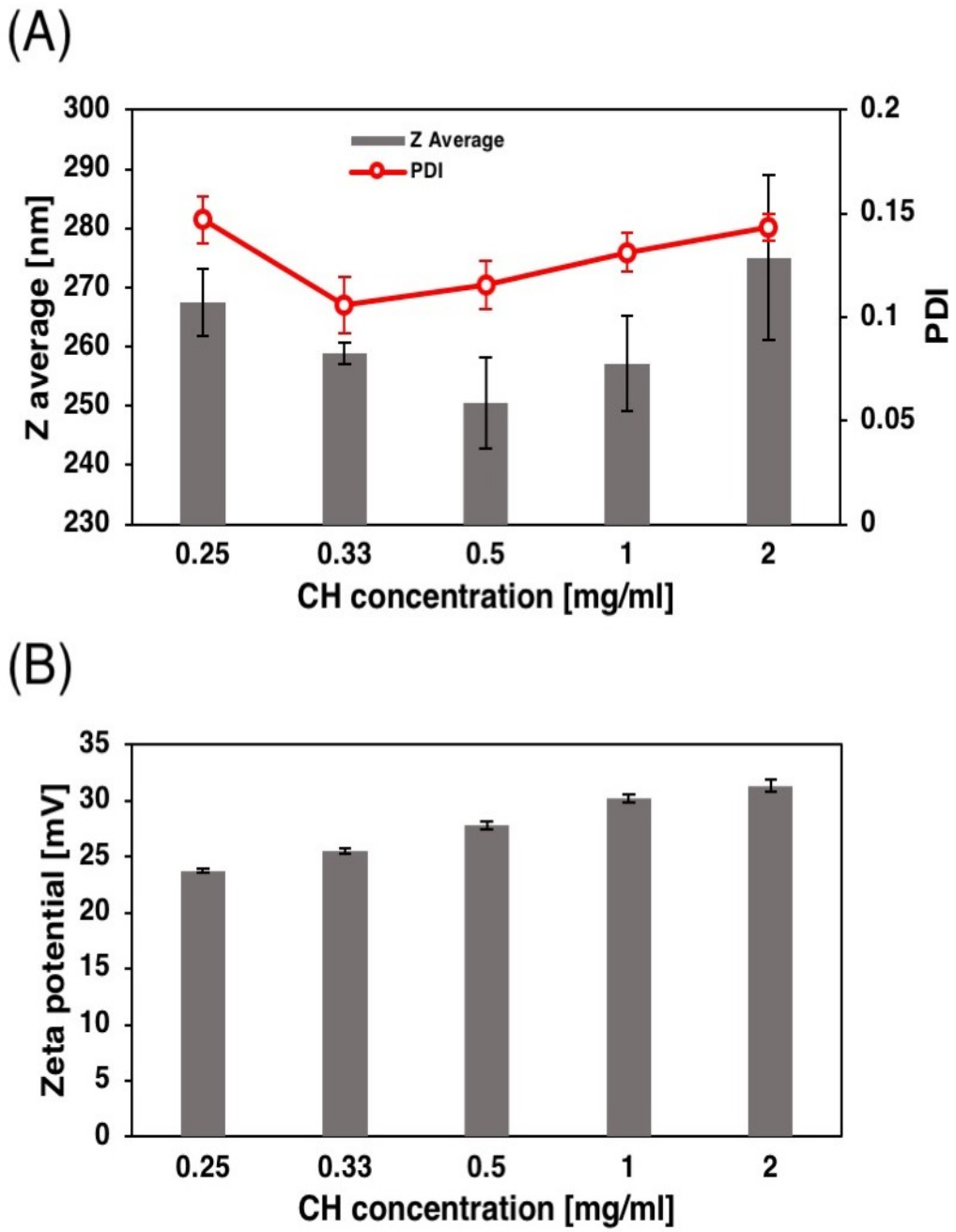

Fig. 2-2 Effects of CH concentration on the particle size and PDI (A) and zeta potential (B) at a CS total concentration of 1 mg/ml; pH of CCNCs was fixed at 5.5; data are presented as the mean ± standard deviation, n = 3

Absorbance at 600 nm (OD 600) was used to monitor the turbidity of CCNCs, as negligible absorbance was observed for both polymers at this wavelength. Therefore, the absorbance measured at this wavelength suggests the formation of NCs. By increasing CH concentration, the turbidity decreased almost linearly (**Fig. 2-3**), which contradicts what was reported previously [28]. The difference could be due to the variation in molecular characteristics of CH, i.e. molecular weight, deacetylation degree, which requires future investigations. In the present work, low molecular weight CH was used instead of high molecular weight CH.

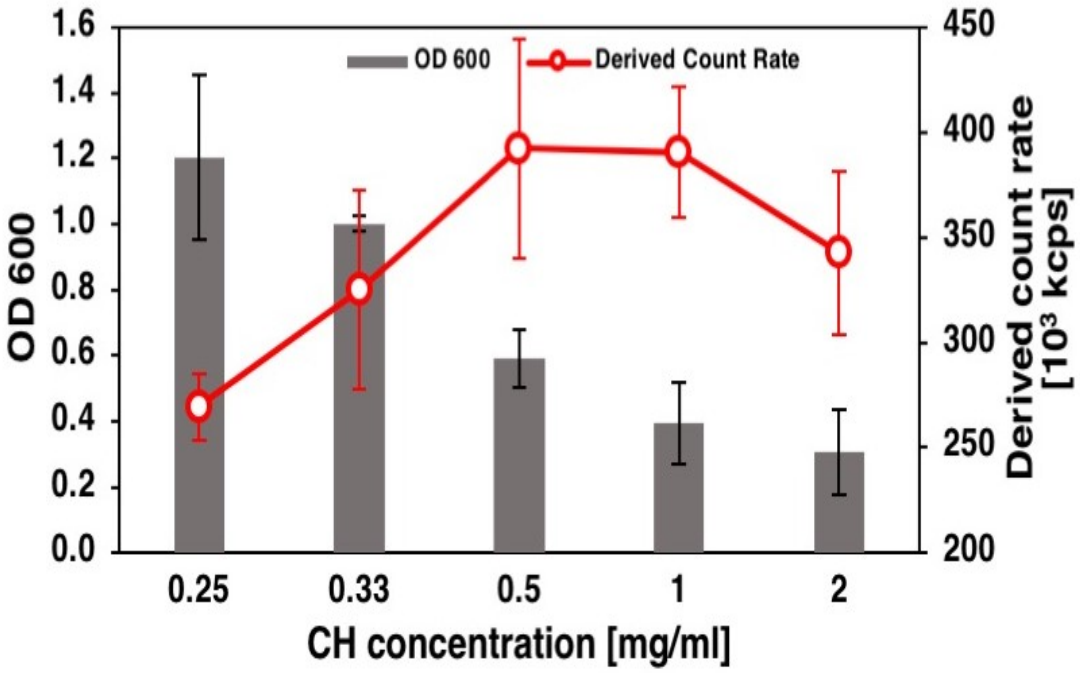

Fig. 2-3 Effects of CH concentration on OD 600 and derived count rate at a CS total concentration of 1 mg/ml; pH of CCNCs was fixed at 5.5; data are presented as the mean ± standard deviation, n = 3

To get insight into the factors controlling the particle size and the formation structure of CCNCs, we investigated the effect of total biopolymer concentration (i.e. [CS] + [CH]) on the characteristics of CCNCs. It revealed that the total biopolymer concentration affects the particle size. Increasing the total biopolymer concentration resulted in larger particles (**Fig. 2-**

4). It indicates that the composition of CS and CH also has an important role in controlling the particle size and structure of CCNCs.

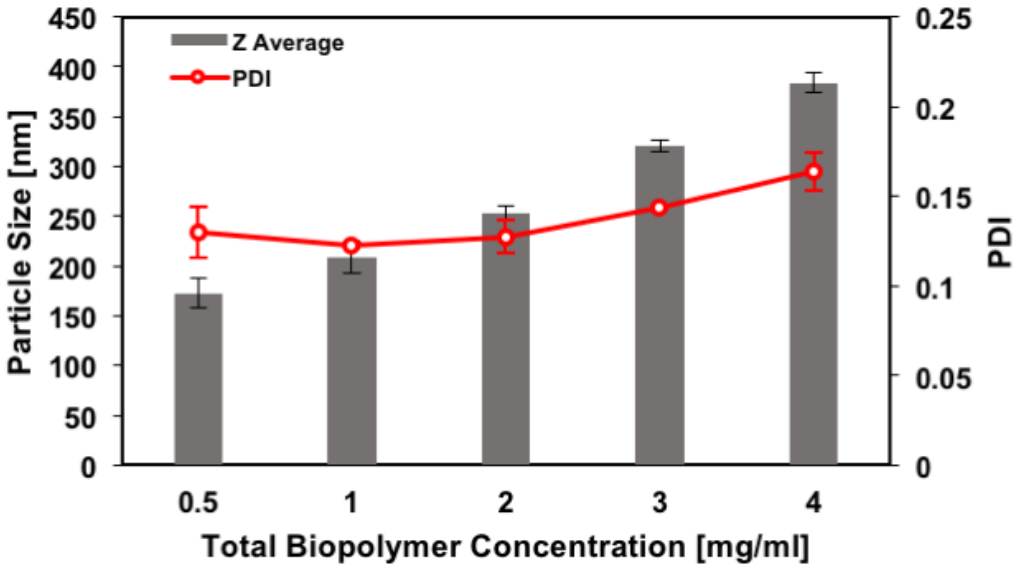

Fig. 2-4 Effect of total biopolymer concentration ([CS] + [CH]) on the particle size and PDI at a CS/CH mass ratio of 1:1; pH of CCNCs solution was fixed at 5.5; data are presented as the mean ± standard deviation, n = 3

2.4.2 Interactions between CS and CH by FT-IR

It has been reported that the interactions between these two biopolymers seem to not only be electrostatic interactions but also hydrophobic interactions arising from the possible interaction between N-acetylglucosamine residues of CH and hydrophobic domains of CS [34]. Nevertheless, few studies are available with regard to the mechanism of the formation of CCNCs. We thus sought to confirm the intermolecular interactions of CS with CH based on the ATR-FTIR spectra of lyophilized CS, CH, and CCNCs (**Fig. 2-5**). The FT-IR spectrum of CS reveals the major characteristic bands at 3288 cm^{-1}, 1644 cm^{-1}, 1533 cm^{-1}, 1240 cm^{-1}, and 1079 cm^{-1}, which correspond to the O-H stretching, amide I, amide II, amide III, and monoanionic symmetric stretching of phosphate, respectively [26, 35]. Meanwhile, the peaks around 1400 cm^{-1} (1447 cm^{-1} and 1395 cm^{-1}) and the small yet beneficial peak at 976 cm^{-1} were

due to the C-N stretching vibrations, the C=O stretching vibrations of COO- and dianionic phosphate symmetric stretching, respectively [35-37]. The FT-IR spectrum of CH shows the primary amine (N-H) bands at around 3200-3400 cm^{-1}, amide I (1657 cm^{-1}), amide II (1567 cm^{-1}), and glycosidic linkage stretching (C-O-C) at around 1068 cm^{-1} [38]. On the other hand, the spectrum of CCNCs shows a representative of both CS and CH spectra with major changes or shifts, suggesting the existence of the intermolecular interactions between the two biopolymers. In the region of 1700 cm^{-1} – 1300 cm^{-1}, several peak changes were noticed. The amide II band became slightly broader and shifted to 1539 cm^{-1}, while the peaks at 1447 cm^{-1} and 1395 cm^{-1} disappeared and shifted to 1403 cm^{-1}, respectively. These results indicate that the electrostatic interactions between the carboxyl and phosphate groups of CS and positively charged CH molecules might play an important role in the association of two biopolymers. Moreover, a marked decrease and minor shift at 1240 cm^{-1} attributed to N-H bending of amide III [39] provides additional evidence for the complexation between CS and CH.

2.4.3 Curcumin-loaded CCNCs

Having studied the effect of CH concentration on the formation of CCNCs in the previous sections, we selected CCNCs with CH concentrations of 0.5, 1, and 2 mg/ml for curcumin loading described in this section. Our choice was based on the colloidal stability and the number of particles, as indicated by high zeta potential (around 30 mV), sufficient derived count rates, and turbidity measurements. There are two commonly used methods to incorporate drugs or bioactive molecules into nanocarriers, i.e. drugs are incorporated before (mixed method) and after nanocarriers formation (adsorption method) [32]. In this study, curcumin was incorporated after CCNCs' formation for the sake of simplicity. Besides, there are no marked differences between the two methods on entrapment efficiency (EE) and the particle

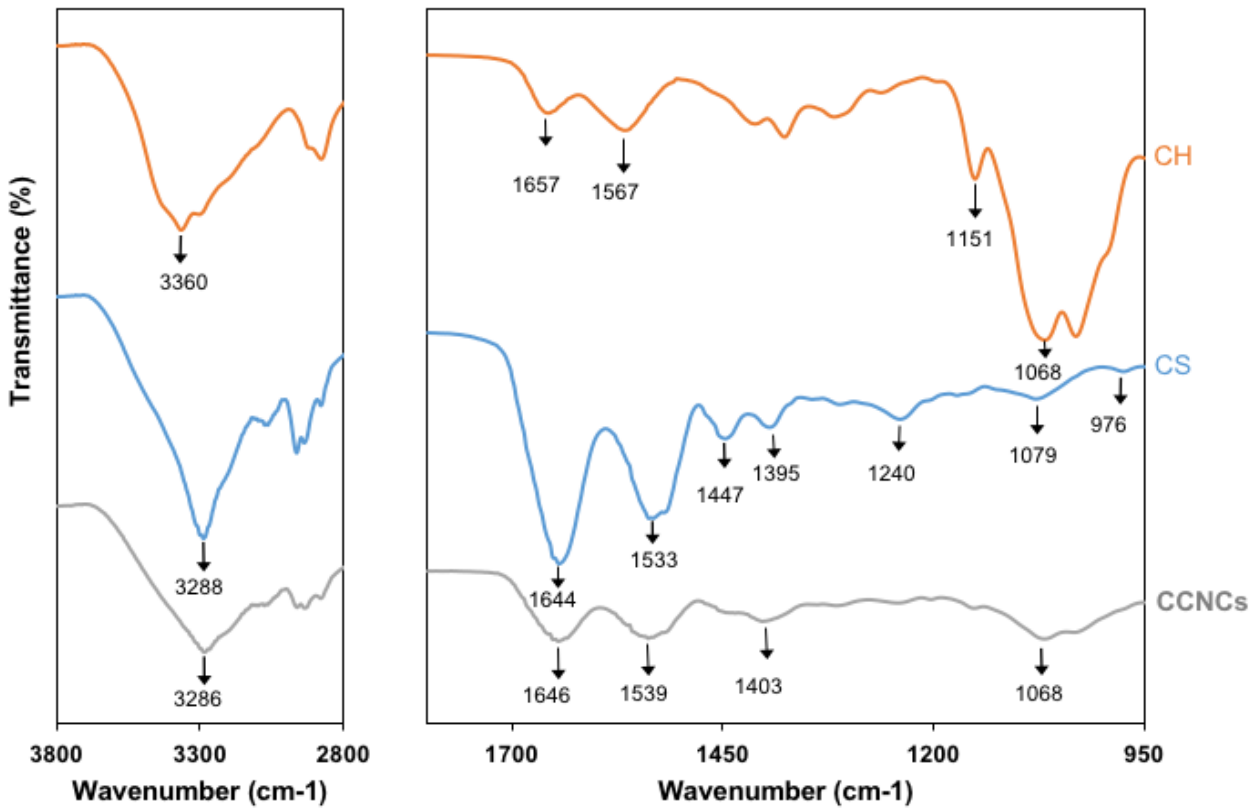

Fig. 2-5 ATR-FTIR spectra of CH, CS, and CCNCs at a CH concentration of 0.5 mg/ml

size (**Table 2-1**). The physical appearance and properties of CCNCs before and after curcumin addition are shown in **Fig. 2-6** and **Table 2-2**. While there was no marked difference in the particle size and PDI at a CH concentration of 0.5 mg/ml (**Table 2-2**), the addition of curcumin caused a notable increase in the particle size and PDI at CH concentrations of 1 and 2 mg/ml, suggesting that curcumin could induce alteration in the structural integrity of CCNCs, conceivably through hydrophobic interactions with CS. The reason for the discrepancy observed at a CH concentration of 0.5 mg/ml was likely to be associated with the higher number of particles as measured by DLS and UV spectrophotometer. A higher number of particles indicates more curcumin can be loaded and distributed evenly as more binding sites for curcumin are available. Thus, the impact of curcumin addition on the integrity of complexes' network would be minimized.

Table 2-1 Physical characteristics of curcumin-loaded CCNCs with varying CH concentrations using two different loading methods and their curcumin entrapment efficiency[a]

CH Concentration [mg/ml]	Mixed Method			Adsorption Method		
	Particle Size [nm]	PDI	EE [%]	Particle Size [nm]	PDI	EE [%]
0.5	250.1±2.1	0.150±0.010	55.5±4.3	254.8±3.7	0.118±0.004	55.9±2.2
1	255.0±8.6	0.162±0.019	31.7±1.3	292.2±6.2	0.171±0.016	33.6±4.3
2	300.4±11.7	0.194±0.018	34.6±5.9	302.8±6.0	0.206±0.015	32.6±4.2

[a]Mixed method: Curcumin was added in CS before nanocomplexes formation; adsorption method: Curcumin was added after nanocomplexes formation; the amount of curcumin loaded was 136 μg; total concentration of CS was 1 mg/ml; final pH was fixed at 5.5; data are reported as the mean ± standard deviation, n = 3.

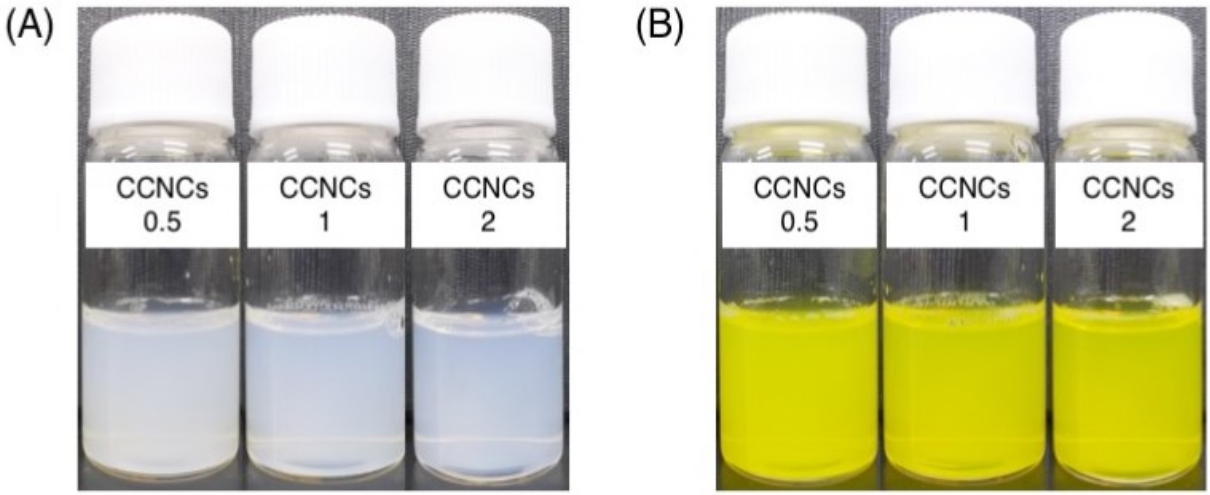

Fig. 2-6 Photographs of freshly prepared unloaded CCNCs (A) and curcumin-loaded CCNCs (B) with different CH concentrations (0.5, 1, and 2 mg/ml); total concentration of CS was 1 mg/ml; final pH was fixed at 5.5; curcumin was loaded at 25 μg/ml

The highest EE of 55.9% was achieved at the lowest CH concentration of 0.5 mg/ml (**Table 2-2**). This may also be attributed to the higher number of particles at a CH concentration of 0.5 mg/ml, as indicated by the derived count rate and turbidity values.

2.4.3.1 A spectroscopic study of curcumin-loaded CCNCs

We utilized spectroscopy techniques including UV-vis and fluorescence spectrophotometer to get a better understanding of the binding between curcumin and CCNCs by monitoring CS and curcumin inherent fluorescent properties. **Fig. 2-7A** shows the absorbance spectra of curcumin in ethanol and CCNCs. The absorbance maxima of curcumin in ethanol was ~425 nm, which is attributed to the π-π* transitions in the enolic form of curcumin [40], while that of curcumin in CCNCs was slightly red-shifted to 428 nm, which is in agreement with a previous report utilizing soy protein to encapsulate curcumin [41]. It is well-known that the sensitivity of CS and curcumin towards variation in the microenvironment could be of use for probing their polarity and structural changes [26, 27, 42].

Table 2-2 Physical characteristics of CCNCs with varying CH concentrations before and after curcumin addition and their curcumin entrapment efficiency[a]

CH Concentration [mg/ml]	Unloaded CCNCs		Curcumin-loaded CCNCs		EE [%]
	Particle Size [nm]	PDI	Particle Size [nm]	PDI	
0.5	250.5±7.7	0.115±0.012	254.8±3.7	0.118±0.004	55.9±2.2
1	257.2±8.0	0.131±0.009	292.2±6.2	0.171±0.016	33.6±4.3
2	275.1±13.9	0.144±0.007	302.8±6.0	0.206±0.015	32.6±4.2

[a]The amount of curcumin added was 136 μg; total concentration of CS was 1 mg/ml; final pH was fixed at 5.5; data are reported as the mean ± standard deviation, n = 3

It has been reported that casein micelles interact with hydrophobic molecules such as ANS, Nile Red, pyrene, vitamin D2 as well as curcumin mainly through tryptophan (Trp) or tyrosine (Tyr) residues [25-27, 43]. β-casein and α_{s1}-casein collectively have three Trp residues, which are primarily located in the interior hydrophobic sites of casein molecules [42]. Hence, the Trp fluorescent signal in the presence of increasing concentrations of curcumin was followed by exciting at 295 nm. As expected, the fluorescence intensity of Trp gradually decreased as curcumin was added (**Fig. 2-7B**), confirming the binding of curcumin with Trp of CS. The decrease was more obvious as more curcumin was incorporated. In addition, the fluorescence maxima of curcumin entrapped in CCNCs was blue-shifted by about 13 nm to 525 nm (**Fig. 2-7C**), as compared with the fluorescence maxima of curcumin in ethanol (λ_{max} = 538 nm), indicating that curcumin was located in a more hydrophobic environment [26, 27]. Although the binding of curcumin with CH could be expected [20, 40], it seemed that curcumin was more favorably bound with hydrophobic domains of CS as evidenced by the fluorescence measurement. At low pH (below 6.5), chitosan behaves as a strong polyelectrolyte and is weakly hydrophobic, while at high pH (above 6.5) its hydrophobicity substantially increases due to the inter-intramolecular interactions among deprotonized chitosan molecules [18, 40]. Therefore, the binding of curcumin with CH at pH 5.5, which was used at this study, was minimized.

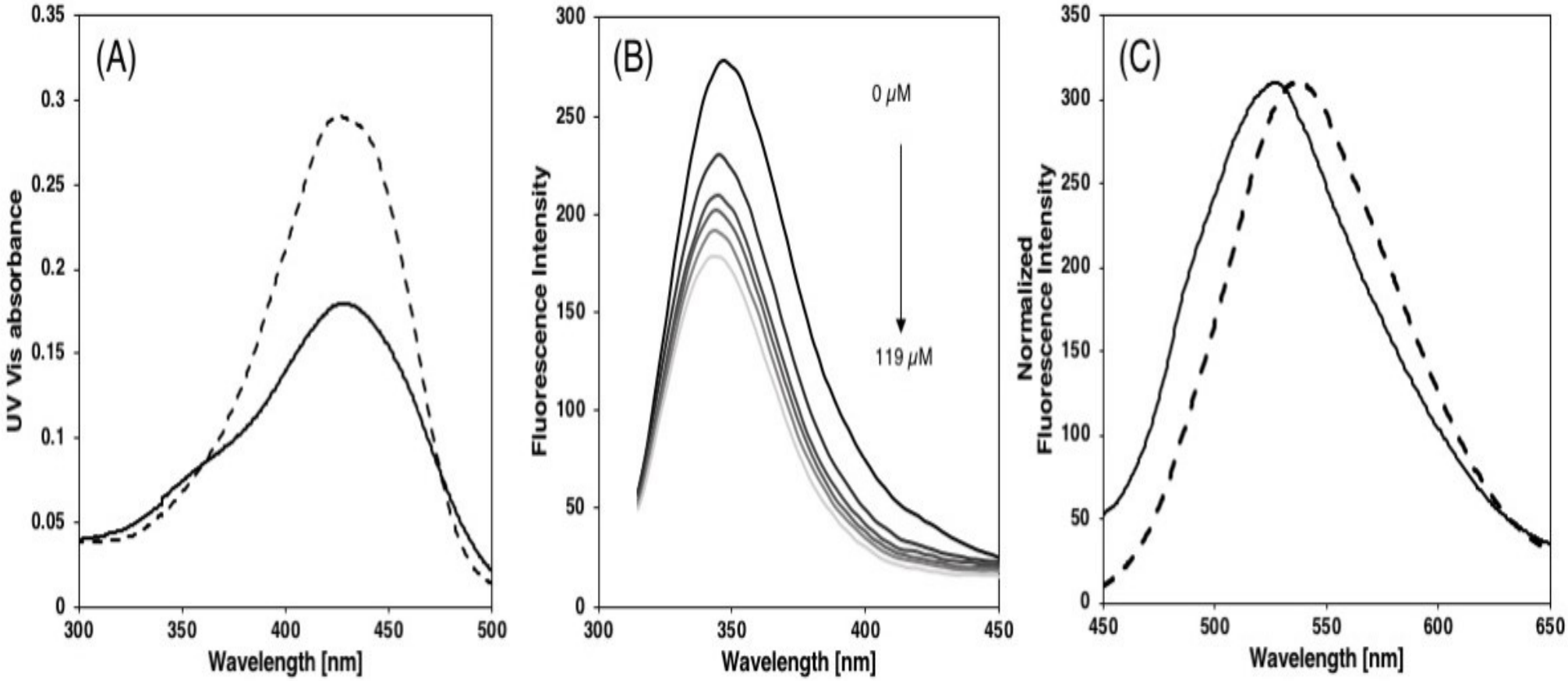

Fig. 2-7 UV-Vis absorbance spectra of curcumin in CCNCs (solid lines) and ethanol (dash lines) showing λ_{max} at 428 and 425 nm, respectively (A); fluorescence emission spectra of CCNCs in the presence of increasing concentration of curcumin (51, 68, 85, 102, 119 μM) (B); fluorescence emission spectra of curcumin in ethanol (dash lines) and in CCNCs (solid lines) excited at 420 nm (C)

2.4.3.2 Thermal stability and antioxidant activity of curcumin in CCNCs

We evaluated the degradation of curcumin entrapped in CCNCs after being heated at 80°C for 2 h. As shown in **Fig. 2-8**, CCNCs with CH concentrations of 1 and 2 mg/ml conferred enhanced protection of curcumin against high temperature as compared with free curcumin dissolved in 5 mM acetate buffer as a control. Approximately 42% of curcumin degraded after being heated for 2 h in the case of control; whereas, around 63 and 58% of curcumin still remained in the case of curcumin-loaded in CCNCs with CH concentrations of 1 and 2 mg/ml, respectively. The enhanced thermal stability of curcumin might be in part due to the protective effect of CCNCs from direct contact with water. CCNCs with a CH concentration of 0.5 mg/ml had the lowest curcumin protection among CCNCs, but its curcumin-protective ability was comparable to that of free curcumin, presumably due to particle instability against heat, as indicated by an increase in the particle size (**Table 2-3**).

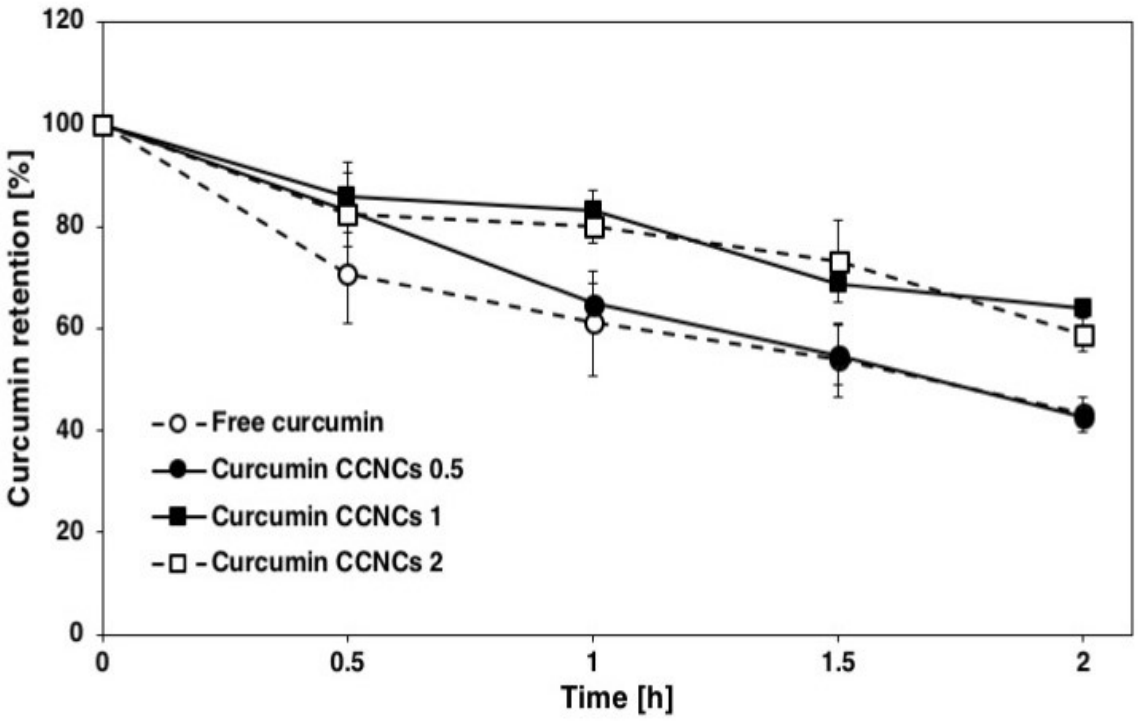

Fig. 2-8 Curcumin retention (%) of curcumin-loaded CCNCs with varying CH concentrations after thermal treatment at 80°C for 2 h; free curcumin dissolved in 5 mM acetate buffer (pH 5.5) with a small amount of ethanol (2.6% v/v) was used as a control; data are reported as the mean ± standard deviation, n = 3

Table 2-3 Particle size and PDI of curcumin-loaded CCNCs with varying chitosan concentrations before and after heat treatment for 2 h[a]

CH Concentration [mg/ml]	Before Heat Treatment for 2 h*		After Heat Treatment for 2 h	
	Particle Size [nm]	PDI	Particle Size [nm]	PDI
0.5	254.8±3.7	0.118±0.004	361.3±22	0.045±0.008
1	292.2±6.2	0.171±0.016	285.7±3.2	0.086±0.006
2	302.8±6.0	0.206±0.015	304.4±2.9	0.120±0.007

[a]These data were taken from **Table 2.2**

Antioxidant activities of free curcumin and curcumin-loaded CCNCs at a concentration of 50 μg/ml were evaluated using the FRAP method, which is based on the ferricyanide reducing capability [30]. The reducing power of curcumin-loaded in CCNCs was slightly lower than that of free curcumin (**Table 2-4**). This could be attributed to the limited accessibility of ferricyanide to curcumin entrapped in the hydrophobic region of CCNCs [44, 45], which in turn reduces the electron transfer rate from curcumin to Fe^{3+}.

2.4.4 Water dispersibility and storage stability of freeze-dried curcumin-loaded CCNCs

To study water dispersibility and storage stability of curcumin-loaded CCNCs, freshly prepared curcumin-loaded CCNCs were freeze-dried in the presence of 5% trehalose, a well-known cryoprotectant, to prevent aggregation of CCNCs induced by the extremely harsh freezing process. Afterward, the freeze-dried curcumin-loaded CCNCs was reconstituted in Milli-Q water. **Fig. 2-9** shows the appearance of free curcumin as a control, redispersed curcumin-loaded CCNCs before and after 1-day of storage at room temperature (25°C). The solubility of free curcumin in water was promoted by trehalose. However, some portions of

curcumin were precipitated after 1-day of storage. The precipitation rate increased after several days of storage. On the other hand, reconstituted curcumin-loaded CCNCs showed enhanced stability and water dispersibility. The amount of curcumin in CCNCs was determined to be approx. 25 μg/ml, which was several orders of magnitude higher than the solubility of curcumin in water (11 ng/ml) [8]. Reconstituted curcumin-loaded CCNCs also showed remarkable storage stability at least for 1 week at room temperature (25°C), as minimal changes in the physicochemical properties were noted (**Table 2-5**).

Table 2-4 Total reducing power of curcumin-loaded in CCNCs[a]

Samples	FRAP [A_{700nm}]	Relative Reducing Power [%][b]
Free Curcumin	0.182±0.008	100
Curcumin-loaded CCNCs with a CH concentration of 0.5 mg/ml	0.161±0.004	88.5
Curcumin-loaded CCNCs with a CH concentration of 1 mg/ml	0.167±0.008	91.8
Curcumin-loaded CCNCs with a CH concentration of 2 mg/ml	0.174±0.006	95.6

[a]Free curcumin dissolved in 5 mM acetate buffer (pH 5.5) with 2.6% v/v ethanol was used as control; curcumin concentration used was 50 μg/ml; total concentration of CS was 1 mg/ml; data are reported as the mean ± standard deviation, n = 3

[b]Relative reducing power was calculated using free curcumin as the reference value

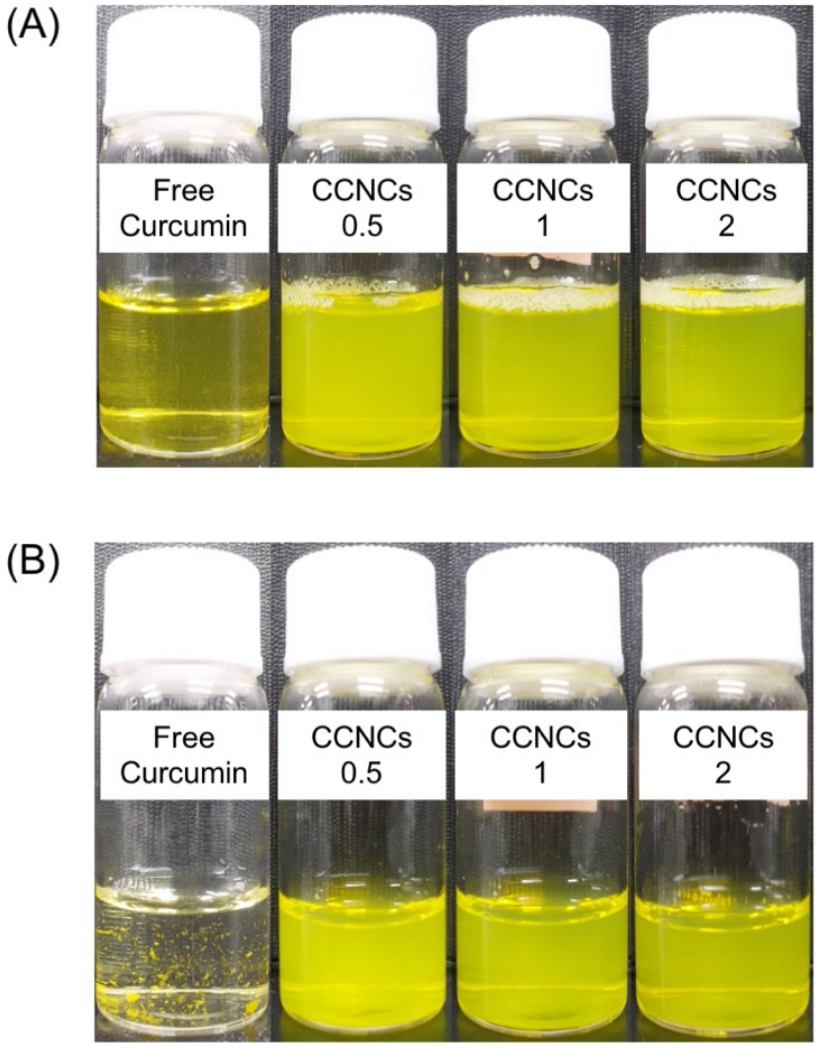

Fig. 2-9 Photographs of reconstitued curcumin-loaded in CCNCs with different CH concentrations (0.5, 1, and 2 mg/ml) and free curcumin before (A) and after 1-day of storage (B) at 25^{o}C; curcumin was loaded at 25 μg/ml

The excellent enhancing of water solubility and stability of curcumin by CS-based carriers was reported previously [26, 27]. Nevertheless, nanocarriers carrying positive charges have some advantages for enhancing cellular uptake and mucoadhesiveness, which is suitable for oral delivery. In this study, CH was simultaneously used for inducing the formation of NCs with CS and for conferring positively charged domains, while CS served as a stabilizer and solubility enhancer for curcumin. Having these two biocompatible polymers along with their merits in the form of CCNCs as a carrier for curcumin is considered advantageous.

Table 2-5 Physical characteristics of reconstituted curcumin-loaded CCNCs after 1-week of storage at 25°C[a]

CH Concentration [mg/ml]	Day 0			Day 7			Curcumin Retention [%]
	Particle Size [nm]	PDI	Zeta Potential [mV]	Particle Size [nm]	PDI	Zeta Potential [mV]	
0.5	263.0±5.6	0.125±0.012	23.4±0.4	255.9±5.1	0.100±0.006	22.8±0.4	89±6
1	264.9±13.1	0.136±0.004	26.7±0.5	259.8±13.9	0.116±0.009	26.8±0.3	91±4
2	280.0±2.8	0.171±0.005	28.8±0.1	268.0±0.7	0.145±0.006	28.3±0.5	85±2

[a]Freeze-dried curcumin-loaded CCNCs was reconstituted in Milli-Q water (final pH 6); the amount of curcumin used was 25 μg; the total concentration of CS was 1 mg/ml; data are reported as the mean ± standard deviation, n = 3

2.5 Conclusions

We have studied the formation of electrostatic interaction-based, biocompatible NCs of CS and CH as a function of CH concentration for encapsulation of curcumin. The number of particles of CCNCs was highly dependent on CH concentration. Curcumin could be successfully loaded into CCNCs with a high entrapment efficiency. The binding of curcumin and CCNCs was due to hydrophobic interaction between CS and curcumin as suggested by the fluorescence study. The enhanced water solubility and stability of curcumin in CCNCs was achieved, suggesting the potential of CCNCs as a delivery vehicle for curcumin in the food and pharmaceutical applications. Future work will be focused on the delivery of curcumin-loaded CCNCs into the cells.

References

[1] O. Naksuriya, S. Okonogi, R. M. Schiffelers and W. E. Hennink. Curcumin Nanoformulations: A Review of Pharmaceutical Properties and Preclinical Studies and Clinical Data related to Cancer Treatment. Biomaterials, 35 (2014) 3365–3383.

[2] E. O. Farombi, S. Shrotriya, H. K. Na, S. H. Kim and Y. J. Surh. Curcumin Attenuates Dimethylnitrosamine-induced Liver Injury in Rats through Nrf2-mediated Induction of Heme Oxygenase-1. Food Chem. Toxicol, 46 (2008) 1279–1287.

[3] C. Zeng, P. Zhong, Y. Zhao, K. Kanchana, Y. Zhang, Z. A. Khan, S. Chakrabarti, L. Wu, J. Wang and G. Liang. Curcumin Protects Hearts from FFA-induced Injury by Activating Nrf2 and Inactivating NF-κB both In Vitro And In Vivo. J. Mol. Cell. Cardiol, 79 (2015) 1–12.

[4] A. J. Ruby, G. Kuttan, K. Dinesh Babu, K. N. Rajasekharan and R. Kuttan. Anti-tumour and Antioxidant Activity of Natural Curcuminoids. Cancer Lett, 94 (1995) 79–83.

[5] C. D. Lao, M. T. Ruffin, D. Normolle, D. D. Heath, S. I. Murray, J. M. Bailey, M. E. Boggs, J. Crowell, C. L. Rock and D. E. Brenner. Dose Escalation of a Curcuminoid Formulation. BMC Complement. Altern. Med, 6 (2006) 10.

[6] R. A. Sharma, S. A. Euden, S. L. Platton, D. N. Cooke, A. Shafayat, H. R. Hewitt, T. H. Marczylo, B. Morgan, D. Hemingway, S. M. Plummer, M. Pirmohamed, A. J. Gescher and W. P. Steward. Phase I Clinical Trial of Oral Curcumin: Biomarkers of Systemic Activity and Compliance. Clin. Cancer Res, 10 (2004) 6847–6854.

[7] P. Anand, A. B. Kunnumakkara, R. A. Newman, B. B. Aggarwal, P. Anand, A. B. Kunnumakkara and R. A. Newman. Bioavailability of Curcumin: Problems and Promises. Mol. Pharm, 4 (2007) 807–818.

[8] H. H. Tønnesen, M. Másson and T. Loftsson. Studies of Curcumin and Curcuminoids. XXVII. Cyclodextrin Complexation: Solubility, Chemical and Photochemical Stability. Int. J. Pharm, 244 (2002) 127–135.

[9] G. Shoba, D. Joy, M. Majeed, R. Rajendran and P. S. S. R. Srinivas. Influence of Piperine on the Pharmacokinetics of Curcumin in Animals and Human Volunteers. Planta Med, 64 (1998) 353–356.

[10] L. Li, F. S. Braiteh and R. Kurzrock. Liposome-encapsulated Curcumin: In Vitro and In Vivo Effects on Proliferation, Apoptosis, Signaling, and Angiogenesis. Cancer, 104 (2005) 1322–1331.

[11] M. Gou, K. Men, H. Shi, M. Xiang, J. Zhang, J. Song, J. Long, Y. Wan, F. Luo, X. Zhao and Z. Qian. Curcumin-loaded Biodegradable Polymeric Micelles for Colon Cancer Therapy In Vitro And In Vivo. Nanoscale, 3 (2011) 1558–1567.

[12] J. Shaikh, D. D. Ankola, V. Beniwal, D. Singh and M. N. V. R. Kumar. Nanoparticle Encapsulation Improves Oral Bioavailability of Curcumin by at Least 9-fold when Compared to Curcumin Administered with Piperine as Absorption Enhancer. Eur. J. Pharm. Sci, 37 (2009) 223–230.

[13] K. Ahmed, Y. Li, D. J. McClements and H. Xiao. Nanoemulsion- and Emulsion-based Delivery Systems for Curcumin: Encapsulation and Release Properties. Food Chem, 132 (2012) 799–807.

[14] J. Sun, C. Bi, H. M. Chan, S. Sun, Q. Zhang and Y. Zheng. Curcumin-loaded Solid Lipid Nanoparticles have Prolonged In Vitro Antitumour Activity, Cellular Uptake and Improved In Vivo Bioavailability. Colloid. Surf. B, 111 (2013) 367–375.

[15] J. Xiao, S. Nian and Q. Huang. Assembly of Kafirin/carboxymethyl Chitosan Nanoparticles to Enhance the Cellular Uptake of Curcumin. Food Hydrocoll, 51 (2015) 166–175.

[16] Y. Luo, K. Pan and Q. Zhong. Casein/pectin Nanocomplexes as Potential Oral Delivery Vehicles. Int. J. Pharm, 486 (2015) 59–68.

[17] F. P. Chen, S. Ou and C. H. Tang. Core-shell Soy Protein-soy Polysaccharide Complex (Nano)particles as Carriers for Improved Stability and Sustained-release of Curcumin. J Agric Food Chem, 64 (2016) 5053-5059.

[18] T. Delair. Colloidal Polyelectrolyte Complexes of Chitosan and Dextran Sulfate Towards Versatile Nanocarriers of Bioactive Molecules. Eur. J. Pharm. Biopharm, 78 (2011) 10–18.

[19] Y. Luo and Q. Wang. Recent Development of Chitosan-based Polyelectrolyte Complexes with Natural Polysaccharides for Drug Delivery. Int. J. Biol. Macromol, 64 (2014) 353–367.

[20] L. H. Chuah, C. J. Roberts, N. Billa, S. Abdullah and R. Rosli. Cellular Uptake and Anticancer Effects of Mucoadhesive Curcumin-containing Chitosan Nanoparticles. Colloid. Surf. B, 116 (2014) 228–236.

[21] B. Hu, Y. Ting, X. Zeng and Q. Huang. Cellular Uptake and Cytotoxicity of Chitosan-caseinophosphopeptides Nanocomplexes Loaded with Epigallocatechin Gallate. Carbohydr. Polym, 89 (2012) 362–370.

[22] A. Anitha, S. Sowmya, P. T. S. Kumar, S. Deepthi, K. P. Chennazhi, H. Ehrlich, M. Tsurkan and R. Jayakumar. Chitin and Chitosan in Selected Biomedical Applications. Prog. Polym. Sci, 39 (2014) 1644–1667.

[23] R. K. Das, N. Kasoju and U. Bora. Encapsulation of Curcumin in Alginate-chitosan-pluronic Composite Nanoparticles for Delivery to Cancer Cells. Nanomedicine Nanotechnology, Biol. Med, 6 (2010) 153–160.

[24] Y. D. Livney. Milk Proteins as Vehicles for Bioactives. Curr. Opin. Colloid Interface Sci, 15 (2010) 73–83.

[25] E. Semo, E. Kesselman, D. Danino and Y. D. Livney. Casein Micelle as a Natural Nano-capsular Vehicle for Nutraceuticals. Food Hydrocoll, 21 (2007) 936–942.

[26] K. Pan, Q. Zhong and S. J. Baek. Enhanced Dispersibility and Bioactivity of Curcumin by Encapsulation in Casein Nanocapsules. J. Agric. Food Chem, 61 (2013) 6036–6043.

[27] A. Sahu, N. Kasoju and U. Bora. Fluorescence Study of the Curcumin-casein micelle Complexation and Its Application as a Drug Nanocarrier to Cancer Cells. Biomacromolecules, 9 (2008) 2905–2912.

[28] A. K. Anal, A. Tobiassen, J. Flanagan and H. Singh. Preparation and Characterization of Nanoparticles Formed by Chitosan-caseinate Interactions. Colloid. Surf. B, 64 (2008) 104–110.

[29] M. Razmi, A. Divsalar, A. A. Saboury, Z. Izadi, T. Haertlé and H. Mansuri-Torshizi. Beta-casein and Its Complexes with Chitosan as Nanovehicles for Delivery of a Platinum Anticancer Drug. Colloid. Surf. B, 112 (2013) 362–367.

[30] T. Ak and I. Gülçin. Antioxidant and Radical Scavenging Properties of Curcumin. Chem. Biol. Interact, 174 (2008) 27–37 .

[31] U. Nobbmann. Derived Count rate−What Is It?,Malvern. Retrieved from http://www.materials-talks.com/blog/2015/06/11/derived-count-rate-what-is-it/ (2015)

[32] L. Yang, S. Gao, S. Asghar, G. Liu, J. Song, X. Wang, Q. Ping, C. Zhang and Y. Xiao. Hyaluronic acid/chitosan Nanoparticles for Delivery of Curcuminoid and Its In Vitro Evaluation in Glioma Cells. Int. J. Biol. Macromol, 72 (2015) 1391–1401.

[33] Q. Hu, T. Wang, M. Zhou, J. Xue and Y. Luo. Formation of Redispersible Polyelectrolyte Complex Nanoparticles from Gallic Acid-chitosan Conjugate and Gum Arabic. Int. J. Biol. Macromol, 92 (2016) 812–819.

[34] S. F. Ausar, I. D. Bianco, R. G. Badini, L. F. Castagna, N. M. Modesti, C. A. Landa and D. M. Beltramo. Characterization of Casein Micelle Precipitation by Chitosans. J. Dairy Sci, 84 (2001) 361–369.

[35] C. Fernández, S. F. Ausar, R. G. Badini, L. F. Castagna, I. D. Bianco and D. M. Beltramo. An FTIR Spectroscopy Study of the Interaction Between α_s-Casein-bound Phosphoryl Groups and Chitosan. Int. Dairy J, 13 (2003) 897–901.

[36] A. Barth. The Infrared Absorption of Amino Acid Side Chains. Prog. Biophys. Mol. Biol, 74 (2000) 141–173.

[37] J. Depciuch, M. Sowa-Kućma, G. Nowak, D. Dudek, M. Siwek, K. Styczeń and M. Parlińska-Wojtan. Phospholipid-protein Balance in Affective Disorders: Analysis of Human Blood Serum Using Raman and FTIR Spectroscopy. A Pilot Study. J. Pharm. Biomed. Anal, 131 (2016) 287–296.

[38] T. T. M. Ho, K. E. Bremmell, M. Krasowska, S. V. MacWilliams, C. J. E. Richard, D. N. Stringer and D. A. Beattie. In situ ATR FTIR Spectroscopic Study of the Formation and Hydration of a Fucoidan/chitosan Polyelectrolyte Multilayer. Langmuir, 31 (2015) 11249–11259.

[39] K. Kaiden, T. Matsui and S. Tanaka. A Study of the Amide III Band by FT-IR Spectrometry of the Secondary Structure of Albumin, Myoglobin, and γ–Globulin. Applied Spectroscopy, 41 (1987) 180-184.

[40] B. Boruah, P. M. Saikia and R. K. Dutta. Binding and Stabilization of Curcumin by Mixed Chitosan-Surfactant Systems: A Spectroscopic Study. J. Photochem. Photobiol. A Chem, 245 (2012) 18–27.

[41] A. Tapal and P. K. Tiku. Complexation of Curcumin with Soy Protein Isolate and Its Implications on Solubility and Stability of Curcumin. Food Chem, 130 (2012) 960–965.

[42] Y. Liu and R. Guo. pH-dependent Structures and Properties of Casein Micelles. Biophys. Chem, 136 (2008) 67–73.

[43] C. A. Gatti, P. H. Risso and M. S. Pires. Spectrofluorometric Study on Surface Hydrophobicity of Bovine Casein Micelles in Suspension and During Enzymic Coagulation. J. Agric. Food Chem, 43 (1995) 2339–2344.

[44] C. Tan, J. Xie, X. Zhang, J. Cai and S. Xia. Polysaccharide-based Nanoparticles by Chitosan and Gum Arabic Polyelectrolyte Complexation as Carriers for Curcumin. Food Hydrocoll, 57 (2016) 236–245.

[45] F. Donsì, M. Sessa, H. Mediouni, A. Mgaidi and G. Ferrari. Encapsulation of Bioactive Compounds in Nanoemulsion-based Delivery Systems. Procedia Food Sci, 1 (2011) 1666–1671.

CHAPTER 3 GENIPIN-STABILIZED CASEINATE-CHITOSAN NANOPARTICLES FOR ENHANCED STABILITY AND ANTI-CANCER ACTIVITY OF CURCUMIN

3.1 Abstract

Nanoparticles formed by the assembly of protein and polysaccharides are of great interest for the delivery of hydrophobic molecules. Herein, the formation of genipin-crosslinked nanoparticles from caseinate (CS) and chitosan (CH) is reported for the delivery of curcumin, a polyphenolic compound from turmeric, to cells. Genipin-crosslinked CS-CH nanoparticles (G-CCNPs) having a diameter of ~250 nm and a low polydispersity index showed excellent stability over a wide pH range, as indicated by dynamic light scattering and transmission electron microscopic measurements. Cellular uptake of curcumin loaded into G-CCNPs by HeLa cells was improved, as measured by confocal laser scanning microscopy (CLSM) and fluorescence-activated cell-sorting analysis. Cell proliferation assays indicated that G-CCNPs were nontoxic and that curcumin's anticancer activity in vitro was also improved by G-CCNPs. Stability of curcumin at neutral pH was enhanced by G-CCNPs. CLSM study revealed that G-CCNPs were poorly internalized by HeLa cells, possibly because of strong cell membrane interactions and a negative zeta potential. Overall, our results suggested that the enhanced curcumin cytotoxicity might be associated with the enhanced stability of curcumin by G-CCNPs and free curcumin released from G-CCNPs into the cell. These biocompatible NPs might be suitable carriers for enhancing curcumin's therapeutic potential.

3.2. Introduction

Nanostructured delivery systems fabricated from polysaccharide-protein interactions have gained increasing interest in the food and pharmaceutical fields because of their facile preparation and biocompatibility [1,2]. The principal driving force for their formation is attractive electrostatic interactions between oppositely charged biopolymers in aqueous solution, although hydrogen bonding and hydrophobic interactions are also important [3]. Among the many available polysaccharides, chitosan (CH) is the most popular for its cationic nature, biodegradability, biocompatibility, and mild toxicity [4–6]. CH is generally obtained by deacetylation of chitin from shrimp shells and, in dilute acidic solution, the amine moieties of CH (pK_a of ~6.5) are proto-nated, allowing expansion of CH linear chains and a resulting high charge density [7]. Nanoparticles (NPs) prepared by molecular self-assembly of CH and protein/peptides have shown promise in solubilizing, stabilizing, and enhancing the bioactivity of a wide range of hydrophilic and hydrophobic drugs and biomolecules, including epigallocatechin-3-gallate [8], doxorubicin hydrochloride [9], lutein [10] and resveratrol [6]. In addition, NPs have also been utilized for gene and protein delivery with encouraging results [11,12]. One of the potential proteins for fabrication of these kinds of NPs is caseinate (CS), a milk protein consisting of four protein types (αS_1, αS_2, β, and κ) with an isoelectric point of 4.7 and an excellent ability for enhancing the solubility and delivery of hydrophobic molecules [13,14]. The formation of CS and CH nano-sized complexes (CCNCs) has been reported, using modulations of CS-CH concentrations, pH, and medium ionic strength to obtain NPs with low polydispersity [15]. However, CCNCs stability is strongly dependent on pH and salt concentrations, which is unfavorable for further applications in which NPs have to be applied under physiological conditions. Chemical crosslinking is a straightforward yet an effective approach for stabilizing NPs. This approach could also be useful for modulating the release profiles of encapsulated biomolecules [16,17]. However, commonly used and effective

chemical crosslinkers, such as glutaraldehyde and diisocyanate, are not suitable for clinical and biological applications because of their possible residual toxicity [18,19]. Recently, genipin has attracted considerable attention as a chemical crosslinker, owing to its nontoxic property and excellent biocompatibility [20–22]. Genipin is an aglycone derived from geniposide of the Gardenia fruit (**Fig. 3-1**). It primarily reacts with amino groups to generate intrinsic fluorescence conjugates that are highly stable against light and enzymes,which enables them to be utilized as bio-imaging probes and fluorescent labeling agents [23]. Genipin-mediated crosslinking has recently been reported to strengthen the colloidal stability and structural integrity of CH-based NPs and CS micelles [24,25]. Genipin-stabilized peptide-CH NPs for encapsulation of a water-soluble compound has been reported [8]. Moreover, genipin-crosslinked aminated starch-coated NPs capable of modulating the release profile of a hydrophobic compound, curcumin has also been demonstrated [26].

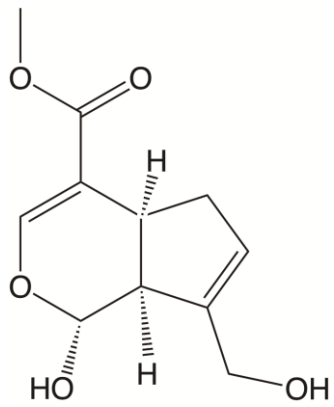

Fig. 3-1 The chemical structure of genipin

Herein, we fabricated genipin-crosslinked CS-CH NPs (G-CCNPs). The role of genipin conjugation was investigated instabilizing CS-CH NPs under various conditions for effective curcumin delivery to cells. Curcumin encapsulation into G-CCNPs was shown to not only provide better stability in neutral pH but also to enhance anticancer activity in vitro in the human cervical cancer cell line HeLa. Furthermore, cellular uptake studies were performed using confocal laser scanning microscopy (CLSM) to gain an insight into G-CCNPs

interactions with HeLa cells as well as how G-CCNPs improved the efficacy of entrapped curcumin over free curcumin in HeLa cells.

3.3 Experimental

3.3.1 Materials

Low molecular weight CH (viscosity of 5–20 mPa·s and degree of deacetylation of 80.7%) and genipin (>97% pure) were purchased from Tokyo Chemical Industry Co., Ltd. (Tokyo, Japan). CS was purchased from Sigma-Aldrich, Inc. (St. Louis, MO, USA). Curcumin was purchased from Wako Pure Chemical Industries, Ltd. (Osaka, Japan). A cell counting kit, WST-8, and Hoechst 4432 solution were purchased from Dojindo Laboratories, Inc. (Kumamoto, Japan). Minimum essential medium (MEM), fetal bovine serum (FBS), penicillin, streptomycin, OPTI-MEM, and Alexa Fluor 488 phalloidin were purchased from Thermo Fisher Scientific, Inc. (Waltham, MA, USA). Dulbecco's phosphate-buffered saline (D-PBS) was purchased from Nacalai Tesque, Inc. (Kyoto, Japan). All other chemicals were analytical grade.

3.3.2 Preparation and characterization of G-CCNPs and curcumin-loaded G-CCNPs

G-CCNPs were prepared by simply mixing CS and CH solutions to yield CS-CH nanocomplexes (CCNCs), followed by crosslinking with genipin and a purification step. Briefly, a CH solution (1 mg/ml) was prepared by dissolving CH in 0.1 M acetic acid under mild stirring until dissolved and then adjusted pH 5.5 with 1 M NaOH. A CS solution (2 mg/ml) was prepared in Milli-Q water and both solutions stored at 4 ^{o}C overnight to facilitate complete hydration before use. CCNCs were formed spontaneously by slowly adding CS solution to an equal volume of CH solution under stirring at room temperature (25 ^{o}C) and the final pH adjusted to 5.5 with 0.1 M HCl or NaOH. Then, the crosslinking reaction with genipin was performed as follows. Genipin (20 mg/ml), dissolved in dimethyl sulfoxide (DMSO), was added into 2 ml of CCNCs to a final concentration of 0.5 mg/ml and allowed to react at 30 ^{o}C

for 24 h to yield G-CCNCs. Unreacted genipin was removed by dialysis against Milli-Q water using a 3.5 kDa molecular weight cut-off cellulose membrane (Spectrum Laboratories, Inc., Rancho Dominguez, CA, USA) at 4 ^{o}C for 3 h. Last, purification was performed to separate NPs from free polymers using a centrifugation method (2500 g, 20 ^{o}C, and 30 min). After two cycles of washing-centrifugation, the resulting G-CCNPs were collected and redispersed in Milli-Q water. The uncrosslinked CS-CH NPs (CCNPs) were prepared in the similar manner as for G-CCNPs, except that no genipin was added and purification was done at 9000 g. For preparation of curcumin-loaded G-CCNPs, a curcumin stock solution (1 mg/ml) was added to the G-CCNPs solution and vortexed for 10 s to allow curcumin entrapment. The hydrodynamic size, polydispersity index (PDI), and zeta potential of G-CCNPs and curcumin-loaded G-CCNPs were measured by dynamic light scattering (DLS; Zetasizer Nano ZS, Malvern Instruments Ltd., Worcestershire, United Kingdom). The curcumin entrapment efficiency (EE) was determined based on a centrifugation method. Briefly, curcumin-loaded G-CCNPs were centrifuged at 9000 g at 20 ^{o}C for 30 min. An aliquot of supernatant containing unloaded curcumin was extracted with acetonitrile (1:1 volume ratio) and filter-centrifuged (Amicon Ultra; molecular weight cut-off, 30 kDa; Millipore Corp., Billerica, MA, USA) at 14 000 g at 20 ^{o}C for 20 min before injection into a reversed-phase high performance liquid chromatograph equipped with an auto sampler (Jasco LC-4000, Jasco Inc., Easton, MD, USA). A C-18 column (InertSustain; GL Sciences, Inc., Tokyo, Japan) was used with a mobile phase of acetonitrile containing 0.1% trifluoroacetic acid (55% by vol) and Milli-Q water at a flow rate of 0.8 ml/min. The EE (%) and loading capacity (LC) of curcumin loaded G-CCNPs were calculated using the following equations:

$$\text{EE}\ (\%) = \frac{\text{Total curcumin added} - \text{unloaded curcumin}}{\text{Total curcumin added}} \times 100\%$$

$$\text{LC}\ (\%) = \frac{\text{Total curcumin entrapped}}{\text{Total mass of G} - \text{CCNPs}} \times 100\%$$

To evaluate G-CCNPs stability under different conditions, G-CCNPs were redispersed in Milli-Q water mixed with an equal volume of Milli-Q water with 2x PBS (pH 7.4) and 70 mM HCl containing 4 mg/ml NaCl (pH 1.2). The samples were equilibrated at room temperature for at least 2 h before being characterized by DLS and transmission electron microscopy (TEM).

3.3.3 Release profile of curcumin from G-CCNPs

The release profiles of curcumin from G-CCNPs were investigated using a dialysis method in two different pH, i.e., pH 7.4 and 5.5. Briefly, 1.6 ml of curcumin-loaded G-CCNPs (20μg/ml) in PBS pH 7.4 and 5.5 was put in a dialysis membrane (Spectra/Por®, 12-14 kDa molecular weight cut-off). The dialysis bags were then immersed in 25 ml of the release medium (10 mM PBS pH 7.4 and 5.5 containing 50% ethanol) and placed in an incubator shaker at 37 ^{o}C and 50 rpm for 6h. 50% ethanol was used in the release medium to provide sink condition, as previously reported [27]. At predetermined time, 200μl of release medium containing curcumin was collected and replaced with the same amount of pre-warmed release medium. The amount of curcumin was determined using HPLC analysis, as previously mentioned.

3.3.4 Cytotoxicity in vitro

Cell viabilities of HeLa cells for free curcumin and unloaded and curcumin-loaded G-CCNPs were determined by WST assay. HeLa cell line was provided by the RIKEN BRC through the National Bio-Resource Project of the MEXT, Japan. HeLa cells were cultured in MEM medium containing 10% FBS and 1% antibiotic-antimycotic (Thermo Fisher Scientific, Inc.). HeLa cells were grown to a density of 5000 cells per well in a 96-well plate (Greiner Bio-One GmbH, Frickenhausen, Germany) and incubated overnight under a 5% CO_2 atmosphere. Then, the medium was removed and the cells exposed to free curcumin, curcumin-loaded or unloaded G-CCNPs in a reduced serum medium (OPTI-MEM, Thermo Fisher

Scientific, Inc.) at varying concentrations. DMSO was used to solubilize free curcumin, with a final DMSO concentration at <0.5%. After a 24-h incubation, the samples were removed and 100 μl of WST-8 cell counting solution in OPTI-MEM added to each well. After a further 3-h incubation, the A_{450} was read using a microplate reader (Bio-Tek Instrument, Inc., Winooski, VT, USA) and cell viabilities expressed as the percentage of living cells over untreated cells.

3.3.5 Cellular uptake studies

Cellular uptake of free curcumin and curcumin-loaded G-CCNPs in HeLa cells was evaluated by CLSM and a flow cytometer. For CLSM studies, HeLa cells were seeded in a multi-well glass bottom dish (Matsunami Glass Industries, Ltd., Osaka, Japan) at a density of 10 000 cells per well and incubated overnight at 37 ºC under CO_2 atmosphere. Then, the medium was removed and samples, dispersed in OPTI-MEM, added to the dish, with curcumin at 10 μg/ml. After 3 and 6 h of incubation, the samples were removed and the cells fixed with 4% paraformaldehyde (Wako Pure Chemical Industries, Ltd.) at 25 ºC for 10 min. The cells were then viewed under an LSM 700 confocal microscope (Carl Zeiss AG, Oberkochen, Germany) equipped with a diode laser. Fluorescein isothiocyanate and Texas Red filter were used to observe the green fluorescence of curcumin and red fluorescence of unloaded G-CCNPs, respectively. For flow cytometric analysis, HeLa cells were seeded in a Nunc cell-culture treated 6-well dish (Thermo Fisher Scientific, Inc.) at a density of 300 000 cells per well and incubated overnight at 37 ºC under CO_2 atmosphere. Then, the medium was removed and samples added to the dish, with curcumin at 10 μg/ml. After 3 and 6 h of incubation, the samples were removed and washed thrice with D-PBS. Then, HeLa cells were trypsinized (Nacalai Tesque, Inc.), washed twice with cold D-PBS, centrifuged (450 g, 4 ºC, and 5 min), and finally redispersed in D-PBS containing 1% FBS. The samples were held in an ice bath until measured. After filtering with a cell strainer, the samples were analyzed using a flow cytometer (Sony cell sorter EC800, Sony Biotechnology Inc., San Jose, CA, USA) at 488 nm.

Quantitative analysis of cell-associated NPs was evaluated by a flow cytometer equipped with 561 nm laser (BD FACS Aria, BD Biosciences Co, San Jose, CA, USA). A yellow/green filter (610/20) was used. Samples were prepared in the similar manner as for quantifying cellular uptake of curcumin in HeLa cells, except that HeLa cells were collected by using a cell scraper to avoid damage on the cell membrane. A total of at least 20000 events was recorded for each sample. Data are reported as mean intensity.

3.3.6 Statistical analysis

The statistical analysis was performed using ANOVA and Student's t-test with Microsoft Excel (Version 2017 for Macintosh, Microsoft Corp, Redmond, WA, USA). P values of < 0.05 were considered statistically significant.

3.4 Results and Discussion

3.4.1 Formation and characterization of G-CCNPs

The formation of biocompatible CCNCs by the electrostatic interactions was studied previously and the stability of these structures against pH and ionic strength found to be poor because of repulsive forces and salt-screening effects [15]. Herein, a crosslinking reaction between CCNCs and genipin, a naturally occurring nontoxic crosslinker was applied to enhance the stability. The genipin concentration, crosslinking reaction pH, reaction temperature, and duration were chosen to be 0.5 mg/ml, 5.5, 30 ^{o}C, and 24 h, respectively. Under these reaction conditions, no visible aggregation of G-CCNCs was observed. The formation of blue color in CCNCs after incubation with a genipin solution was considered evidence of a successful crosslinking reaction, as has been previously reported [22,24,25]. The crosslinking mechanism of CCNCs and genipin involved two reactions [28]. The first reaction was believed to be a nucleophilic attack on the olefinic carbon atom at the genipin C-3 by primary amine groups of CS or CH, while the later reactions was a nucleophilic substitution of the genipin ester group to form a secondary amide. After genipin crosslinking, centrifugal

purification was carried out to remove free polymers and collect G-CCNPs. The hydrodynamic size, PDI, and zeta potential before and after crosslinking are shown in **Table 3-1**. No notable differences in particle sizes were observed, suggesting that no interparticle crosslinking reaction took place and NPs structures remained unaffected. A decrease in the NPs zeta potential from +32.6 to +24.7 mV after crosslinking was noticed, which was because of the consumption of primary amines in the genipin-crosslinking reaction.

Table 3-1. Z-average size, PDI, and surface charge of CCNPs and G-CCNPs redispersed in Milli-Q water

Samples	Particle Size [nm]	PDI	Zeta Potential [mV][a]
CCNPs	256.6 ±7.7	0.201 ±0.013	+32.9 ±0.5
G-CCNPs	238.6 ±13.9	0.076 ±0.022	+24.7 ±1.3

Data, mean ±standard deviation, *n*=3

[a]Zeta potential measured at pH 5.5

3.4.2 Stability of G-CCNPs

G-CCNPs stability against pH and ionic strength was evaluated by preparing G-CCNPs in HCl containing 2 mg/ml NaCl (pH 1.2) and PBS (pH 7.4), with CCNPs used as a control. Changes in physical characteristics (hydrodynamic size and PDI) of CCNPs and G-CCNPs were recorded by DLS after a 2-h incubation at 25 ^{o}C. A marked increase in CCNPs hydrodynamic size and PDI was observed after dispersal in PBS (**Fig. 3-2A**). At pH 7.4, CH molecules at CCNPs surfaces would be deprotonated, as their pK_a is around 6.5 [29], and the electrostatic interactions thus would be weakened, leading to swollen particles. At pH 1.2, a marked decrease in CCNPs hydrodynamic size was noted. Also, CCNPs appearance changed from a slightly turbid to a clear transparent solution, indicating NPs disruption. This visual observation was confirmed by a drastic drop in the light scattering intensity (data not shown), as measured by DLS. The obtained CCNPs hydrodynamic size from DLS at pH 1.2 could have

arisen from CS in the aqueous solution. At pH 1.2, both CS and CH are positively charged, such that repulsive interactions are dominant and counteract NPs formation. In contrast, G-CCNPs hydrodynamic size and PDI under different conditions remained fairly constant, suggesting that covalent crosslinking with genipin overcame destabilization induced by pH and ionic strength (**Figs. 3-2A and 3-2B**). In addition, TEM analysis confirmed the DLS results (**Fig. 3-2C**), with both CCNPs and G-CCNPs showing spherical shapes in water. Notably, G-CCNPs structural integrity appeared unaffected in simulated gastric fluid (SGF; pH 1.2) and simulated intestinal fluid (SIF; pH 7.4) while that of CCNPs was considerably altered.

3.4.3 Curcumin-loaded G-CCNPs and release profile of curcumin from G-CCNPs

Having confirmed that G-CCNPs were quite stable under various pH conditions, curcumin was loaded to a final concentration of 25 μg/ml into these NPs using the adsorption method, in which curcumin was added after G-CCNPs formation, to simplify the preparation step and increase entrapment efficiency. After loading, slight increases in hydrodynamic size and PDI were observed, suggesting that curcumin was successfully loaded into G-CCNPs. The entrapment efficiency and loading capacity of curcumin in G-CCNPs were 88.6 and 4.2%, respectively (**Table 3-2**). The high entrapment efficiency was because of curcumin binding to G-CCNPs through hydrophobic interactions, presumably with CS's hydrophobic tryptophan, as has been suggested previously [30].

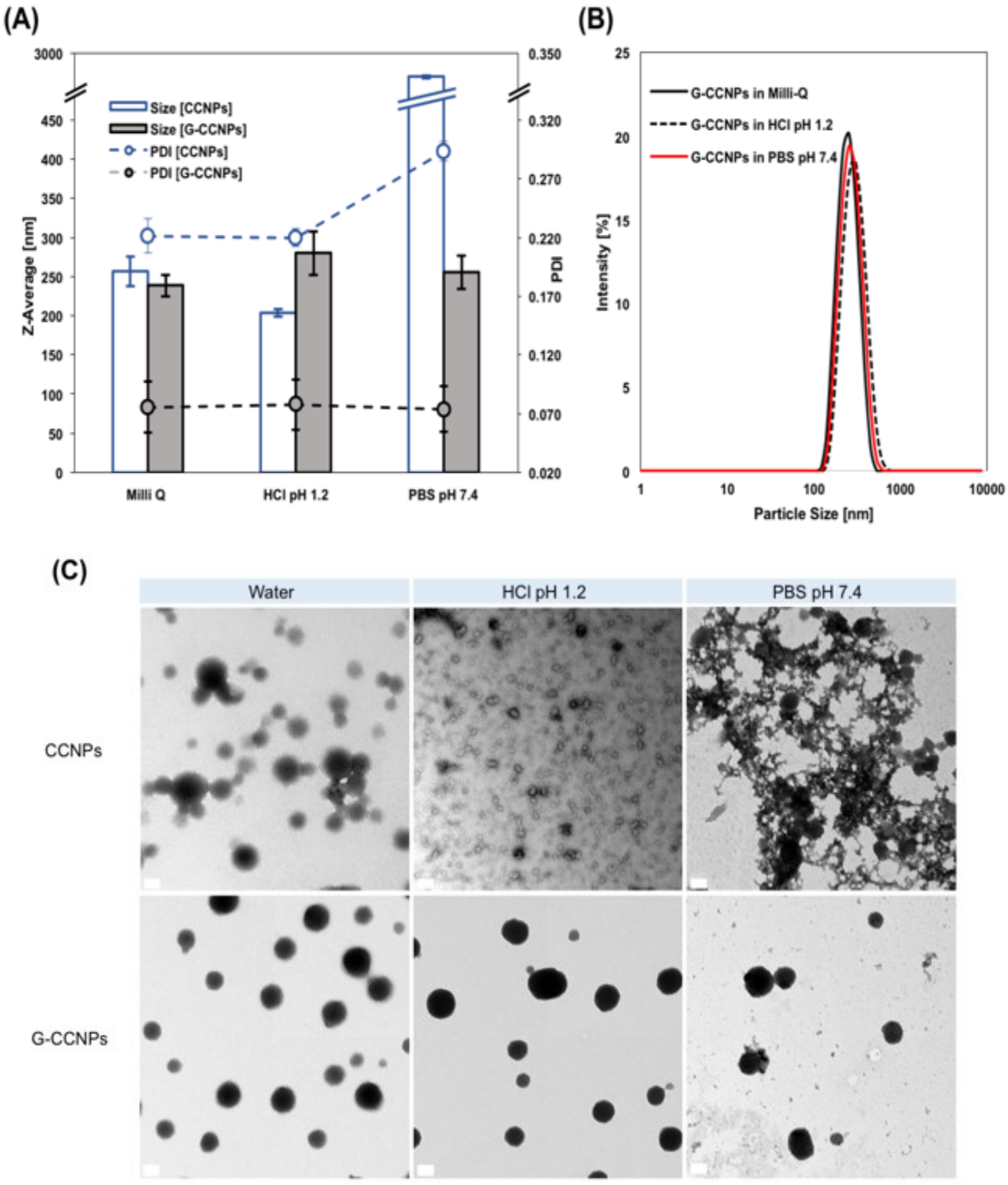

Fig. 3-2 (A) Particle sizes and PDI of G-CCNPs under various conditions determined by DLS. Uncrosslinked NPs (CCNPs) used as control. (B) Size distribution of G-CCNPs under various conditions. (C) TEM images of CCNPs and G-CCNPs under various conditions. Scale bars, 100 nm

Table 3-2. Characteristics of curcumin-loaded G-CCNPs[a]

Samples	Size [nm]	PDI	EE [%]	LC [%]
Curcumin G-CCNPs	272.9 ±13.1	0.077 ±0.011	88.6 ±0.2	4.2 ±0.2

[a]An aliquot of 1 mg/ml curcumin stock solution dissolved in DMSO added after G-CCNPs redispersed in Milli-Q water.

Data, mean ±standard deviation, *n*=3

The release of curcumin from G-CCNPs was studied in pH 7.4 and 5.5 which simulates a physiological condition and acidic environment of cancer, respectively. The release of curcumin from G-CCNPs in both pH conditions showed a biphasic profile where a burst release was observed within 1 h and followed by a sustained release for up to 6 h (**Fig. 3-3**). The release of curcumin was faster in pH 5.5 than in pH 7.4. It might be attributed to the degree of protonation of CH [31]. At low pH, CH undergoes protonation, resulting in the swelling of G-CCNPs matrix. Therefore, curcumin can be released faster. At the neutral pH, CH is deprotonated, which limits G-CCNPs swelling behavior. Hence, curcumin release was reduced. These results suggest that G-CCNPs might be useful to release curcumin effectively in acidic environment of cancer cells.

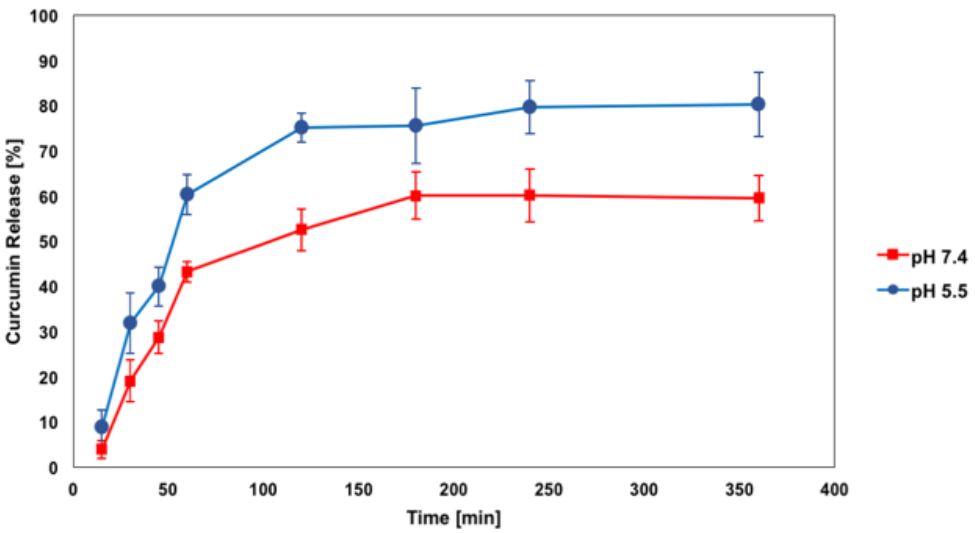

Fig. 3-3 Release profile of curcumin from G-CCNPs in two different pHs. Data, mean ± standard deviation, *n* = 3.

3.4.4 Cytotoxicity in vitro of free curcumin and curcumin-loaded G-CCNPs

The cytotoxicity of free curcumin *in vitro* was evaluated by exposing HeLa cells to curcumin and curcumin-loaded and unloaded G-CCNPs. HeLa cells were treated with samples possessing various curcumin concentrations for 24 h and cell viability determined by WST-8 assay. Cytotoxicity results showed that no decrease in cell viability was observed in the presence of unloaded G-CCNPs at all concentrations used, indicating that G-CCNPs were biocompatible and nontoxic (**Fig. 3-4**). Cell viability decreased in a concentration-dependent manner in the presence of free curcumin or curcumin-loaded G-CCNPs. However, the cytotoxicity of curcumin-loaded G-CCNPs was enhanced compared with that of free curcumin, with the IC_{50} values of free curcumin and curcumin-loaded G-CCNPs for these cells at 10 and 6.5 μg/ml, respectively. The obtained IC_{50} value for free curcumin was comparable with those

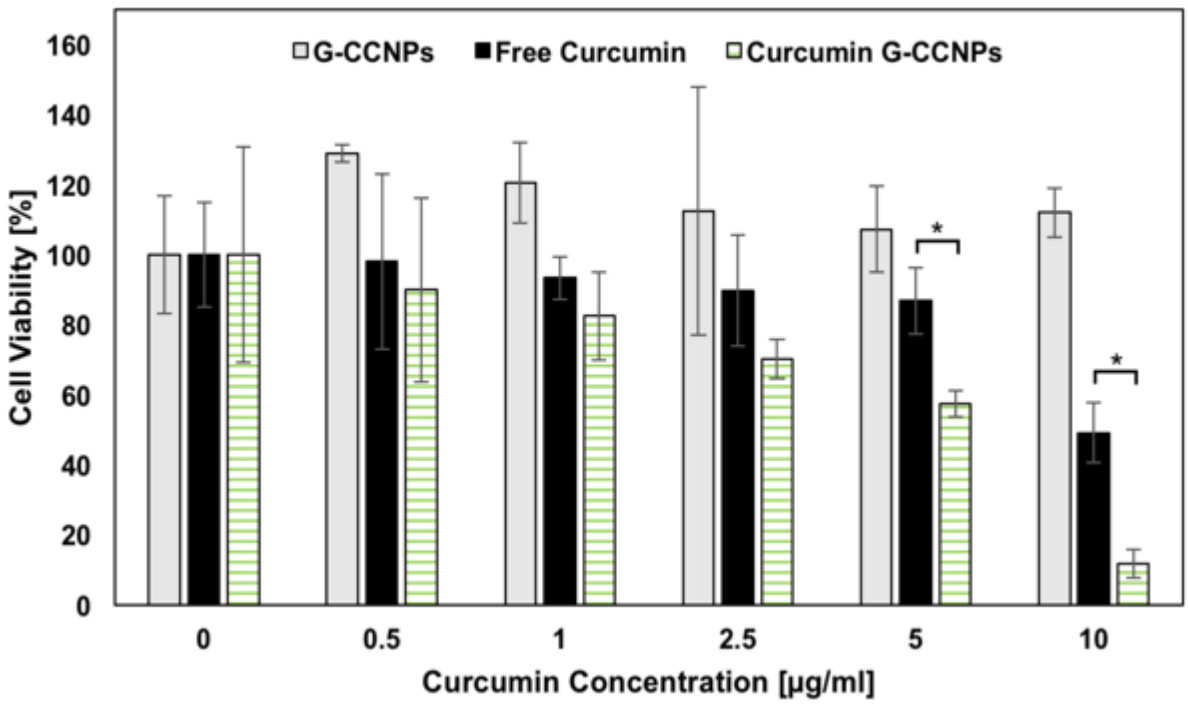

Fig. 3-4 Cytotoxicity *in vitro* of free curcumin and curcumin-loaded and unloaded G-CCNPs in HeLa cells by WST-8 assay after a 24-h incubation. Data, mean ± standard deviation, n=3, *$p < 0.05$

in previous reports [32,33]. Curcumin has been shown to have the ability to induce cytotoxicity *in vitro* in various cancer cell lines through apoptosis-related induction and the regulation of important oncogenic molecules [34–36]. Additionally, cytotoxicity *in vitro* in normal cell lines (L929) was also evaluated. Both free curcumin and curcumin-loaded G-CCNPs were less toxic toward normal cells than cancer cells (**Fig. 3-5**). The increased cytotoxicity of curcumin towards cancer cells might be due to the differences in cell structure and the ability of curcumin to modulate important signalling molecules in cancer cells [31, 37].

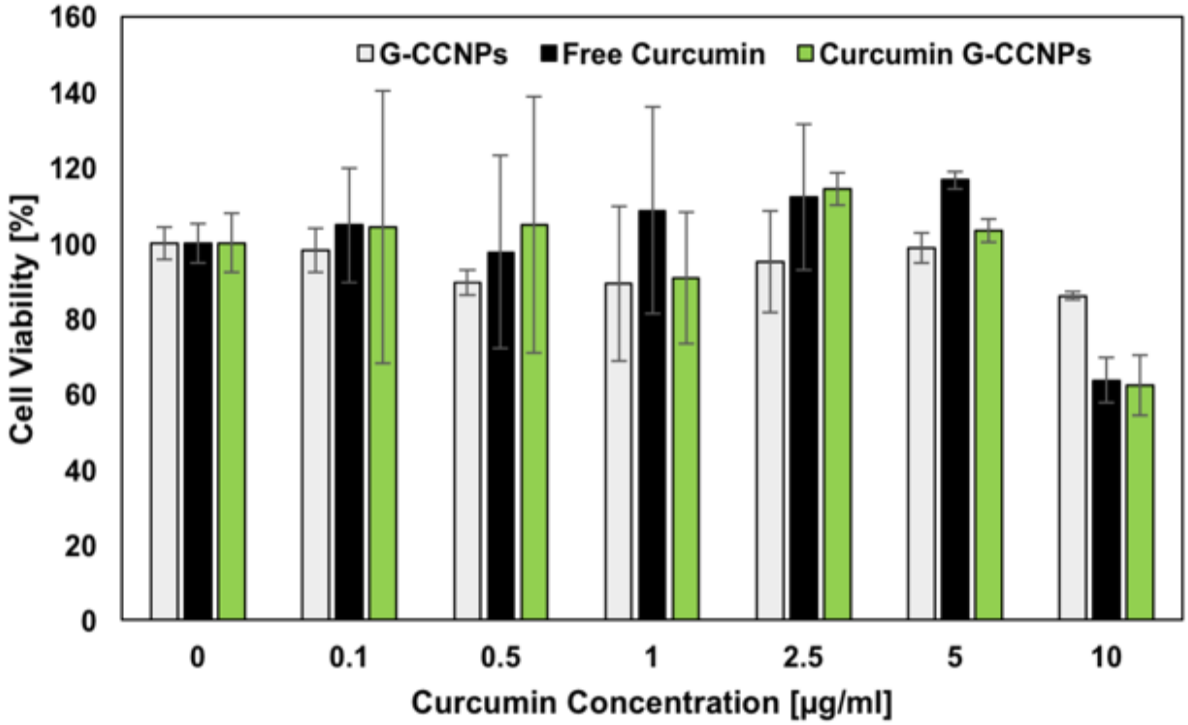

Fig. 3-5 Cytotoxicity *in vitro* of free curcumin, curcumin-loaded G-CCNPs, and unloaded G-CCNPs in normal cells (L929) by WST-8 assay after a 24-h incubation.
Data, mean ± standard deviation, $n = 3$

3.4.5 Cellular uptake of free curcumin and curcumin-loaded G-CCNPs

The enhanced cytotoxicity *in vitro* of curcumin-loaded G-CCNPs was confirmed by evaluating the intracellular uptake of free curcumin and curcumin-loaded G-CCNPs by HeLa cells using CLSM and flow cytometric analysis. The intrinsic green fluorescence of curcumin was used to visualize intracellular curcumin delivery to HeLa cells. Both free curcumin and curcumin-loaded G-CCNPs showed a slight green fluorescence signal after a 3-h incubation and curcumin signals were predominantly observed in the cytoplasm, consistent with previous studies (**Fig. 3-6**) [38,39]. However, the green signal from free curcumin decreased after a 6-h incubation because of rapid curcumin degradation in the serum-free medium (**Fig. 3-7**). In contrast, the green signal from curcumin-loaded G-CCNPs continued, even after a 6-h incubation, indicating that curcumin stability was enhanced by entrapment in G-CCNPs. Flow cytometric analysis further confirmed that intracellular delivery by curcumin-loaded G-CCNPs was enhanced compared with that of free curcumin. The mean fluorescence intensity of curcumin-loaded G-CCNPs was higher than that of free curcumin at 3 and 6 h (**Fig. 3-8**). These results suggest that G-CCNPs could be used as a potential carrier for enhanced curcumin delivery to cancer cells.

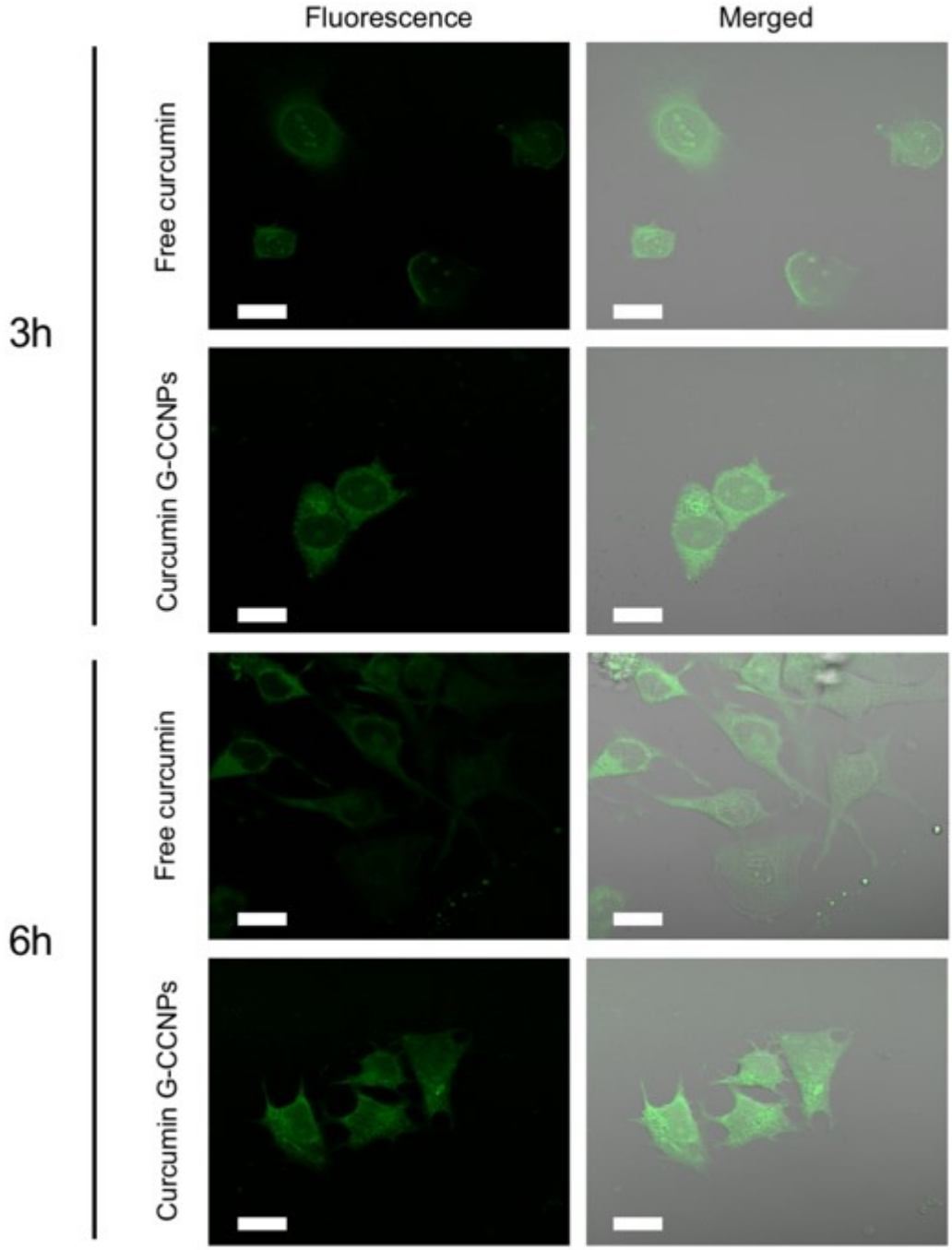

Fig. 3-6 Cellular uptake of free curcumin and curcumin G-CCNPs in HeLa cells determined by CLSM. Cells incubated for 3 and 6 h at a final concentration of 10 μg/ml curcumin. At 40× magnification, curcumin emits green fluorescence at 488 nm, and scale bars, 20 μm

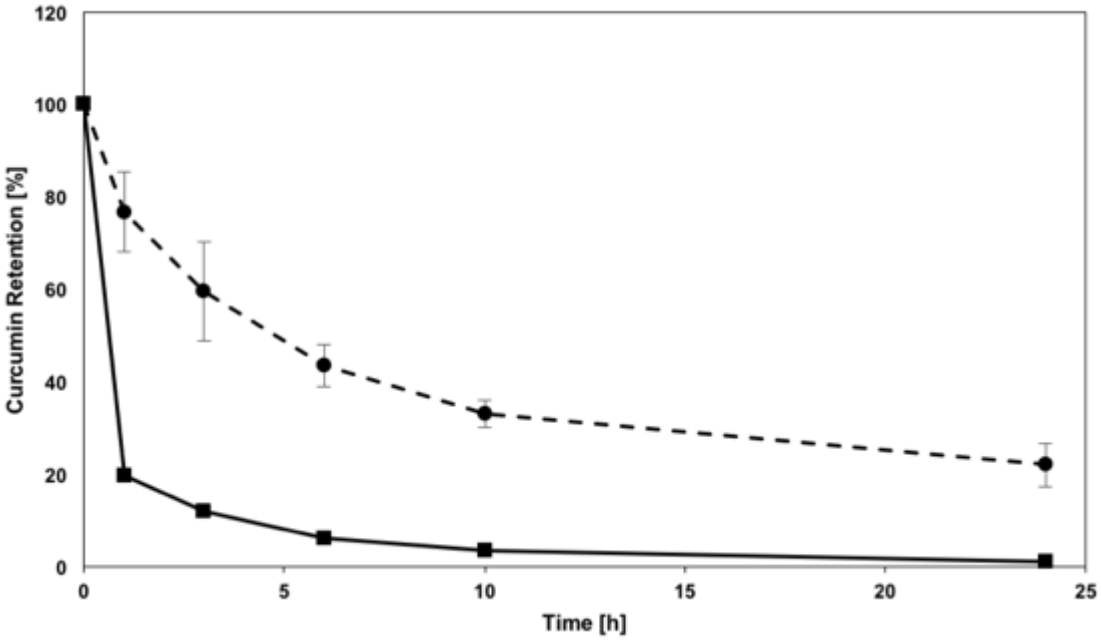

Fig. 3-7 Stability of free curcumin (solid lines) and curcumin G-CCNPs (dash lines) in serum-free medium (OPTI-MEM) at 37ºC under 5% CO_2 atmosphere. The initial concentration of curcumin was 10 μg/ml. Data, mean ± standard deviation, n = 3

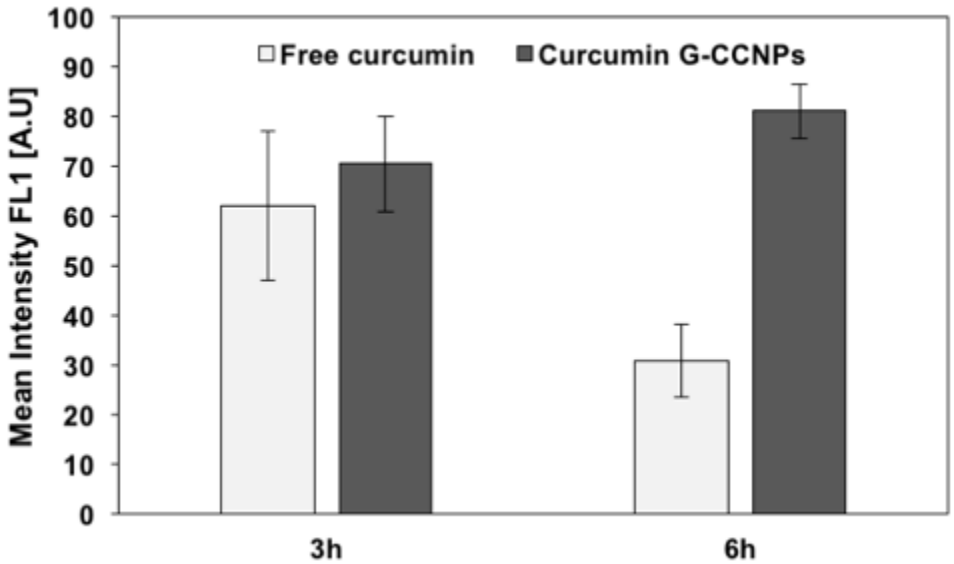

Fig. 3-8 Mean fluorescence intensity of curcumin in HeLa cells after incubation with free curcumin and curcumin-loaded G-CCNPs for 3 and 6 h at a final concentration of 10 μg/ml curcumin, determined by flow cytometric analysis. Cell density, 3 x 10^5 cells/well and data, mean ± standard deviation, n=3

3.4.6 Cellular uptake of G-CCNPs

Further insight into the mechanism of this enhanced cytotoxicity *in vitro* of curcumin-loaded G-CCNPs in HeLa cells was investigated by examining the cellular uptake of G-CCNPs using CLSM. G-CCNPs displayed intrinsic red fluorescence that derived from the genipin-crosslinking reaction. Localization of G-CCNPs within these cells was precisely determined through the *z*-stack mode of CLSM. Alexa Fluor 488 phalloidin (green) and Hoechst (blue) were used to stain F-actin associated with the cell membrane and nucleus, respectively. The *z*-stack images of HeLa cells after incubation with G-CCNPs for 3 h showed a greater red fluorescence signal, from G-CCNPs, on cell surfaces and not inside the cells, which suggests that G-CCNPs were poorly internalized by these cells (**Fig. 3-9**). In addition to the physical characteristics of NPs, such as size, shape, and surface properties, NPs cellular uptake also depends on the cell type [40]. Thus, cancer cell line A549 was used to confirm the cellular uptake traffic of G-CCNPs. Similarly, G-CCNPs appeared to attach and localize on cell surfaces (**Fig. 3-10**). Indeed, enhanced cytotoxicity of curcumin-loaded G-CCNPs in A549 cells was observed, compared with that of free curcumin (**Fig. 3-11**). The present results contradicted some previous reports that CH-based NPs are effectively internalized by cells through endocytosis-related pathways, such as macro-pinocytosis [41] and clathrin-mediated endocytosis [42]. Endocytosis-mediated internalization of CH-based or coated-NPs is related to their relatively small size and their positive surface charges [41,42]. In comparison, poor internalization of CH-based NPs has also been observed by other researchers [43–45], possibly because of NPs aggregation [43,45]. The possible localization of G-CCNPs on cell surfaces from particle aggregation was assessed by evaluating the stability of G-CCNPs in serum-free medium, OPTI-MEM, in a CLSM study using DLS. After incubation at 37 ^{o}C under 5% CO_2 for 6 h, no appreciable changes in the hydrodynamic size and PDI of G-CCNPs were found, suggesting that particle aggregation did not occur (**Fig. 3-12**).

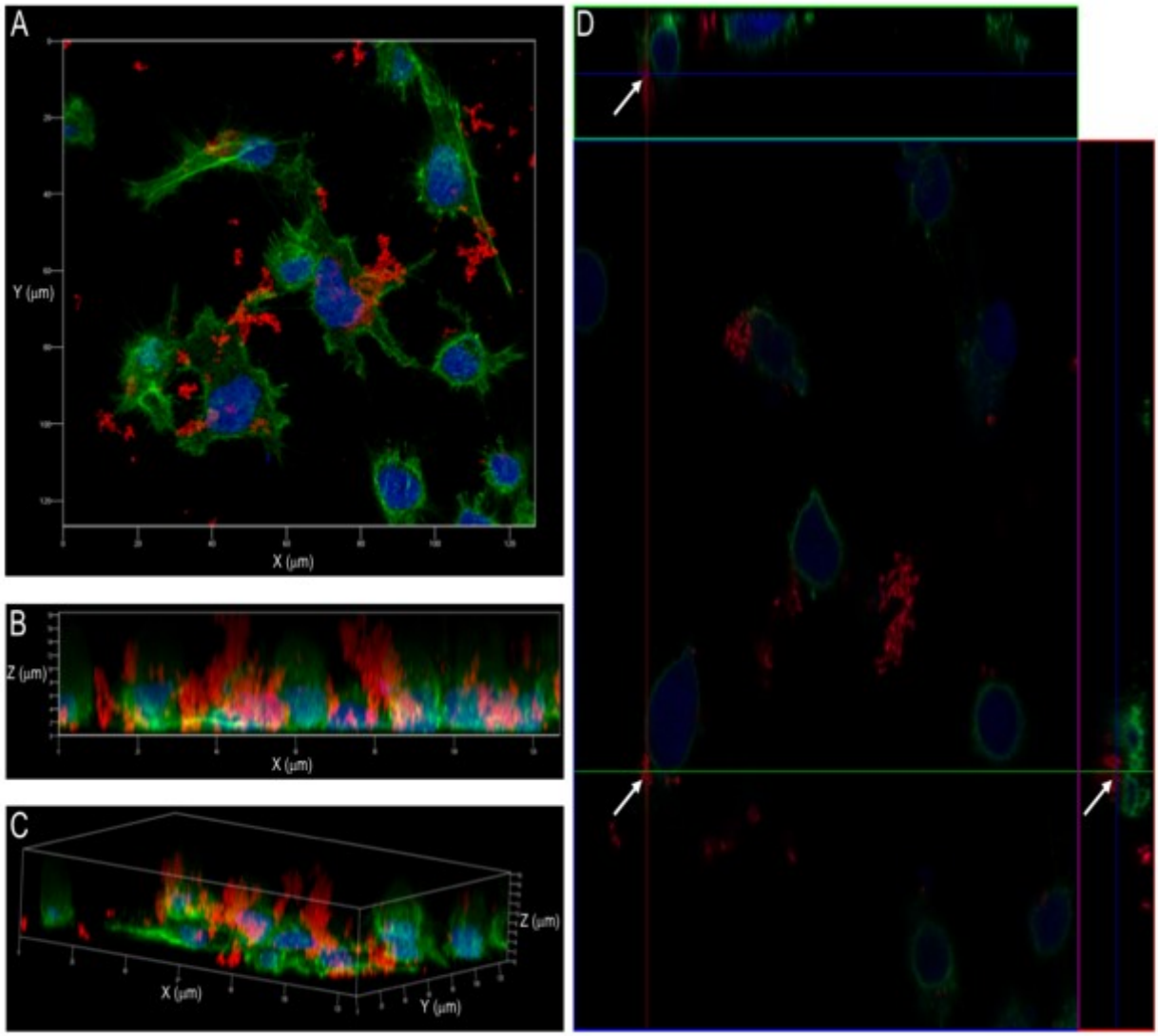

Fig. 3-9 Cellular uptake of G-CCNPs (red, genipin) in HeLa cells examined by *z*-stack 3D CLSM. Phalloidin (green) and Hoechst (blue) used to stain F-actin on cell membrane and nucleus, respectively. Observation done for 3 h at a 63× magnification and *x*-axis shows bottom of cells. (A) 2D image with *x*, *y* planes, (B) 2D image with *x*, *z* planes, (C) 3D image, and (D) orthogonal view of *z*-stack image. Intersection points (white arrow) indicate location of G-CCNPs within cells and G-CCNPs were located on cell membranes

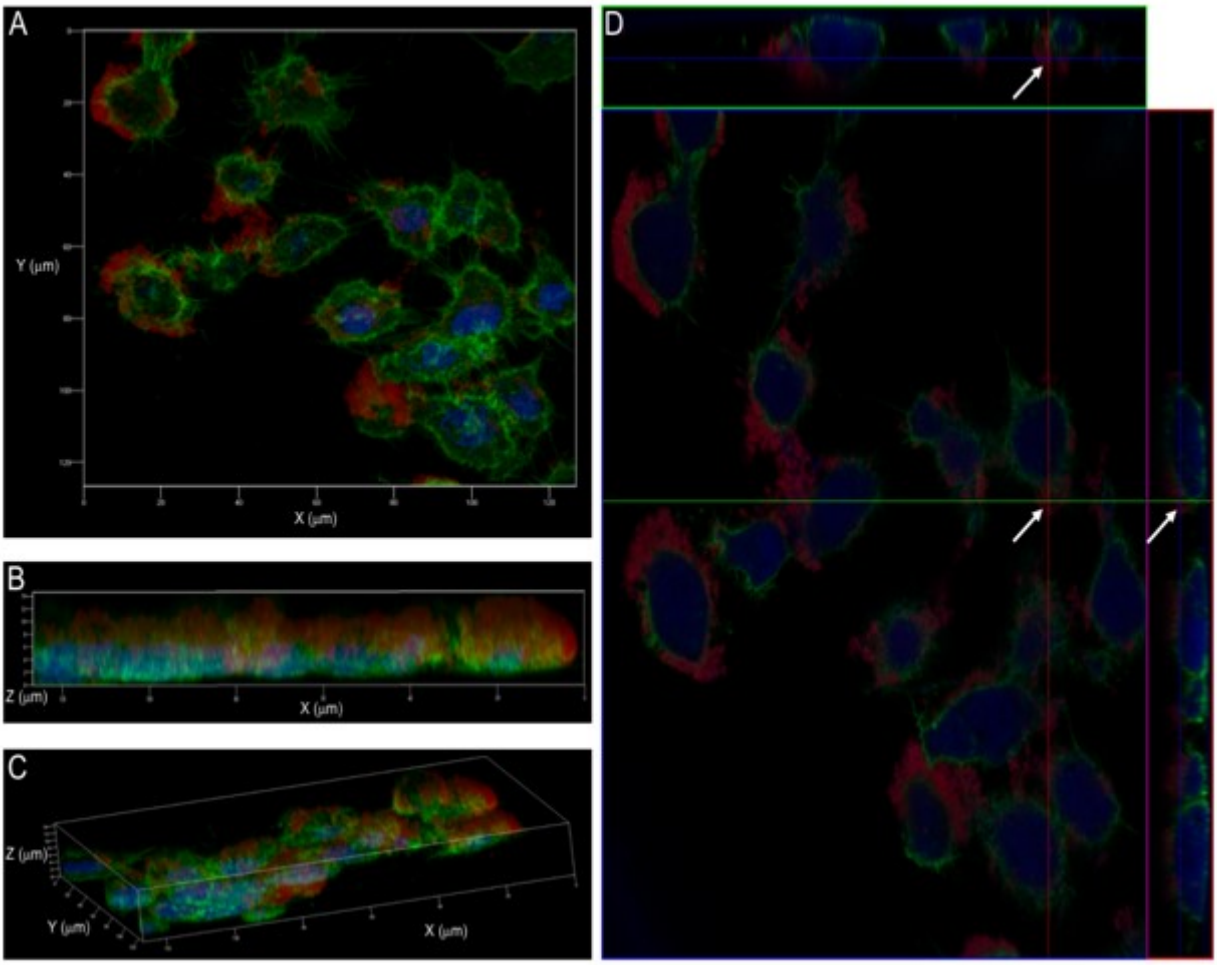

Fig. 3-10 Cellular uptake of G-CCNPs (red, genipin) in A549 cells examined by *z*-stack 3D CLSM. Phalloidin (green) and Hoechst (blue) used to stain F-actin on cell membrane and nucleus, respectively. Observation done for 3h at a 63× magnification and *x*-axis shows bottom of cells. (A) 2D image with *x*, *y* planes. (B) 2D image with *x*, *z* planes. (C). 3D image. (D) Orthogonal view of *z*-stack image. Intersection points (white arrow) indicate the location of G-CCNPs within A549 cells. G-CCNPs were located on cell membranes

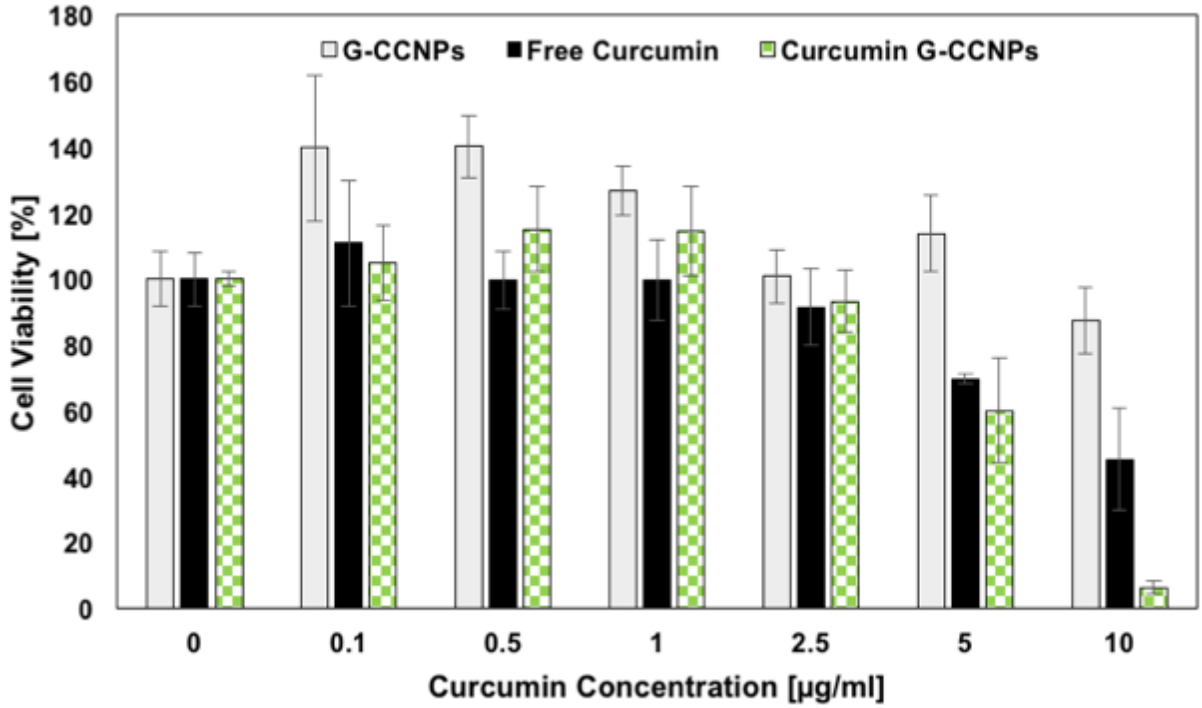

Fig. 3-11 Cytotoxicity *in vitro* of free curcumin, curcumin-loaded G-CCNPs, and unloaded G-CCNPs in A549 cells by WST-8 assay after a 24-h incubation.

Data, mean ± standard deviation, $n = 3$

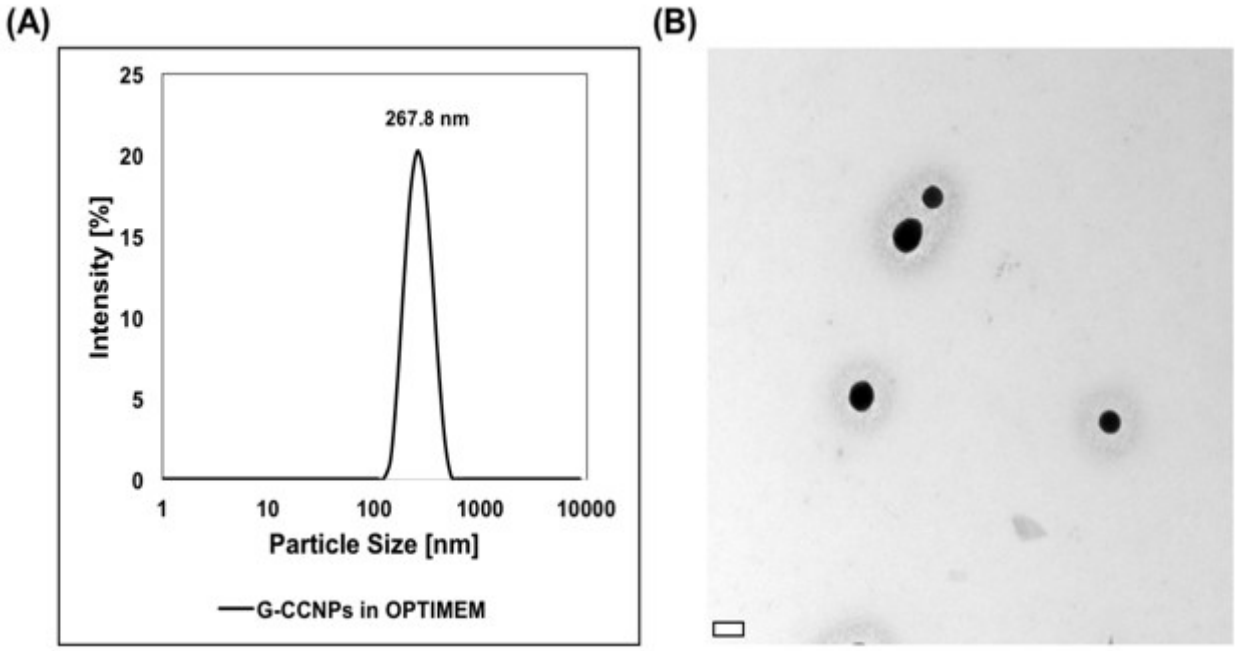

Fig. 3-12 (A) Size distribution of G-CCNPs in OPTI-MEM by DLS. G-CCNPs incubated for 6h at 37 ºC under 5% CO_2 atmosphere. (B) TEM image of G-CCNPs in OPTI-MEM and scale bar, 200 nm

However, the zeta potential decreased from +24.7 to -13.2 mV (**Table 3-3**). A decrease in zeta potential and charge reversal might have explained the lack of intracellular G-CCNPs delivery [46]. Besides, the colloidal stability of G-CCNPs is rather poor as the zeta potential value does not reach ±30 mV [47]. Alternatively, G-CCNPs binds strongly with cell membrane phospholipids, causing disarrangement of lipid structures and thus hindering cellular internalization [48]. The quantification of cell-associated G-CCNPs was further determined by flow cytometric analysis and the result is shown in **Fig. 3-13**. A marked increase in the fluorescence intensity of cells incubated with G-CCNPs as compared with cells only was observed, implying that G-CCNPs were likely to be bound to the surface of the cells.

Table 3-3. Characteristics of G-CCNPs in OPTI-MEM determined by DLS

Sample	Size [nm]	PDI	Zeta [mV][a]
G-CCNPs	267.8 ± 8.9	0.078 ± 0.003	-13.2 ± 2.2

Samples incubated for 6 h at 37 ºC under 5% CO_2 atmosphere before measurements

Data, mean ± standard deviation, $n = 3$

[a]Zeta potential measurements conducted in PBS at pH 7.4

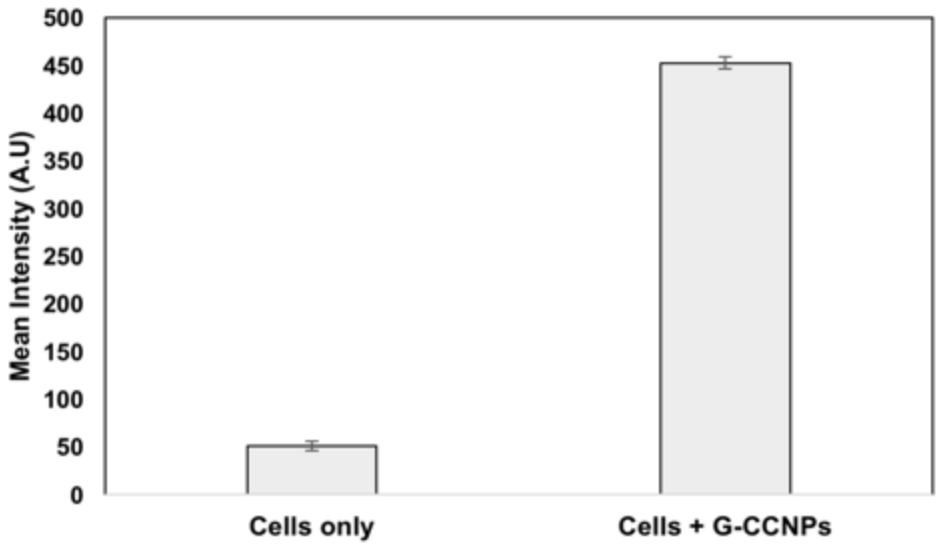

Fig. 3-13 Quantitative analysis of cell-associated G-CCNPs by a flow cytometer. HeLa cells incubated for 3h by G-CCNPs. Data, mean ± standard deviation, $n = 3$

3.4.7 Discussion on G-CCNPs as a potential carrier for curcumin

A nano drug delivery system capable of improving therapeutic potential of curcumin is of interest. G-CCNPs could improve cytotoxicity *in vitro* of curcumin in HeLa cells as determined by WST-8 assay. The enhanced cytotoxicity *in vitro* of curcumin by G-CCNPs might be attributed to the stability enhancement of curcumin in the serum-free medium at neutral pH which in turn increases the intracellular uptake of curcumin, as examined by CLSM (Fig. 3-6) and flow cytometric analysis (Fig. 3-8). NPs intracellular uptake through endocytosis could be useful for stabilizing and improving efficiency of drug delivered to the cells, which might also explain the enhanced cytotoxicity *in vitro* of curcumin by G-CCNPs. Interestingly, G-CCNPs seemed to be bound to the cell membrane as suggested by the combined results from CLSM (Fig. 3-9) and flow cytometric analysis (Fig. 3-13). *In vitro* release study revealed that curcumin was released in a sustained manner by G-CCNPs at neutral pH (Fig. 3-3). Thus, it might be that curcumin was possibly released from G-CCNPs into the medium and/or to the cell membranes and then was taken up by the cells to exert cytotoxicity. In summary, the improved stability of encapsulated curcumin in neutral pH and the subsequent release of curcumin into the medium and/or after attachment of curcumin-loaded G-CCNPs on cell membranes could be a potential mechanism for enhanced cytotoxicity *in vitro* and intracellular uptake of curcumin to cells. NPs intracellular uptake into cells is mostly desired for enhanced efficacy and the delivery of drugs and bioactive molecules. For instance, aminated starch coated iron oxide NPs was capable of enhancing cytotoxicity of curcumin through significant NPs internalization along with the increased production of radical oxygen species (ROS) [26]. However, drug delivery without NPs internalization has shown promise as an alternative approach, which would allow bypassing a complex endocytotic pathway and reduce possible toxicity induced by internalized NPs [49,50]. To our knowledge, this is the first report showing that protein-polysaccharide-based NPs enhanced the cytotoxicity *in vitro* of a hydrophobic

molecule, curcumin, in cancer cells with negligible NPs internalization. The results obtained here clearly indicated that G-CCNPs could be used as a nontoxic and effective delivery vehicle for hydrophobic or hydrophilic drugs or bioactive molecules in the fields of food, medicine, and pharmacy.

3.5 Conclusions

The formation of biocompatible CS-CH NPs was demonstrated, utilizing electrostatic interactions and stabilization by genipin-crosslinking, a naturally occurring crosslinking agent. Crosslinked NPs (G-CCNPs) exhibited near homogeneous particle size distribution with positive surface charges in water. G-CCNPs showed significant stability enhancement under various pH conditions, compared with the uncrosslinked counterpart. G-CCNPs were able to encapsulate curcumin with high entrapment efficiency (~90%) through hydrophobic interactions. The interaction of G-CCNPs with HeLa cells was studied, and *z*-stack CLSM images revealed that G-CCNPs were mainly found on cell surfaces but not internalized into cells. These NPs might have strongly interacted with cell membranes, preventing their cellular internalization. However, these results suggest that G-CCNPs improved *in vitro* anticancer curcumin activity over free curcumin in HeLa cells. The mechanism by which G-CCNPs improved curcumin bioactivity might be related to enhanced curcumin stability and its following release from G-CCNPs into cells by passive curcumin diffusion.

References

[1] P. Zimet and Y. D. Livney. Beta-lactoglobulin and Its Nanocomplexes with Pectin as Vehicles for ω-3 Polyunsaturated Fatty Acids. Food Hydrocoll, 23 (2009) 1120-1126.

[2] C. G. De Kruif, F. Weinbreck and R. De Vries. Complex Coacervation of Proteins and Anionic Polysaccharides. Curr. Opin. Colloid Interface Sci, 9 (2004) 340-349.

[3] S. L. Turgeon, M. Beaulieu, C. Schmitt and C. Sanchez. Protein-polysaccharide Interactions: Phase-ordering Kinetics, Thermodynamic and Structural Aspects. Curr. Opin. Colloid Interface Sci, 8 (2003) 401-414.

[4] L. Plapied, N. Duhem, A. des Rieux and V. Préat. Fate of Polymeric Nanocarriers for Oral Delivery. Curr. Opin. Colloid Interface Sci, 16 (2011) 228-237.

[5] S. N. Tammam, H. M. E. Azzazy, H. G. Breitinger and A. Lamprecht. Chitosan Nanoparticles for Nuclear Targeting: The Effect of Nanoparticle Size and Nuclear Localization Sequence Density. Mol. Pharm, 12 (2015) 4277-4289.

[6] Y. O. Jeon, J. S. Lee and H. G. Lee. Improving Solubility, Stability, and Cellular Uptake of Resveratrol by Nanoencapsulation with Chitosan and γ-Poly (Glutamic Acid). Colloids Surfaces B Biointerfaces, 147 (2016) 224-233.

[7] M. R. Kasimova, A. Velázquez-Campoy and H. M. Nielsen. On the Temperature Dependence of Complex Formation Between Chitosan and Proteins. Biomacromolecules, 12 (2011) 2534-2543.

[8] B. Hu, M. Xie, C. Zhang and X. Zeng. Genipin-structured Peptide-Polysaccharide Nanoparticles with Significantly Improved Resistance to Harsh Gastrointestinal Environments and Their Potential for Oral Delivery of Polyphenols. J. Agric. Food Chem, 62 (2014)12443-12452.

[9] J. Qi, P. Yao, F. He, C. Yu and C. Huang. Nanoparticles with Dextran/chitosan Shell and BSA/chitosan Core-Doxorubicin Loading and Delivery. Int. J. Pharm, 393 (2010) 177-185.

[10] D. Y. Hong, J. S. Lee and H. G. Lee. Chitosan/poly-γ-glutamic acid Nanoparticles Improve the Solubility of Lutein. Int. J. Biol. Macromol, 85 (2016) 9-15.

[11] Z. X. Liao, S. F. Peng, Y. L. Chiu, C. W. Hsiao, H. Y. Liu, W. H. Lim, H. M. Lu and H. W. Sung. Enhancement of Efficiency of Chitosan-based Complexes for Gene Transfection with Poly (γ-glutamic acid) by Augmenting Their Cellular Uptake and Intracellular Unpackage. J. Control. Release, 193 (2014) 304-315.

[12] K. Sonaje, Y. J. Chen, H. L. Chen, S. P. Wey, J. H. Juang, H. N. Nguyen, C. W. Hsu, K. J. Lin and H. W. Sung. Enteric-coated Capsules Filled with Freeze-dried Chitosan/poly (γ-glutamic acid) Nanoparticles for Oral Insulin Delivery. Biomaterials, 31 (2010) 3384-3394.

[13] T. Koupantsis, E. Pavlidou and A. Paraskevopoulou. Flavour Encapsulation in Milk Proteins-CMC Coacervate-type Complexes. Food Hydrocoll, 37 (2014) 134-142.

[14] E. Semo, E. Kesselman, D. Danino and Y. D. Livney. Casein Micelle as A Natural Nano-capsular Vehicle for Nutraceuticals. Food Hydrocoll, 21 (2007) 936-942.

[15] A. K. Anal, A. Tobiassen, J. Flanagan and H. Singh. Preparation and Characterization of Nanoparticles Formed by Chitosan-caseinate Interactions. Colloids Surfaces B Biointerfaces, 64 (2008) 104-110.

[16] W. He, M. Parowatkin, V. Mailänder, M. Flechtner-Mors, R. Graf, A. Best, K. Koynov, K. Mohr, U. Ziener, K. Landfester and D. Crespy. Nanocarrier for Oral Peptide Delivery Produced by Polyelectrolyte Complexation in Nanoconfinement. Biomacromolecules, 16 (2015) 2282-2287.

[17] N. Reddy, R. Reddy and Q. Jiang. Crosslinking Biopolymers for Biomedical Applications. Trends Biotechnol, 33 (2015) 362-369.

[18] P. Taddei, V. Chiono, A. Anghileri, G. Vozzi, G. Freddi and G. Ciardelli. Silk Fibroin/gelatin Blend Films Crosslinked with Enzymes for Biomedical Applications. Macromol. Biosci, 13 (2013) 1492-1510.

[19] J. Fang, Y. Zhang, S. Yan, Z. Liu, S. He, L. Cui and J. Yin. Poly (L-glutamic acid)/Chitosan Polyelectrolyte Complex Porous Microspheres as Cell Microcarriers for Cartilage Regeneration. Acta Biomater, 10 (2014) 276-288.

[20] F. L. Mi, H.-W. Sung, S.-S. Shyu, C.-C. Su and C.-K. Peng. Synthesis and Characterization of Biodegradable TPP/genipin Co-crosslinked Chitosan Gel Beads. Polymer, 44 (2003) 6521-6530.

[21] F. L. Mi, Y. C. Tan, H. F. Liang and H. W. Sung. In Vivo Biocompatibility and Degradability of a Novel Injectable-chitosan-based Implant. Biomaterials, 23 (2002) 181-191.

[22] X. Song, H. Wu, S. Li, Y. Wang, X. Ma and M. Tan. Ultrasmall Chitosan-genipin Nanocarriers Fabricated from Reverse Microemulsion Process for Tumor Photothermal Therapy in Mice. Biomacromolecules, 16 (2015) 2080-2090.

[23] Y. Zhang, L. Mao, J. Liu and T. Liu. Self-fluorescent Drug Delivery Vector Based on Genipin-crosslinked Polyethylenimine Conjugated Globin Nanoparticle. Mater. Sci. Eng. C, 71 (2017) 17-24.

[24] M. A. Pujana, L. Pérez-Álvarez, L. C. C. Iturbe and I. Katime. Biodegradable Chitosan Nanogels Crosslinked with Genipin. Carbohydr. Polym, 94 (2013) 836-842.

[25] N. F. N. Silva, A. Saint-Jalmes, A. F. De Carvalho and F. Gaucheron. Development of Casein Microgels from Cross-linking of Casein Micelles by Genipin. Langmuir, 30 (2014) 10167-10175.

[26] C. Saikia, M.K. Das, A. Ramteke and T.K. Maji. Effect of Crosslinker on Drug Delivery Properties of Curcumin Loaded Starch Coated Iron Oxide Nanoparticles. Int. J. Biol. Macromol, 93 (2016) 1121-1132.

[27] C. Chang, T. Wang, Q. Hu, M. Zhou, J. Xue and Y. Luo. Pectin Coating Improves Physicochemical Properties of Caseinate/zein Nanoparticles as Oral Delivery Vehicles for Curcumin. Food Hydrocoll, 70 (2017) 143-151.

[28] M. F. Butler, Y. F. Ng and P. D. A. Pudney. Mechanism and Kinetics of the Crosslinking Reaction Between Biopolymers Containing Primary Amine Groups and Genipin. J. Polym. Sci. Part A Polym. Chem, 41(2003) 3941-3953.

[29] Y. Huang, Y. Cai and Y. Lapitsky. Factors Affecting the Stability of Chitosan/tripolyphosphate Micro- and Nanogels: Resolving the Opposing Findings. J. Mater. Chem. B, 3 (2015) 5957-5970.

[30] M. Esmaili, S. M. Ghaffari, Z. Moosavi-Movahedi, M. S. Atri, A. Sharifizadeh, M. Farhadi, R. Yousefi, J. M. Chobert, T. Haertlé and A. A. Moosavi-Movahedi. Beta Casein-micelle as a Nano Vehicle for Solubility Enhancement of Curcumin: Food Industry Application. LWT - Food Sci. Technol, 44 (2011) 2166-2172.

[31] A. Anitha, V.G. Deepagan, V.V.D. Rani, D. Menon, S.V. Nair and R. Jayakumar. Preparation, Characterization, In Vitro Drug Release and Biological Studies of Curcumin Loaded Dextran Sulphate-chitosan Nanoparticles. Carbohydr. Polym, 84 (2011) 1158-1164.

[32] A. Sahu, U. Bora, N. Kasoju and P. Goswami. Synthesis of Novel Biodegradable and Self-assembling Methoxy Poly(ethylene glycol)-palmitate Nanocarrier for Curcumin Delivery to Cancer Cells. Acta Biomater, 4 (2008) 1752-1761.

[33] J. Liu, L. Xu, C. Liu, D. Zhang, S. Wang, Z. Deng, W. Lou, H. Xu, Q. Bai and J. Ma. Preparation and Characterization of Cationic Curcumin Nanoparticles for Improvement of Cellular Uptake. Carbohydr. Polym, 90 (2012) 16-22.

[34] J. Ravindran, S. Prasad and B. B. Aggarwal. Curcumin and Cancer Cells: How Many Ways Can Curry Kill Tumor Cells Selectively? AAPS J, 11 (2009) 495-510.

[35] M. M. Yallapu, S. Khan, D. M. Maher, M. C. Ebeling, V. Sundram, N. Chauhan, A. Ganju, S. Balakrishna, B. K. Gupta, N. Zafar, M. Jaggi and S. C. Chauhan. Anti-Cancer Activity of Curcumin Loaded Nanoparticles in Prostate Cancer. Biomaterials, 35 (2014) 8635-8648.

[36] M. S. Zaman, N. Chauhan, M. M. Yallapu, R. K. Gara, D. M. Maher, S. Kumari, M. Sikander, S. Khan, N. Zafar, M. Jaggi and S. C. Chauhan. Curcumin Nanoformulation for Cervical Cancer Treatment. Sci. Rep, 6 (2016) 20051.

[37] A. Kunwar, A. Barik, B. Mishra, K. Rathinasamy, R. Pandey and K.I Priyadarsini. Quantitative Cellular Uptake, Localization and Cytotoxicity of Curcumin in Normal and Tumor Cells. Biochim. Biophys. Acta, 1780 (2008) 673-679.

[38] M. T. Fatima, A. Chanchal, P. S. Yavvari, S. D. Bhagat, M. Gujrati, R. K. Mishra and A. Srivastava. Cell Permeating Nano-Complexes of Amphiphilic Polyelectrolytes Enhance Solubility, Stability, and Anti-Cancer Efficacy of Curcumin. Biomacromolecules, 17 (2016) 2375-2383.

[39] X. Yang, Z. Li, N. Wang, L. Li, L. Song, T. He, L. Sun, Z. Wang, Q. Wu, N. Luo, C. Yi and C. Gong. Curcumin-Encapsulated Polymeric Micelles Suppress the Development of Colon Cancer In Vitro and In Vivo. Sci. Rep, 5 (2015) 10322.

[40] H. Y. Nam, S. M. Kwon, H. Chung, S. Y. Lee, S. H. Kwon, H. Jeon, Y. Kim, J. H. Park, J. Kim, S. Her, Y. K. Oh, I. C. Kwon, K. Kim and S. Y. Jeong. Cellular Uptake Mechanism and Intracellular Fate of Hydrophobically Modified Glycol Chitosan Nanoparticles. J. Control. Release, 135 (2009) 259-267.

[41] Y. C. Huang and T. H. Kuo. O-carboxymethyl Chitosan/fucoidan Nanoparticles Increase Cellular Curcumin Uptake. Food Hydrocoll, 53 (2016) 261-269.

[42] M. Huang, Z. Ma, E. Khor and L. Y. Lim. Uptake of FITC-chitosan Nanoparticles by A549 Cells. Pharm. Res, 19 (2002) 1488-1494.

[43] J. Malmo, K. M. Vårum and S. P. Strand. Effect of Chitosan Chain Architecture on Gene Delivery: Comparison of Self-branched and Linear Chitosans. Biomacromolecules, 12 (2011) 721-729.

[44] J. P. Fuenzalida, T. Weikert, S. Hoffmann, C. Vila-Sanjurjo, B. M. Moerschbacher, F. M. Goycoolea and S. Kolkenbrock. Affinity Protein-based FRET Tools for Cellular Tracking of Chitosan Nanoparticles and Determination of the Polymer Degree of Acetylation. Biomacromolecules, 15 (2014) 2532-2539.

[45] Z. Garaiova, S. P. Strand, N. K. Reitan, S. Lélu, S. T. Størset, K. Berg, J. Malmo, O. Folasire, A. Bjørkøy and C. De L. Davies. Cellular Uptake of DNA-chitosan Nanoparticles: The Role of Clathrin- and Caveolae-mediated Pathways. Int. J. Biol. Macromol, 51 (2012) 1043-1051.

[46] D. Hu, Z. Xu, Z. Hu, B. Hu, M. Yang and L. Zhu. PH-triggered Charge-reversal Silk Sericin-based Nanoparticles for Enhanced Cellular Uptake and Doxorubicin Delivery. ACS Sustain. Chem. Eng, 5 (2017) 1638-1647.

[47] F. Han, S. Li, R. Yin, H. Liu and L. Xu. Effect of Surfactants on the Formation and Characterization of a New Type of Colloidal Drug Delivery System: Nanostructured Lipid Carriers. Colloid Surf A Physicochem Eng Asp, 315 (2008) 210-216.

[48] Y. Zhang, S. Tekobo, Y. Tu, Q. Zhou, X. Jin, S. A. Dergunov, E. Pinkhassik and B. Yan. Permission to Enter Cell by Shape: Nanodisk vs Nanosphere. ACS Appl. Mater. Interfaces, 4 (2012) 4099-4105.

[49] D. Hofmann, C. Messerschmidt, M. B. Bannwarth, K. Landfester and V. Mailänder. Drug Delivery Without Nanoparticle Uptake: Delivery by a Kiss-and-run Mechanism on the Cell Membrane. Chem. Commun, 50 (2014) 1369-1371.

[50] S. Snipstad, S. Westrøm, Y. Mørch, M. Afadzi, A. K. O. Åslund and C. De L. Davies. Contact-mediated Intracellular Delivery of Hydrophobic Drugs from Polymeric Nanoparticles. Cancer Nanotechnol, 6 (2015) 3.

CHAPTER 4 NANOPARTICLES FORMED FROM THE ASSEMBLY OF REDUCED ALBUMIN AND GLYCOL CHITOSAN FOR PACLITAXEL DELIVERY

4.1 Abstract

Cancer continues to pose health problems for people all over the world. Nanoparticles (NPs) have emerged as a promising platform for effective cancer chemotherapy. NPs formed by the assembly of proteins and chitosan (CH) through non-covalent interactions attract great interest. However, the poor water solubility of CH limits its practical application. Herein, the formation of reduced bovine serum albumin (rBSA) and glycol chitosan (GC) nanoparticles (rBG NPs) was demonstrated for paclitaxel (PTX) delivery. The effects of a rBSA/GC mass ratio and pH on the particle size, polydispersity index (PDI), the number of particles, and the surface charge were evaluated. The formation mechanism and stability of these NPs were determined by compositional analysis and dynamic light scattering (DLS). The effect of pH on the physical characteristics of rBG NPs was notable, particularly at pH 6.5. The effect of mass ratio was found to be substantial when rBSA concentration was higher. Hydrophobic and electrostatic interactions were driving forces for the formation of rBG NPs and these NPs were stable at physiological conditions. PTX was successfully encapsulated into rBG NPs with high encapsulation efficiency (~90%). PTX-loaded rBG NPs had a particle size of about 400 nm with low PDI (0.2) and positive charge. rBG NPs could be internalized by HeLa cells, possibly via endocytosis. Cytotoxicity *in vitro* study revealed that PTX-loaded rBG NPs had lower anti-cancer activity as compared with Taxol-like formulation at 24 h, but had quite similar activity at 48 h, possibly due to the slow release of PTX into the cells. Our study suggests that rBG NPs could be used as a potential nano carrier for hydrophobic drugs.

4.2. Introduction

Cancer remains a leading cause of death across the globe, which accounts for 13% of all death incidence [1]. The current treatments for cancer are surgery, radiation therapy, and chemotherapy, which involves the systemic administration of anti-cancer drug to the body. However, most of anti-cancer drugs used in chemotherapy are poorly soluble in water, which leads to poor drug bioavailability [2]. The conventional and commercial approach for solubilizing hydrophobic anti-cancer drugs is by using surfactants and organic solvents, as exemplified in paclitaxel (PTX) injection formulation (Taxol®) that uses considerable amount of cremophor EL and dehydrated ethanol. However, the use of Taxol® in cancer treatment has been associated with hypersensitivity reactions, hyperlipidaemia and peripheral neuropathy occurrence [3].

In the recent years, nano-size drug delivery systems (DDS) have gained tremendous attention for more effective and safer cancer treatment owing to their ability to solubilize or encapsulate hydrophobic drugs, reduce non-specific toxicity, control pharmacokinetics and pharmacodynamics of the drugs, and enhance drugs penetration into tumors via enhanced permeability and retention (EPR) effect [1,2,4]. Various nano-size DDS have been explored, including polymeric-based nanoparticles (NPs), liposome, nanoemulsion, metallic and inorganic-based nanocarriers [5–9]. In particular, organic-based nano-size DDS are preferred over inorganic counterpart because of less toxic and better biocompatibility and biodegradability [10]. Proteins and polysaccharides are attractive components for development of NPs for cancer treatment due to their excellent biocompatibility [11,12]. NPs fabricated from proteins and polysaccharides have emerged as a promising NPs for improving water solubility, stability, controlled release, and bioactivity of the drugs and/or therapeutic molecules [13–18]. NPs can be simply formed by the complexation between proteins and polysaccharides in the

aqueous solution via non-covalent forces, importantly through the electrostatic interactions [19].

Albumin is an important protein largely found in the blood (35-50 g/L in human serum) for transportation of many biomolecules, including fatty acids, hormones, and nutrients. Albumin is synthesized in the liver and has a globular structure [20]. Albumin has been widely exploited for nano-size DDS due to its non-toxic properties, biodegradability, biocompatibility, low immunogenicity, highly water soluble, and well-characterized [21,22]. In fact, human serum albumin (HSA)-based NPs (Abraxane) has been commercially used for cancer treatment. Bovine serum albumin (BSA) (**Fig. 4-1A**), albumin obtained from bovine serum, has been extensively used as a drug nano carrier due to its similarity with HSA, cost-effective, and well-received in the pharmaceutical industry [21]. BSA has a molecular weight of 69.3 kDa with 583 amino acid residues and contains 17 disulfide bonds and one free thiol (Cys34). BSA has an isoelectric point (p*I*) of 4.7 and possesses two tryptophan (Trp) residues at position 212 (Trp212) present in a hydrophobic pocket at sub domain IIA and at position 134 (Trp134) at sub domain IB, which is exposed to solvent [20–22]. BSA is negatively charged in the solution, which can interact with cationic polymers/polysacccharides. Among existed polycations, chitosan (CH) has been recognized as a promising material for development of nano-size DDS due to its cationic nature, non-toxic profile, biodegradability, biocompatibility [23]. CH is amino polysaccharides obtained from deacetylation of chitin and is composed of 1,4-linked 2-amino-2-deoxy-*β-D*-glucan and 1,4 linked 2-acetamido-2-deoxy-*β-D*-glucan [24]. NPs formed from the assembly of CH and albumins has been previously demonstrated for encapsulation and delivery of anti-cancer drugs such as doxorubixin (DOX) [18], alprazolam [25], paclitaxel (PTX) [26], ibuprofen [27], and as a gene carrier [28]. However, one limitation in utilizing CH as a drug nano carrier is its poor water solubility and possible aggregation at physiological conditions (neutral pH and high salt concentrations) because its pK_a is only 6.5 [23,24].

In this study, we fabricated NPs from the assembly between reduced BSA (rBSA) and glycol chitosan (GC) (**Fig. 4-1B**), a water soluble derivative of CH, for encapsulation and delivery of hydrophobic anti-cancer drug, PTX (**Fig. 4-1C**). The formation of nanocomplexes from rBSA and GC (rBG NPs) was studied as a function of a rBSA/GC mass ratio and pH. The physical characteristics and stability of these NPs were evaluated by dynamic light scattering (DLS) and compositional analysis. Finally, the ability of rBG NPs as PTX nano-size DDS was demonstrated.

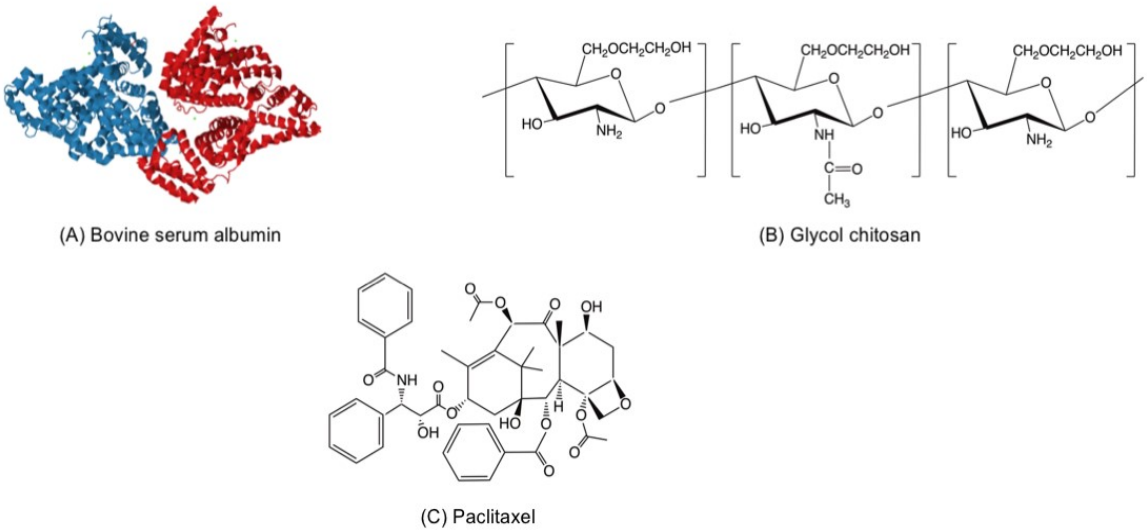

Fig. 4-1 The crystal structure of (A) BSA (PDB-ID:3v03). The chemical structure of (B) GC and (C) PTX.

4.3 Experimental

4.3.1 Materials

Bovine serum albumin (free fatty acid, 98% purity), glycol chitosan (free amine group ≥ 60%, degree of polymerization of min. 400), methanol, acetonitrile (HPLC grade), ethanol, urea, and Tris(2-carboxyethyl)phosphine hydrochloride (TCEP.HCl) were purchased from Wako Pure Chemical Industries, Ltd. (Osaka, Japan). Paclitaxel and L-cysteine were purchased from Tokyo Chemical Industry Co., Ltd. (Tokyo, Japan). The Quick Start™ Bradford Protein Assay was purchased from Bio-Rad, Inc. (Hercules, CA, USA). Tween 80, rhodamine B

isothiocyanate (RBITC), and dimethyl sulfoxide (DMSO) were purchased from Sigma-Aldrich, Inc (St. Louis, MO, USA). 5,5-dithio-bis-(2-nitrobenzoic acid) (DTNB) was purchased from Kishida Chemical Co., Ltd. (Osaka, Japan). A cell counting kit, WST-8, and Hoechst 4432 solution were purchased from Dojindo Laboratories, Inc. (Kumamoto, Japan). Minimum essential medium (MEM), fetal bovine serum (FBS), penicillin, streptomycin, and OPTI-MEM were purchased from Thermo Fisher Scientific, Inc. (Waltham, MA, USA). Dulbecco's phosphate-buffered saline (D-PBS) was purchased from Nacalai Tesque, Inc. (Kyoto, Japan). Cremophor EL was obtained from Fluka Biochemika, Germany. All other chemicals were analytical grade.

4.3.2 Preparation and Formation of rBG NPs

Reduction of BSA. The reduction of BSA (rBSA) was carried out using TCEP.HCl under denaturing conditions [29]. Briefly, BSA (100 mg) and TCEP.HCl (86 mg) were separately dissolved in 5 mL reducing buffer (25 mM Tris-HCl, 8 M urea, and 0.1 mM EDTA). Then, the BSA solution were mixed with TCEP.HCl solution and incubated at 25 ^{o}C for 4 h. The solution was then dialyzed against 500 mL of 1 mM HCl using a 12-14 kDa dialysis membrane (Spectra/Por®, Repligen Corp., Waltham, MA, USA) for 3 days at 4 ^{o}C with 4 changes to remove excess urea and TCEP.HCl. The protein concentration in rBSA solution was measured by the Bradford assay. The number of free thiols per BSA molecule was determined by the Ellman's assay. L-cysteine was used to obtain a standard calibration curve for quantifiying the number of free thiols. Under these experimental conditions, the number of free thiols per BSA molecule generated after reduction process was about 21. The rBSA solution was stored at 4 ^{o}C before use.

Purification of glycol chitosan. GC was purified by dialysis and filtration methods [30]. Briefly, GC (10 mg/mL) was dissolved in Mili-Q water under a gentle magnetic stirring, and the pH was adjusted to 5.5. The GC solution was then dialyzed against Milli-Q water using a

12-14 kDa membrane for overnight at room temperature and filtered using a 0.4 μm membrane filter. Finally, the GC solution was lyophilized for 48 h and stored at 4 ºC before use.

Formation of rBG NPs. The formation of rBG NPs was carried out by simply mixing rBSA and GC solutions to yield rBG NPs. Briefly, a GC solution (2 mg/ml) was prepared by dissolving lyophilized GC in 10 mM acetate buffer pH 5.5 under stirring until completely dissolved and stored at 4 ºC overnight for complete hydration. A rBSA solution (2 mg/ml) was prepared from the stock solution by diluting with 1 mM HCl. rBG NPs were formed by slowly adding rBSA solution to an equal volume of GC solution under mild stirring at room temperature (25 ºC), and the final pH adjusted to the desired values with 0.1 M HCl or NaOH.

The composition of rBSA and GC in the NPs. The composition of rBSA and GC in the NPs was determined by a centrifugation method. In general, 1 mL of rBG NPs solution was centrifuged (18000 *g*, 20 ºC, 30 min), and the supernatant was collected. The amount of rBSA in rBG NPs was measured by the Bradford assay, whereas the amount of GC in rBG NPs was estimated using RBITC-labelled GC. The fluorescent labelling protocol of GC was carried out based on the previous method [31] with a slight modification as follows. Briefly, 0.1 g of GC was dissolved in 10 mL Milli-Q water, and an equal volume of methanol was added and stirred for 2h. 6.5 mL of methanolic solution of RBITC (0.2 mg/mL) was then added to the GC solution and stirred for overnight under light protection. Purification was then carried out by centrifugal filtration (Amicon Ultra; molecular weight cut-off, 30 kDa; Millipore Corp., Billerica, MA, USA) and dialysis against 1 L of Milli-Q water (12-14kDa, Spectra/Por®, Repligen Corp., Waltham, MA, USA). Finally, the pH of the RBITC-GC solution was adjusted to 5.5 and then lyophilized. The degree of labelling was calculated to be 0.08 (% mol/mol). The concentration of GC was estimated using a standard curve generated from the absorbance of RBITC-GC at 556 nm.

Stability of rBG-NPs in various buffers. Briefly, 1 mL of rBG NPs solution was purified using a centrifugation method (9000 *g*, 20 ^{o}C, 30 min) under a 10 μl glycerol bed. The supernatant was removed, and the precipitated rBG NPs were washed 2 times with Milli-Q water. The purified rBG NPs were then redispersed in PBS or the desired buffer solutions and stored at 37 ^{o}C for 1 day. The particle size and polydispersity index (PDI) of rBG NPs in various buffers were noted.

4.3.3 PTX-loaded rBG NPs

PTX was loaded into rBG NPs using adsorption and mixed method. In the adsorption method, a small amount of ethanolic PTX solution (4 mg/mL) was added into 2 mL of rBG NPs solution and gently stirred for 10 min. In the mixed method, PTX was first added into rBSA solution, and then the mixture was added slowly into the GC solution under gentle magnetic stirring. In some cases, PTX-loaded rBG NPs were freeze-dried using 5% trehalose as a cryoprotectant.

4.3.4 Characterization of rBG NPs and PTX-loaded rBG NPs

The Z-average particle size, PDI, derived count rate, and zeta potential of the NPs were measured by dynamic light scattering (DLS; Zetasizer Nano ZS, Malvern Instruments Ltd., Worcestershire, United Kingdom). The shape and morphology of the NPs was observed by transmission electron microscopy (TEM) (JEM 2010, JEOL) at an accelerating voltage of 120 kV. The NPs were stained with 2% uranyl acetate before imaged. The structural characteristics of rBSA was analyzed by a circular dichroism (CD) spectropolarimeter (J-725G, JASCO, Tokyo, Japan) and a fluorescence spectrophotometer (LS55C, Perkin Elmer, Waltham, MA, USA). The encapsulation efficiency (EE) was determined by an extraction method. Briefly, an aliquot of PTX-loaded rBG NPs were mixed with an ethanol at a 1:4 volume ratio and filtered (0.2 μm; Milex®-LG; Millipore Corp., Billerica, MA, USA) before injection into a reversed-phase high performance liquid chromatograph equipped with an auto sampler (Jasco LC-4000,

Jasco Inc., Easton, MD, USA). A C-18 column (InertSustain; GL Sciences, Inc., Tokyo, Japan) was used with a mobile phase of acetonitrile (60% by vol) and Milli-Q water at a flow rate of 0.8 ml/min. The EE (%) of PTX-loaded rBG NPs were calculated using the following equation:

$$\text{EE (\%)} = \frac{\text{Total PTX loaded}}{\text{Total PTX added}} \times 100\%$$

4.3.5 Release profile in vitro of PTX from rBG NPs

The release profile of PTX from rBG NPs was carried out using a dialysis method at pH 7.4. Briefly, 1.5 ml of lyophilized PTX-loaded rBG NPs (25 μg/ml) in PBS pH 7.4 was put in a dialysis membrane (Spectra/Por®, 12-14 kDa molecular weight cut-off). The dialysis bags were then immersed in 25 ml of the release medium (10 mM PBS pH 7.4 containing 5% ethanol and 1% Tween 80) and placed in an incubator shaker at 37 ºC and 60 rpm for 10h. 5% ethanol and 1% Tween 80 was used to provide sink condition [32][33]. At predetermined time, 500 μl of release medium containing PTX was collected and replaced with the same amount of pre-warmed release medium. The amount of PTX was determined using HPLC analysis, as described aboved.

4.3.6 Cellular studies *in vitro*

Cellular uptake of rBG NPs. Cellular uptake of rBG NPs in HeLa cells was evaluated by CLSM. RBITC-GC was used to detect fluorescent signal of rBG NPs. Briefly, HeLa cells were seeded in a multi-well glass bottom dish (Matsunami Glass Industries, Ltd., Osaka, Japan) at a density of 10 000 cells per well and incubated 24 h at 37 ºC under CO_2 atmosphere. Then, the medium was removed and 200 μl of RBITC-labelled rBG NPs, dispersed in OPTI-MEM, added to the dish. After 2 h of incubation, the samples were removed and washed thrice with D-PBS. The cells were then fixed with 4% paraformaldehyde (Wako Pure Chemical Industries, Ltd.) at 25 ºC for 10 min. Later, nuclear staining of HeLa cells was done using Hoechst 4432, according to the manufacturer's instruction. Finally, the cells were viewed under an LSM 700

confocal microscope (Carl Zeiss AG, Oberkochen, Germany) equipped with a diode laser. Rhodamine filter were used to observe the red fluorescence of RBITC-labelled rBG NPs.

Cytotoxicity studies in vitro. The cytotoxicity of rBG NPs and PTX-loaded rBG NPs against HeLa cells were evaluated by WST assay. The cytotoxicity of Taxol-like formulation was also evaluated as a positive control. HeLa cell line was provided by the RIKEN BRC through the National Bio-Resource Project of the MEXT, Japan. HeLa cells were grown in MEM medium containing 10% FBS and 1% antibiotic-antimycotic (Thermo Fisher Scientific, Inc.). HeLa cells were seeded at a density of 5000 cells per well in a 96-well plate (Greiner Bio-One GmbH, Frickenhausen, Germany) and incubated 24 h under a 5% CO_2 atmosphere. Then, the medium was removed and washed with D-PBS. Afterward, the cells were exposed to Taxol-like formulation, rBG NPs, and PTX-loaded rBG NPs in a reduced serum medium (OPTI-MEM, Thermo Fisher Scientific, Inc.) at varying concentrations. After 24 and 48 h of incubation, the samples were removed and 100 µl of WST-8 cell counting solution in OPTI-MEM added to each well. After a 3 h of incubation, the A_{450} was read using a microplate reader (Bio-Tek Instrument, Inc., Winooski, VT, USA) and cell viabilities expressed as the percentage of living cells over untreated cells.

4.3.7 Statistical analysis

The statistical analysis was performed using ANOVA and Student's t-test with Microsoft Excel (Version 2017 for Macintosh, Microsoft Corp, Redmond, WA, USA). P values of < 0.05 were considered statistically significant.

4.4 Results and Discussion

4.4.1 Formation and characterization of rBG NPs

Reduction of BSA. The formation of rBG NPs involved the initial reduction of BSA and the complexation between rBSA and GC under certain environmental conditions. The reduction of BSA would be expected to increase hydrophobicity as the hidden hydrophobic domain would be exposed due to the alteration of the structure of BSA [34]. The number of free thiols per BSA molecule would also increase due to the breakdown of disulfide bridges. An increase in hydrophobicity and the number of free thiols of BSA would benefit the stability of rBG NPs by forming stronger hydrophobic interaction with GC and BSA self-crosslinking through thiol-disulfide exchange reactions and/or oxidation of free thiols [35]. In this study, TCEP.HCl was selected as a disulfide reductant due to its less sensitivity against oxygen and good activity in a broad range of pH, as compared with other commonly used reductants such as dithiothreitol (DTT) [36]. The number of free thiols per BSA was about 21, corresponding to ~ 60 % of the maximum number of free thiols that can be generated. The structural characteristics of rBSA was evaluated by CD analysis and fluorescence spectroscopy. The CD spectrum of native BSA shows negative bands at 222 nm and 208 nm (**Fig. 4-2 left**), which are characteristics of α-helix structure [37]. On the other hand, CD spectrum of rBSA shows a denatured-like form, indicating that the secondary structure of BSA was changed. The fluorescence intensity of BSA decreased and a slight red-shift in the emission maxima was seen after reduction, suggesting that protein unfolding took place (**Fig. 4-2 right**) [38].

Transformation from globular state (folding) to linear form (unfolding) [35] would also be expected to enhance the electrostatic complexation between BSA and GC.

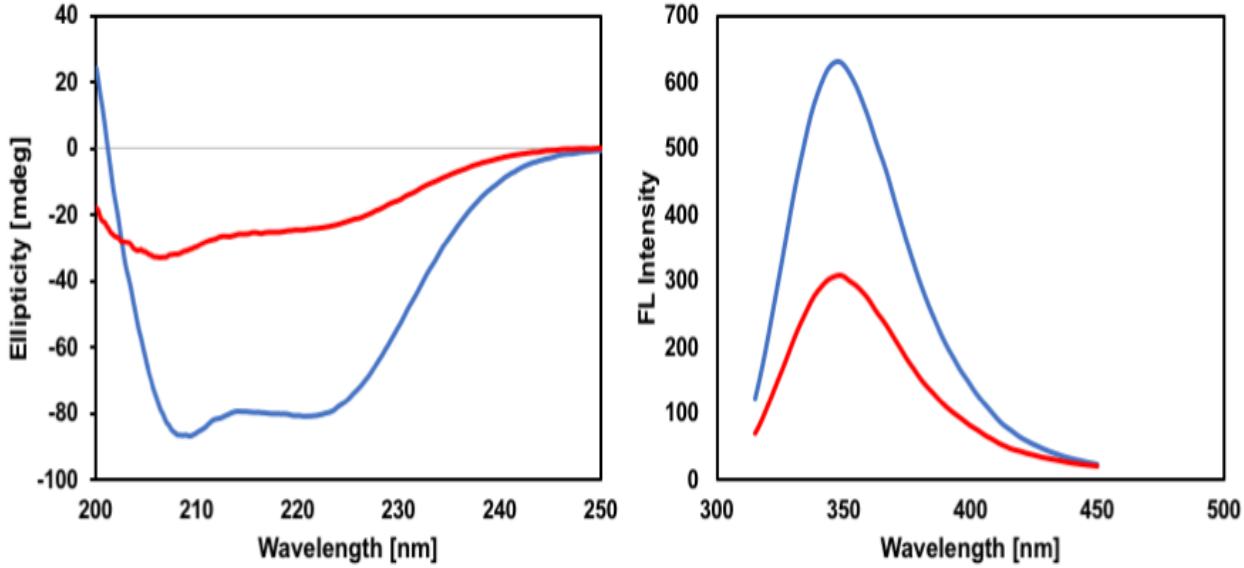

Fig. 4-2 CD (left) and fluorescence emission (right) spectra of native BSA (blue) and rBSA (red). The samples were excited at 295 nm for fluorescence emission spectra.

Effect of rBSA/GC mass ratio. The formation of rBG NPs was then carried out by mixing rBSA and GC in an aqueous solution with very low ionic strength (5 mM acetate buffer). Considering that the physical characteristics of NPs were affected by the initial mass ratio of proteins/polysacccharides, we investigated the effect of rBSA/GC mass ratio on the physical properties of rBG NPs (particle size, PDI, zeta potential, and derived count rates) by DLS measurements. The electrostatic interactions would be expected to occur at the pH above the isoelectric point (pI) of BSA (~4.9) and below the neutral pH (~7) where GC was protonoted. Thus, we set the conditions at a fixed pH value of 5.7, total biopolymer concentration of 2 mg/mL, predetermined in the preliminary study, and varied rBSA/GC mass ratios (4:1, 2:1, 1:1, and 1:2), for this experiment. The Z-average diameter (particle size) at varied rBSA/GC mass ratios remained the same with an average diameter of ~250 nm, except at a rBSA/GC mass ratio of 1:2, where a marked increase in the particle size (~350 nm) was observed (**Fig.**

4-3A). The PDI values within all mass ratios remained the same with an average of 0.2, indicating quite narrow particle size distributions. Irrespective of the rBSA/GC mass ratios, the zeta potentials of rBG NPs were positive (+30 mV). The zeta potentials tended to increase with increasing GC concentrations although a slight decrease in the zeta potential at the highest GC concentration (at a rBSA/GC mass ratio of 1:2) was seen (**Fig. 4-3B**). The derived count rates of rBG NPs showed a decreasing trend with increasing GC concentrations (**Fig. 4-3C**). The derived count rates can be used to estimate the number of particles in the solution [39]. These findings indicate that higher rBSA concentrations are required to form rBG NPs with smaller particle size and higher number of particles. Considering the colloidal stability of rBG NPs, we selected a rBSA/GC mass ratio of 1:1 for the following experiment due to a higher zeta potential value (+35 mV) with small and sufficient number of particles.

Effect of pH. The effect of pH on the particle size, PDI, zeta potential, and the derived count rate of rBG NPs were studied by DLS analysis (**Fig. 4-4**). The Z-average diameter showed an increasing trend (from 70 ± 2 nm to 367 ± 36 nm) with increasing pH from 4.9 to 6.5. Similarly, the number of particles increased with an increase in the pH values. In contrast, the zeta potential values showed a decreasing trend with increasing pH, with the lowest zeta potential value of + 24 mV at a pH of 6.5. An increase in the particle size and a decrease in the zeta potential values might be due to bridging effects and charge neutralization of the complex [40] as pH was increased from 4.9 to 6.5. The PDI values also showed a decreasing trend with increasing pH from 4.9 to 6.5, with the lowest PDI of ~0.2 at pHs of 5.7 and 6.5.

The composition of rBG NPs. To get an insight into the nature of interaction between rBSA and GC and to confirm the findings from DLS analysis, we evaluated the composition of rBSA and GC in rBG NPs using a centrifugation method, assuming that the centrifugal forces are not affecting the original structure of rBG NPs. The amount of rBSA in rBG NPs was determined using the Bradford assay, while the amount of GC was estimated using

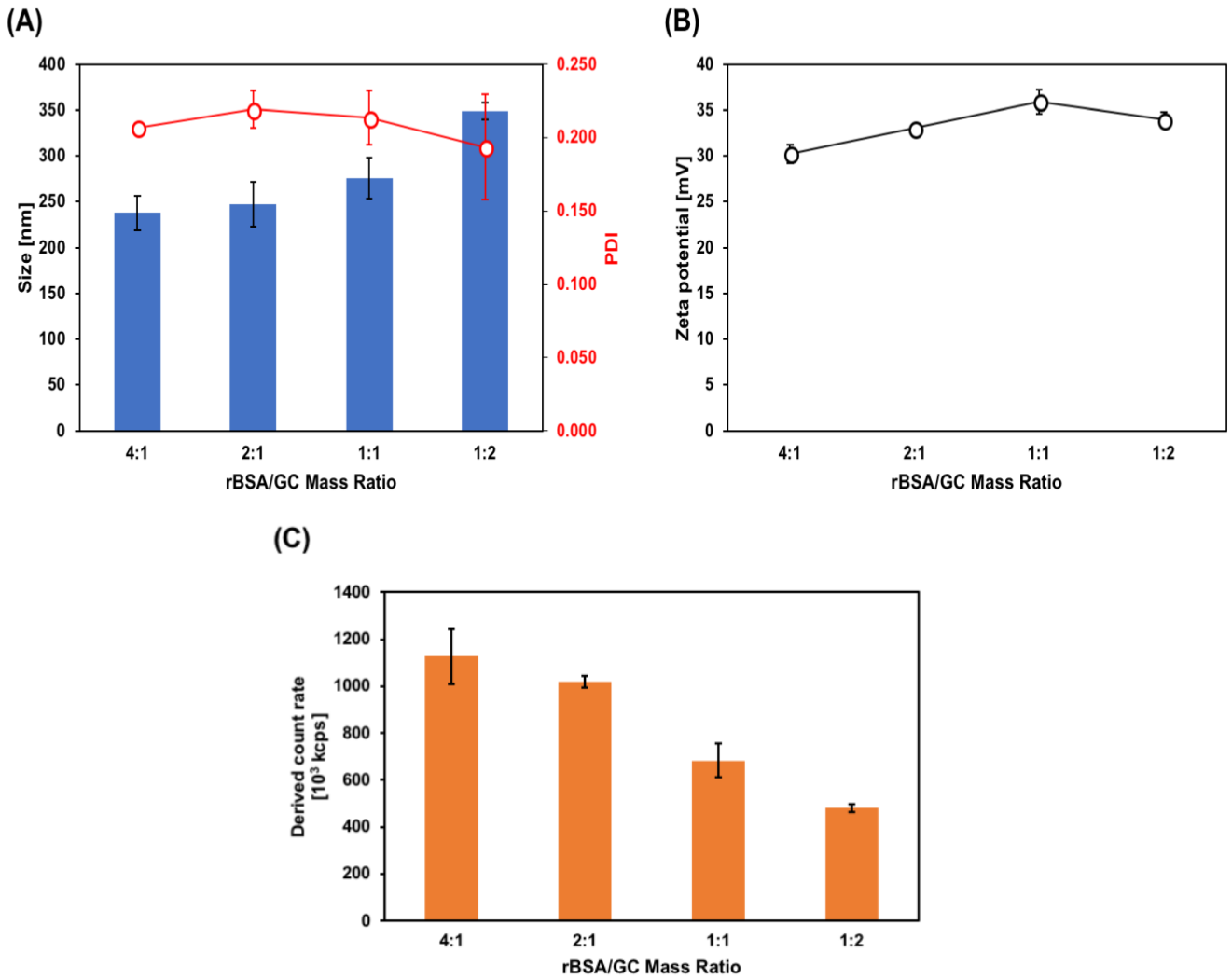

Fig. 4.3 The effect of rBSA/GC mass ratio on (A) particle size and PDI, (B) zeta potential, and (C) derived count rate. Total rBSA + GC concentration was 2 mg/mL and pH 5.7.

RBITC-labelled GC. It should be mentioned that RBITC conjugation into GC was optimized such that the formation of RBITC-GC NPs was prevented, as previously reported [41]. The amount of rBSA and GC in rBG NPs was studied as a function of rBSA/GC mass ratio and pH, with similar experimental conditions as previously discussed. The compositional analysis showed that the amount of rBSA and GC was not greatly affected by a rBSA/GC mass ratio, although the amount of GC involved in rBG NPs tended to be higher at higher rBSA concentrations, particularly at a rBSA/GC mass ratio of 4:1 (**Fig. 4-5**). In contrast, the pH appeared to affect the amount of rBSA and GC in rBG NPs. Increasing the pH from 4.9 to 6.5

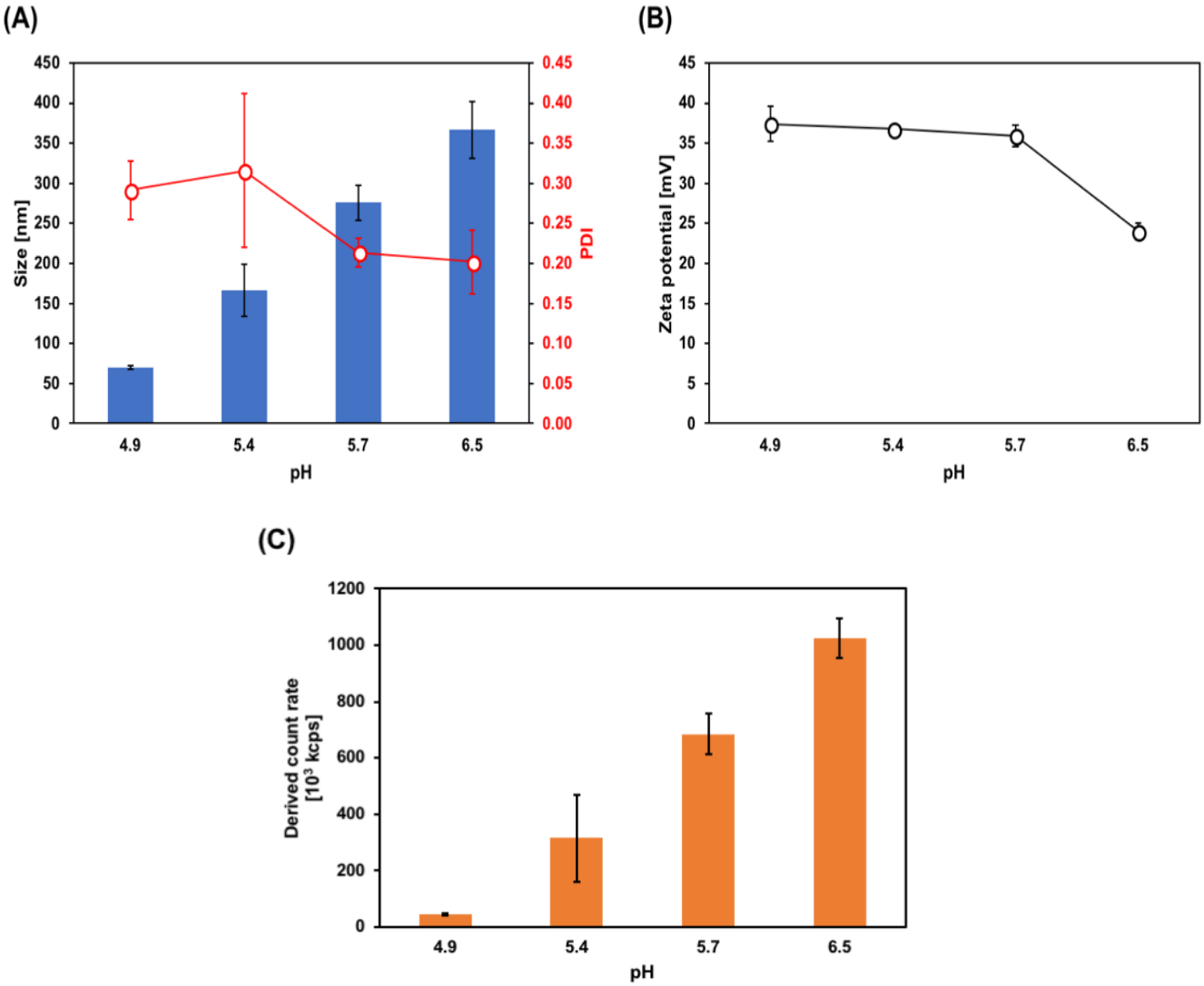

Fig. 4-4 The effect of pH on (A) particle size and PDI, (B) zeta potential, and (C) derived count rate. Total rBSA + GC concentration was 2 mg/mL and rBSA/GC mass ratio of 1:1.

increased the percentage of rBSA (from 67 ± 3 % to 97 ± 1 %) and GC (from 3.6 ± 1 % to 15.1 ± 3 %) present in rBG NPs, indicating that the complexation of rBSA and GC was promoted at slightly higher pH near the pK_a of GC (~8). This result might be attributed to the neutralization of the complex at this pH, which increases the amount of rBSA and GC present in rBG NPs. It is also suggested that other non-covalent forces such as hydrophobic interactions play an important role in the complexation of BSA and native chitosan (CH) [42], which may be applicable in the case of GC and rBSA.

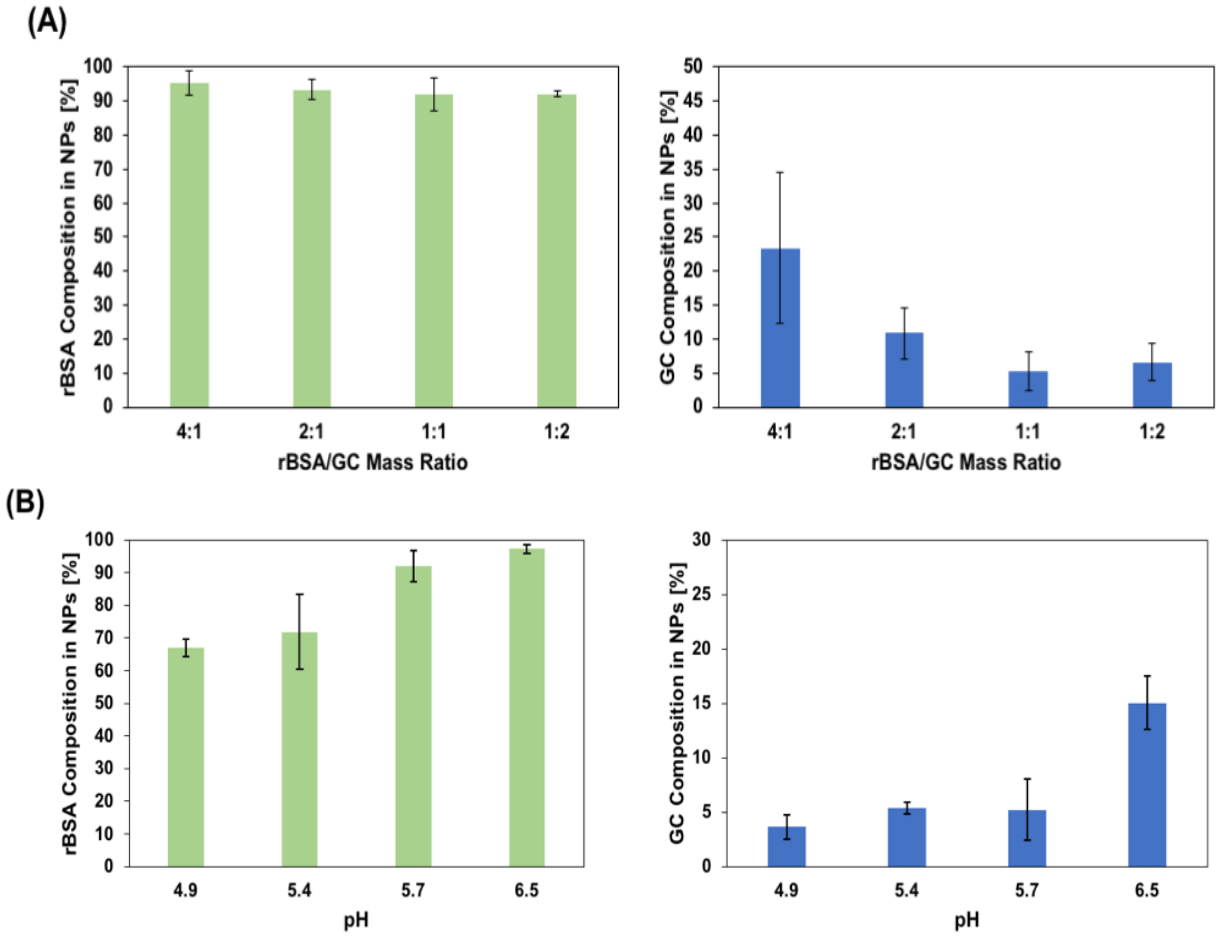

Fig. 4-5 Composition of rBSA and GC in rBG NPs as a function of (A) rBSA/GC mass ratio and (B) pH. The amount of rBSA/GC in the NPs was estimated by concentration difference of rBSA/GC in total added and in supernatant before and after centrifugation (18000 *g*). The concentration of rBSA and GC in supernatant was determined by Bradford assay and fluorescent labelled-GC.

Stability and morphology of rBG NPs. To evaluate the stability of rBG NPs against various buffers and to understand the interaction affecting the formation of rBG NPs, rBG NPs formed at a rBSA/GC mass ratio of 1:1 and pH 6.5 were purified by a centrifugation method and redispersed in PBS pH 7.4, PBS with 25 mM glutathione (GSH), PBS with 100 mM Tween 20, and PBS with 100 mM urea. The particle size and PDI were measured by DLS after a 1-day incubation at 37 ^{o}C. A marked increase in the particle size was noticed after rBG NPs were incubated in PBS containing 100 mM Tween 20, suggesting that hydrophobic interactions play

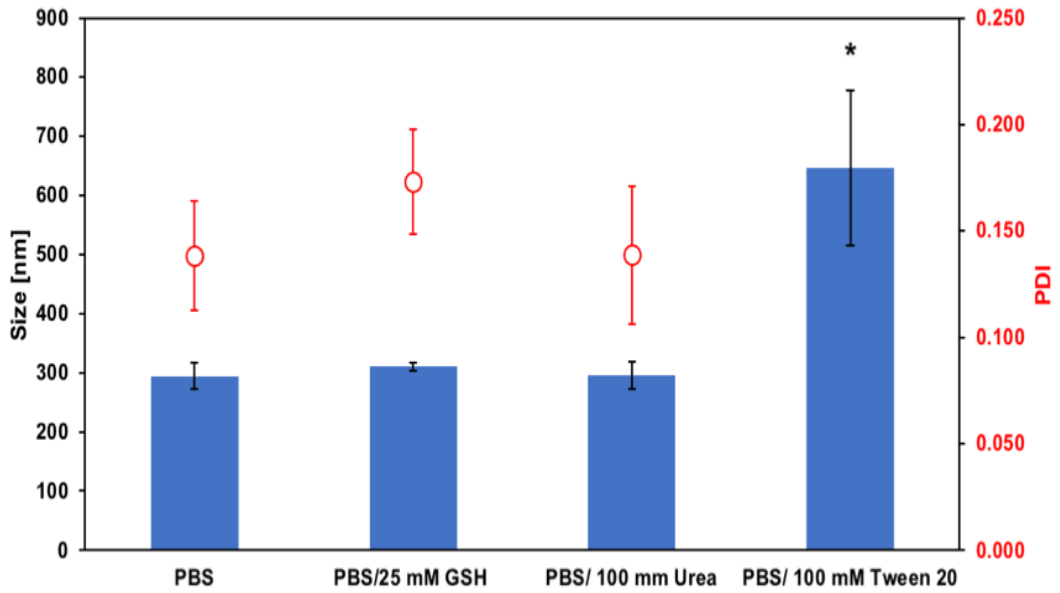

Fig. 4-6 Effect of destabilizing compounds on the particle size and PDI of rBG NPs. rBG NPs were incubated at 37 ^{o}C for 1 day. PDI value of rBG NPs in PBS/100 mM Tween 20 was excluded (PDI > 0.5). * indicates significant at $p < 0.05$.

a dominant role in the formation and stability of NPs (**Fig. 4-6**). In contrast, urea, which is responsible for breaking strong hydrogen bonds [43] was not effective in destabilizing rBG NPs, indicating that hydrogen bonding is not a critical force in rBG NPs. A slight increase in PDI was observed when rBG NPs were incubated in PBS with GSH, although GSH seemed to not affect the particle size. Also, the number of free thiols in rBG NPs dramatically decreased after incubated in PBS (data not shown). This suggests that the self-crosslinking of rBG NPs through the free thiols of rBSA might occur.

The morphology of rBG NPs was examined using TEM. **Fig. 4-7** shows a representative TEM image of rBG NPs formed at a rBSA/GC mass ratio of 1:1 and pH 6.5. rBG NPs had nearly spherical in shape and smaller particle size, as compared with DLS measurements. Some agglomeration of particles were observed. The smaller size and agglomeration of particles were possibly due to the drying effect during sample preparation.

The structure and formation mechanism of rBG NPs. DLS, compositional analysis, and stability test against various destabilizing agents suggest that rBG NPs possess a core-shell

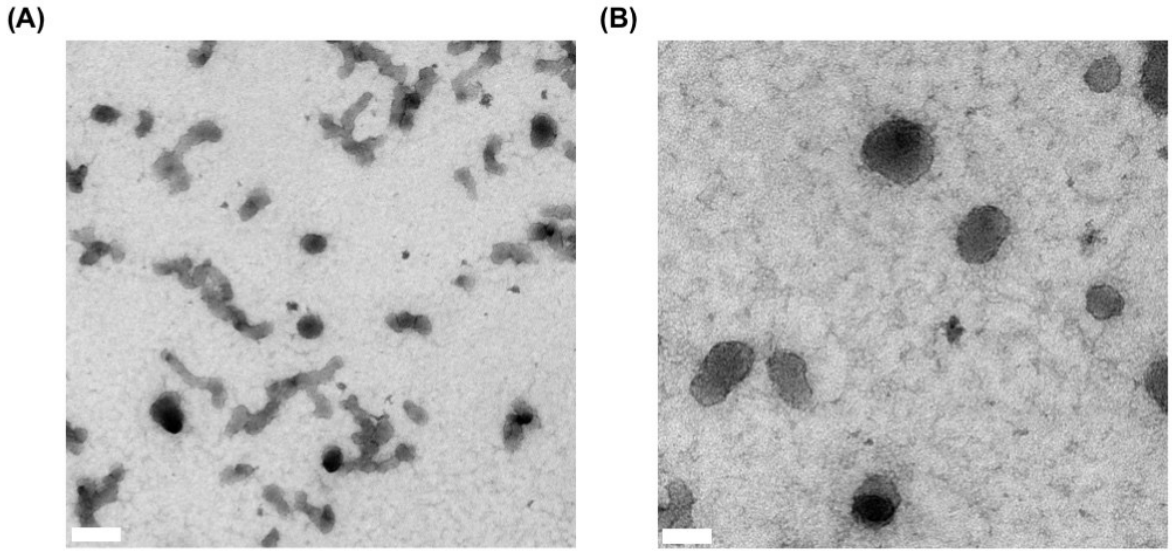

Fig. 4-7 Representative TEM image of rBG NPs (A), and that rBG NPs with higher magnification (B). The NPs were prepared at total biopolymer concentration of 2 mg/mL, rBSA/GC mass ratio of 1:1, and pH 6.5. Scale bars are 200 nm (A) and 100 nm (B).

structure and their formation is mainly promoted by both hydrophobic and electrostatic interactions. rBSA is prone to self-aggregation in the aqueous solution due to its exposed hydrophobic domains, especially at a pH near its pI (~5). rBSA self-aggregation conceivably form the core of rBG NPs, whereas GC acts as a stabilizer to prevent strong rBSA self-aggregation via the electrostatic interactions at a pH where rBSA and GC are oppositely charged (~5 < pH < ~8). According to DLS and compositional analysis, the complexation between rBSA and GC is strengthen at a relatively higher pH (6.5). Beyond this pH value, either precipitation or complex dissociation was observed (data not shown), suggesting that the electrostatic interactions are also critical in stabilizing the complexation between rBSA and GC. In addition, the free thiols in BSA generated after reduction process might also contribute in enhancing the stability of rBG NPs via thiol crosslinking reaction.

4.4.2 PTX-loaded rBG NPs and release profile of PTX from rBG NPs

To evaluate the ability of rBG NPs to encapsulate and deliver a hydrophobic anti-cancer drug, we selected PTX as a representative model drug. rBG NPs formed at a rBSA/GC mass ratio of 1:1 and pH 6.5 was utilized for encapsulation of PTX. PTX was encapsulated into rBG NPs using mixed and adsorption method at a final concentration of 100 μg/ml. The properties of PTX-loaded rBG NPs were evaluated by DLS (**Table 4-1**). The particle size of PTX-loaded rBG NPs using adsorption method was 349 ± 26 nm, which is quite similar to that of blank rBG NPs. In contrast, after loading PTX using mixed method, an increase in the particle size (421 ± 29 nm) was observed, which might be due to the PTX-induced rBSA self-aggregation [44]. No difference was observed in PDI and the derived count rate between the two methods. The encapsulation efficiencies (EE) of PTX in rBG NPs using mixed and adsorption method were 96 ± 5 and 84 ± 13 %, respectively (**Table 4-1**). The high encapsulation efficiency was due to effective PTX binding to rBG NPs through hydrophobic interactions, with rBSA's hydrophobic domains.

Table 4-1. Characteristics of PTX-loaded rBG NPs

Samples	Size [nm]	PDI	Derived count rate [10^3 kcps]	EE [%]
Mixed Method	421 ± 29	0.212 ±0.015	1069 ± 212	96 ± 5
Adsorption Method	349 ± 26	0.194 ±0.010	1170 ± 128	84 ± 13

Data, mean ±standard deviation, *n*=3

The release of PTX from rBG NPs was evaluated using a dialysis method at pH 7.4 (10 mM PBS) which simulates a physiological condition. 1% Tween 80 and 5% ethanol were used in the release medium to ensure that PTX is soluble and can freely diffuse to the outside of the dialysis bag. Without addition of ethanol, PTX could be precipitated inside the dialysis bag

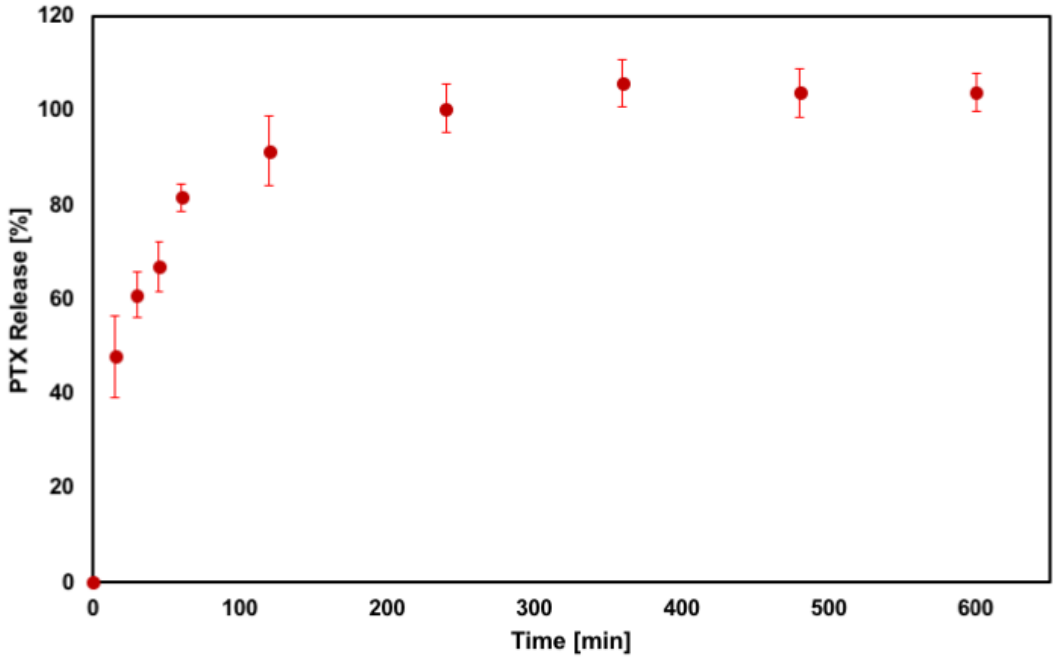

Fig. 4-8 Release profile of PTX from rBG NPs at pH 7.4. Data are reported as mean ± standard deviation, n =3

because the solubility of PTX in PBS was below 0.5 μg/ml, and the results obtained could be misleading [32]. The release profile of PTX from rBG NPs showed a burst release within 15 min and followed by a sustained release for up to 2 h (**Fig. 4-8**). The release of PTX from rBG NPs was completed within 4 h. This quick release PTX profile might be attributed to the presence of ethanol in the release medium, which can diffuse from the release medium to the inside of the dialysis bag. Thus, PTX could be released much faster due to weakened hydrophobic interaction between PTX and rBG NPs.

4.4.3 Cellular studies *in vitro*

Cellular uptake of rBG NPs. The cellular uptake of rBG NPs was evaluated in HeLa cells using CLSM. GC was labelled by RBITC to yield red fluorescence signal that can be used to follow the intracellular fate of rBG NPs. HeLa cells were incubated with rBG NPs for 2 h at 37 ^{o}C. Hoechst 4432 (blue) were used to stain nucleus. The *z*-stack mode of CLSM was employed to precisely determined the spatial location of rBG NPs within HeLa cells. **Fig. 4-9**

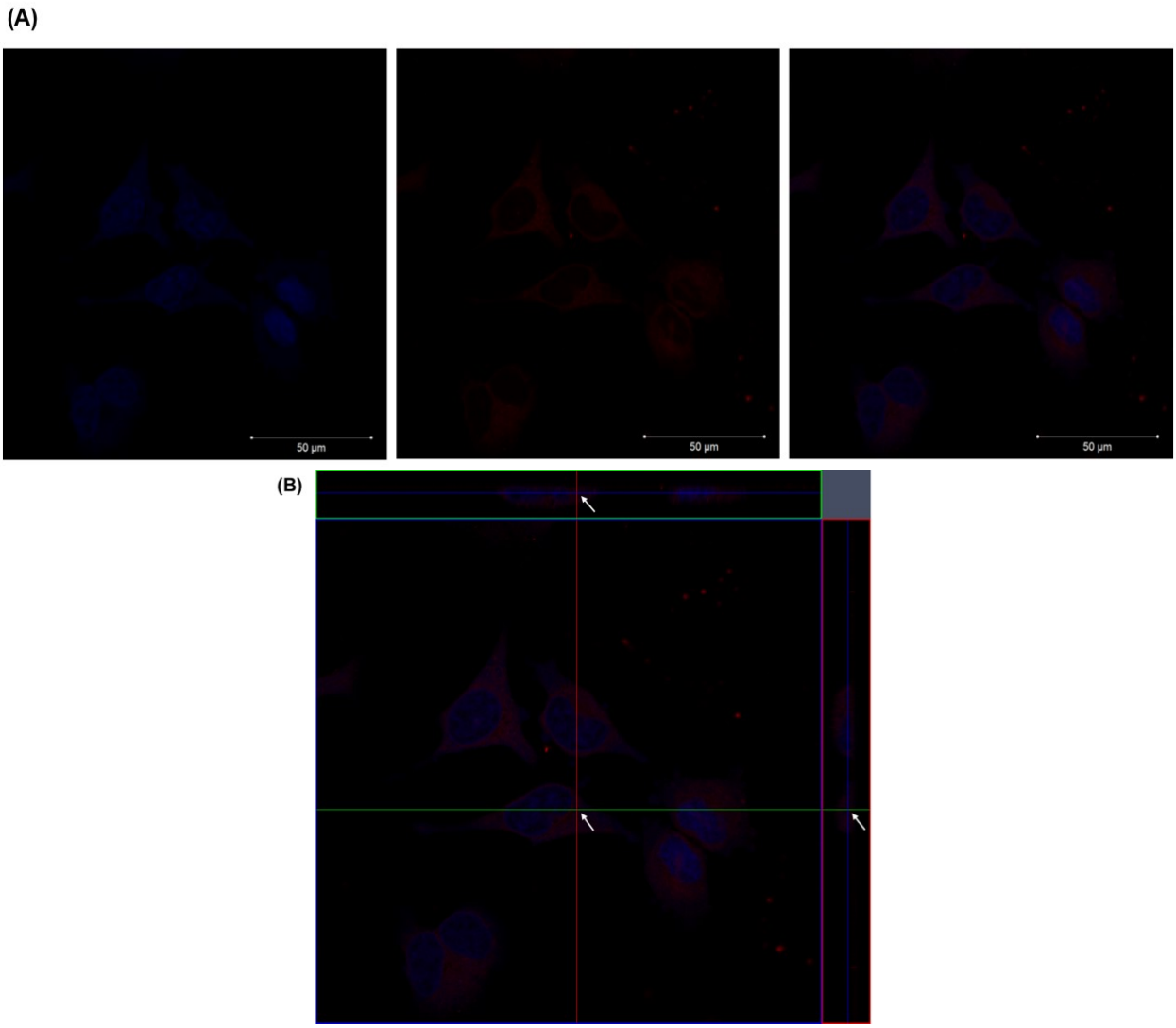

Fig. 4-9 Cellular uptake of rBG NPs (red) in HeLa cells at 37 ºC for 2 h examined by z-stack 3D CLSM. Hoechst (blue) used to stain nucleus (A) and orthogonal view of z-stack image (B). Intersection points (white arrow) indicate that location of rBG NPs was inside cells.

showed that a considerable red fluorescence signal could be found inside the cells, which suggests that rBG NPs were internalized. NPs can undergo internalization via endocytosis-related pathways such as macro-pinocytosis, caveola- and clathrin-mediated endocytosis [45]. To find out whether endocytosis is the pathway for rBG NPs, the cellular uptake was performed for 2 h at 4 ºC, where the internalization via endocytosis decreases due to changes in the cell membrane fluidity [46]. **Fig. 4-10** showed that most of the red fluorescence signals were not found inside the cells, implying that the intracellular transport of rBG NPs is through

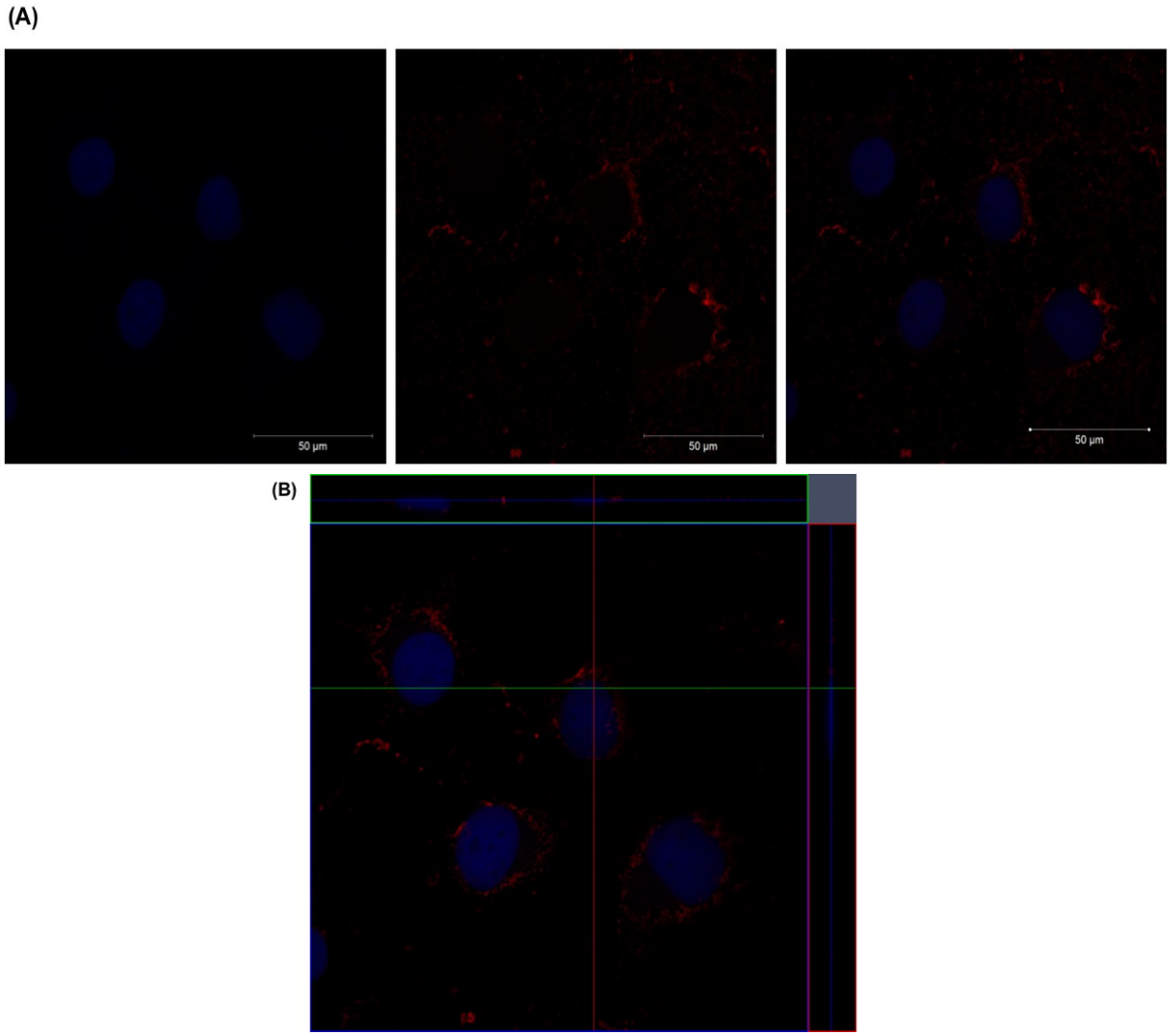

Fig. 4-10 Cellular uptake of rBG NPs (red) in HeLa cells at 4 ºC for 2 h examined by z-stack 3D CLSM. Hoechst (blue) used to stain nucleus (A) and orthogonal view of z-stack image (B). Z-stack image indicates that rBG NPs were poorly internalized by the cells.

endocytic-related pathway. Although further cellular experiments need to be carried out to confirm the intracellular fate of rBG NPs in more details, previous reports revealed that endocytosis-related pathways are a predominant intracellular transport for GC-based NPs [47][48].

Cytotoxicity in vitro of PTX-loaded rBG NPs. The cytotoxicity *in vitro* of PTX-loaded rBG NPs was evaluated on HeLa cells. Taxol-like formulation and blank rBG NPs served as a positive and negative control, respectively. HeLa cells were treated with samples containing

various PTX concentrations for 24 and 48 h and cell viability determined by WST-8 assay. The cytotoxicity *in vitro* results for 24 h of incubation are shown in **Fig. 4-11A**. Cell viability was

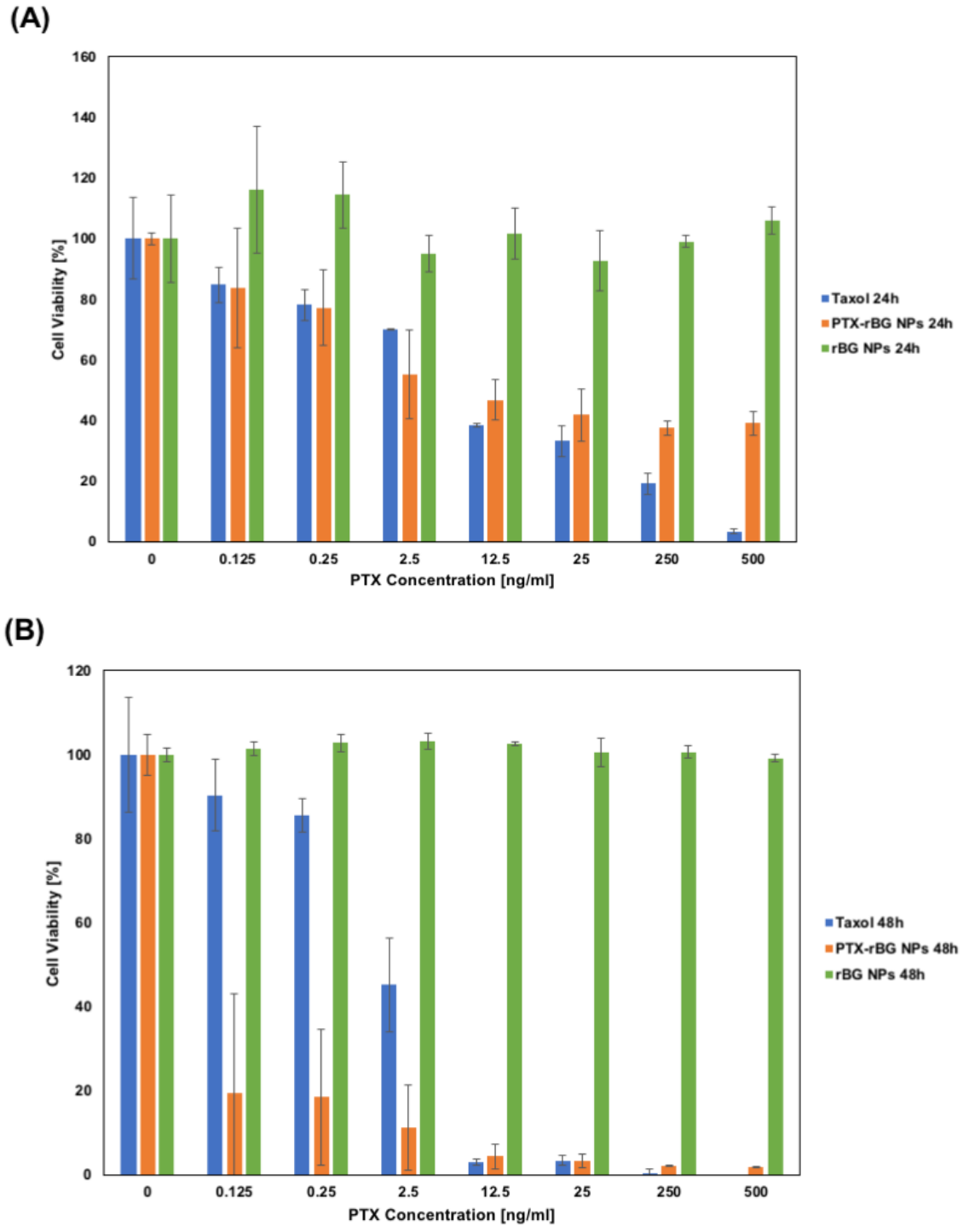

Fig. 4-11 Cytotoxicity *in vitro* of Taxol-like formulation, PTX-loaded rBG NPs, and unloaded rBG NPs in HeLa cells by WST-8 assay after 24 h (A) and 48 h (B) incubation.
Data, mean ± standard deviation, $n = 3$

not considerably affected by exposure with blank rBG NPs, indicating that rBG NPs was biocompatible and nontoxic. Cell viability decreased with increasing PTX concentrations after exposure of Taxol-like formulation and PTX-loaded rBG. However, the cytotoxicity of PTX-loaded rBG NPs was lower compared with that of Taxol-like formulation. After prolonging incubation time to 48 h, the cytotoxicity of PTX-loaded rBG NPs was comparable to that of Taxol-like formulation (**Fig. 4-11B**). These results suggest that PTX was slowly released from rBG NPs. The discrepancy observed between *in vitro* release of PTX and the cellular experiment requires more reliable, proper, accurate experimental method to precisely determine *in vitro* release of hydrophobic molecules from NPs, in particular.

.

4.5 Conclusions

The formation of core-shell NPs based on the complexation between rBSA and GC (rBG NPs) was demonstrated. The electrostatic and hydrophobic interactions played dominant roles in the formation and stability of rBG NPs, as determined by DLS and compositional analysis. The particle size of rBG NPs was tunable by simply adjusting a rBSA/GC mass ratio and pH. rBG NPs was spherical in shape and had excellent stability at the neutral pH (10 mM PBS pH 7.4). rBG NPs had the ability to encapsulate hydrophobic anti-cancer drug, PTX with high encapsulation efficiency through hydrophobic interactions. CLSM analysis revealed that rBG NPs could be effectively internalized into cells, possibly via endocytosis-pathway. WST-8 assay showed that PTX-loaded rBG NPs had a comparable cytotoxicity *in vitro* on HeLa cells compared with Taxol-like formulation after a 48 h of incubation, which might be due to the slow release of PTX from these NPs. Ultimately, rBG NPs showed little toxicity, suggesting that these NPs hold great promise for use as a hydrophobic drug nano-carrier in the pharmaceutical and medical applications.

References

[1] A. Wicki, D. Witzigmann, V. Balasubramanian, J. Huwyler. Nanomedicine in Cancer Therapy: Challenges, Opportunities, and Clinical Applications. J. Control. Release, 200 (2015) 138–157.

[2] T.A. Debele, S.L. Mekuria, H.C. Tsai. Polysaccharide Based Nanogels in the Drug Delivery System: Application as the Carrier of Pharmaceutical Agents. Mater. Sci. Eng. C. 68 (2016) 964–981.

[3] H. Gelderblom, J. Verweij, K. Nooter, A. Sparreboom. Cremophor EL: The Drawbacks and Advantages of Vehicle Selection for Drug Formulation. Eur. J. Cancer, 37 (2001) 1590–1598.

[4] A. Jhaveri, P. Deshpande, V. Torchilin. Stimuli-sensitive Nanopreparations for Combination Cancer Therapy. J. Control. Release, 190 (2014) 352–370.

[5] X. Huang, W. Liao, Z. Xie, D. Chen, C.Y. Zhang. A pH-responsive Prodrug Delivery System Self-Assembled From Acid-labile Doxorubicin-conjugated Amphiphilic pH-sensitive Block Copolymers. Mater. Sci. Eng. C, 90 (2018) 27–37.

[6] Y. Liu, T. Yang, S. Wei, C. Zhou, Y. Lan, A. Cao, J. Yang, W. Wang. Mucus adhesion- and penetration-enhanced Liposomes for Paclitaxel Oral Delivery. Int. J. Pharm, 537 (2018) 245–256.

[7] L. Chen, B. Chen, L. Deng, B. Gao, Y. Zhang, C. Wu, N. Yu, Q. Zhou, J. Yao, J. Chen. An Optimized Two-vial Formulation Lipid Nanoemulsion of Paclitaxel for Targeted Delivery to Tumor. Int. J. Pharm, 534 (2017) 308–315.

[8] H. Sun, Y. Liu, X. Bai, X. Zhou, H. Zhou, S. Liu, B. Yan. Induction of Oxidative Stress and Sensitization of Cancer Cells to Paclitaxel by Gold Nanoparticles with Different Charge Densities and Hydrophobicities. J. Mater. Chem. B, 6 (2018) 1633–1639.

[9] R.K. Das, A. Pramanik, M. Majhi, S. Mohapatra. Magnetic Mesoporous Silica Gated with Doped Carbon Dot for Site Specific Drug Delivery, Fluorescence and MR Imaging. Langmuir, 34 (2018) 5253–5262.

[10] J.P. Fuenzalida, F.M. Goycoolea. Polysaccharide-protein Nanoassemblies: Novel Soft Materials for Biomedical and Biotechnological Applications. Curr. Protein Pept. Sci, 16 (2015) 89–99.

[11] J. Yang, S. Han, H. Zheng, H. Dong, J. Liu. Preparation and Application of Micro/Nanoparticles Based on Natural Polysaccharides. Carbohydr. Polym, 123 (2015) 53–66.

[12] A.O. Elzoghby, W.M. Samy, N.A. Elgindy. Protein-based Nanocarriers as Promising Drug and Gene Delivery Systems. J. Control. Release, 161 (2012) 38–49.

[13] J.K. Yan, W.Y. Qiu, Y.Y. Wang, J.Y. Wu. Biocompatible Polyelectrolyte Complex Nanoparticles from Lactoferrin and Pectin as Potential Vehicles for Antioxidative Curcumin. J. Agric. Food Chem, 65 (2017) 5720–5730.

[14] M.A. Razi, R. Wakabayashi, Y. Tahara, M. Goto, N. Kamiya. Genipin-stabilized Caseinate-chitosan Nanoparticles for Enhanced Stability and Anti-cancer Activity of Curcumin. Colloids Surfaces B Biointerfaces, 164 (2018) 308–315.

[15] A. Akbari, J. Wu. Cruciferin Coating Improves the Stability of Chitosan Nanoparticles at Low pH. J. Mater. Chem. B, 4 (2016) 4988–5001.

[16] D. Hu, Z. Xu, Z. Hu, B. Hu, M. Yang, L. Zhu. pH-triggered Charge-reversal Silk Sericin-based Nanoparticles for Enhanced Cellular Uptake and Doxorubicin Delivery. ACS Sustain. Chem. Eng, 5 (2017) 1638–1647.

[17] S. Wang, T. Xu, Y. Yang, Z. Shao. Colloidal Stability of Silk Fibroin Nanoparticles Coated with Cationic Polymer for Effective Drug Delivery. ACS Appl. Mater. Interfaces, 7 (2015) 21254–21262.

[18] Y. Wang, S. Xu, W. Xiong, Y. Pei, B. Li, Y. Chen. Nanogels Fabricated from Bovine Serum Albumin and Chitosan via Self-assembly for Delivery of Anticancer Drug. Colloids Surfaces B Biointerfaces, 146 (2016) 107–113.

[19] A.B. Kayitmazer. Thermodynamics of Complex Coacervation. Adv. Colloid Interface Sci, 239 (2017) 169–177.

[20] M.T. Larsen, M. Kuhlmann, M.L. Hvam, K.A. Howard. Albumin-based Drug Delivery: Harnessing Nature to Cure Disease. Mol. Cell. Ther, 4 (2016) 3.

[21] A.O. Elzoghby, W.M. Samy, N.A. Elgindy. Albumin-based Nanoparticles as Potential Controlled Release Drug Delivery Systems. J. Control. Release, 157 (2012) 168–182.

[22] R.R. Kudarha, K.K. Sawant. Albumin Based Versatile Multifunctional Nanocarriers for Cancer Therapy: Fabrication, Surface Modification, Multimodal Therapeutics and Imaging Approaches. Mater. Sci. Eng. C, 81 (2017) 607–626.

[23] S. Yu, B. Sun, S. Gao, S. Guo, K. Zhao. Biomedical Applications of Chitosan and Its Derivatives Nanoparticles. Polymers, 10 (2018) 462.

[24] N.P. Birch, J.D. Schiffman. Characterization of Self-assembled Polyelectrolyte Complex Nanoparticles Formed From Chitosan and Pectin. Langmuir, 30 (2014) 3441–3447.

[25] S. Jana, N. Maji, A.K. Nayak, K.K. Sen, S.K. Basu. Development of Chitosan-based

Nanoparticles Through Inter-polymeric Complexation for Oral Drug Delivery. Carbohydr. Polym, 98 (2013) 870–876.

[26] M. Esfandyari-Manesh, A. Mohammadi, F. Atyabi, S.M. Nabavi, S.M. Ebrahimi, E. Shahmoradi, B.S. Varnamkhasti, M.H. Ghahremani, R. Dinarvand. Specific Targeting Delivery to MUC1 Overexpressing Tumors By Albumin-chitosan Nanoparticles Conjugated to DNA Aptamer. Int. J. Pharm, 515 (2016) 607–615.

[27] N. Varga, M. Benko, D. Sebok, I. Dékány. BSA/polyelectrolyte Core-shell Nanoparticles for Controlled Release of Encapsulated Ibuprofen. Colloids Surfaces B Biointerfaces, 123 (2014) 616–622.

[28] M. Karimi, P. Avci, R. Mobasseri, M.R. Hamblin, H. Naderi-Manesh. The Novel Albumin-chitosan Core-shell Nanoparticles for Gene Delivery: Preparation, Optimization and Cell Uptake Investigation. J. Nanoparticle Res, 15 (2013).

[29] Y. Sun, Y. Huang. Disulfide-crosslinked Albumin Hydrogels. J. Mater. Chem. B, 4 (2016) 2768–2775.

[30] H. Koo, K.H. Min, S.C. Lee, J.H. Park, K. Park, S.Y. Jeong, K. Choi, I.C. Kwon, K. Kim. Enhanced Drug-loading and Therapeutic Efficacy of Hydrotropic Oligomer-conjugated Glycol Chitosan Nanoparticles for Tumor-targeted Paclitaxel Delivery. J. Control. Release, 172 (2013) 823–831.

[31] O. Ma, M. Lavertu, J. Sun, S. Nguyen, M.D. Buschmann, F.M. Winnik, C.D. Hoemann. Precise Derivatization of Structurally Distinct Chitosans with Rhodamine B Isothiocyanate. Carbohydr. Polym, 72 (2008) 616–624.

[32] S.A. Abouelmagd, B. Sun, A.C. Chang, Y.J. Ku, Y. Yeo. Release Kinetics Study of Poorly Water-Soluble Drugs from Nanoparticles: Are We Doing It Right? Mol. Pharm, 12 (2015) 997–1003.

[33] R. Reul, T. Renette, N. Bege, T. Kissel. Nanoparticles for Paclitaxel Delivery: A Comparative Study of Different Types of Dendritic Polyesters and Their Degradation Behavior. Int. J. Pharm, 407 (2011) 190–196.

[34] F. Chen, J. Wu, C. Zheng, J. Zhu, Y. Zhang, X. You, F. Cai, V. Shah, J. Liu, L. Ge. TPGS Modified Reduced Bovine Serum Albumin Nanoparticles as A Lipophilic Anticancer Drug Carrier for Overcoming Multidrug Resistance. J. Mater. Chem. B, 4 (2016) 3959–3968.

[35] T. Lin, P. Zhao, Y. Jiang, Y. Tang, H. Jin, Z. Pan, H. He, V.C. Yang, Y. Huang. Blood-brain-barrier-penetrating Albumin Nanoparticles for Biomimetic Drug Delivery via Albumin-binding Protein Pathways for Antiglioma Therapy. ACS Nano, 10 (2016)

9999–10012.

[36] J.C. Han, G.Y. Han. A Procedure for Quantitative Determination of Tris(2-Carboxyethyl)Phosphine, An Odorless Reducing Agent More Stable and Effective than Dithiothreitol. Anal. Biochem, 220 (1994) 5–10.

[37] N.J. Greenfield. Using Circular Dichroism Spectra to Estimate Protein Secondary Structure. Nat. Protoc, 1 (2006) 2876–2890.

[38] J.T. Vivian, P.R. Callis. Mechanisms of Tryptophan Fluorescence Shifts in Proteins. Biophys. J, 80 (2001) 2093–2109.

[39] Q. Hu, T. Wang, M. Zhou, J. Xue, Y. Luo. Formation of Redispersible Polyelectrolyte Complex Nanoparticles from Gallic Acid-chitosan Conjugate and Gum Arabic. Int. J. Biol. Macromol, 92 (2016) 812–819.

[40] O.G. Jones, D.J. McClements. Recent Progress in Biopolymer Nanoparticle and Microparticle Formation by Heat-treating Electrostatic Protein-polysaccharide Complexes. Adv. Colloid Interface Sci, 167 (2011) 49–62.

[41] H.P. Jae, S. Kwon, M. Lee, H. Chung, J.H. Kim, Y.S. Kim, R.W. Park, I.S. Kim, B.S. Sang, I.C. Kwon, Y.J. Seo. Self-assembled Nanoparticles Based on Glycol Chitosan Bearing Hydrophobic Moieties as Carriers for Doxorubicin: In Vivo Biodistribution and Anti-tumor Activity. Biomaterials, 27 (2006) 119–126.

[42] L. Bekale, D. Agudelo, H.A. Tajmir-Riahi. Effect of Polymer Molecular Weight on Chitosan-protein Interaction. Colloids Surfaces B Biointerfaces, 125 (2015) 309–317.

[43] J.E. Chung, S. Tan, S.J. Gao, N. Yongvongsoontorn, S.H. Kim, J.H. Lee, H.S. Choi, H. Yano, L. Zhuo, M. Kurisawa, J.Y. Ying. Self-assembled Micellar Nanocomplexes Comprising Green Tea Catechin Derivatives and Protein Drugs for Cancer Therapy. Nat. Nanotechnol, 9 (2014) 907–912.

[44] G. Gong, Y. Xu, Y. Zhou, Z. Meng, G. Ren, Y. Zhao, X. Zhang, J. Wu, Y. Hu. Molecular Switch for the Assembly of Lipophilic Drug Incorporated Plasma Protein Nanoparticles and In Vivo Image. Biomacromolecules, 13 (2012) 23–28.

[45] J. Zhao, M.H. Stenzel. Entry of Nanoparticles Into Cells: The Importance of Nanoparticle Properties. Polym. Chem, 9 (2018) 259–272.

[46] W. He, Z. Jin, Y. Lv, H. Cao, J. Yao, J. Zhou, L. Yin. Shell-crosslinked Hybrid Nanoparticles for Direct Cytosolic Delivery for Tumor Therapy. Int. J. Pharm, 478 (2015) 762–772.

[47] P. Pereira, S.S. Pedrosa, J.M. Wymant, E. Sayers, A. Correia, M. Vilanova, A.T. Jones, F.M. Gama. SiRNA Inhibition of Endocytic Pathways to Characterize the Cellular

Uptake Mechanisms of Folate-functionalized Glycol Chitosan Nanogels. Mol. Pharm, 12 (2015) 1970–1979.

[48] C. Yang, S. Gao, F. Dagnæs-Hansen, M. Jakobsen, J. Kjems. Impact of PEG Chain Length on the Physical Properties and Bioactivity of PEGylated Chitosan/siRNA Nanoparticles In Vitro and In Vivo. ACS Appl. Mater. Interfaces, 9 (2017) 12203–12216.

CHAPTER 5 SUMMARY AND FUTURE WORK

5.1 Summary

In the past two decades, nanotechnology has generated great attention of researchers in various fields. In the fields of food, pharmacy and medicine, nanoparticles (NPs) are considered a promising material for a creation of new therapy for many diseases, especially cancer and degenerative diseases. The application of NPs in the biological systems requires a careful selection of constituting materials for fabrication of NPs in terms of cost, availability, and safety. Due to their biodegradability, biocompatibility, and low immunogenicity, proteins and polysaccharides are attractive materials for development of NPs for effective cancer treatment. In this thesis, we investigated the formation of NPs between proteins and chitosan (CH) and evaluated their feasibility for encapsulation and delivery of hydrophobic therapeutic molecules.

In Chapter 2, we described the formation of electrostatic-based nanocomplexes (NCs) between caseinate (CS) and chitosan (CH) (CCNCs) and evaluated the ability of these NCs for encapsulation of curcumin. The particle size, polydispersity index (PDI), turbidity, number of particles, and zeta potential of these NCs were found to be dependent on the total biopolymer concentration and the concentration of CS/CH in these NCs. Higher CS concentrations resulted in higher turbidity and lower number of particles and zeta potential, at least in the range studied. The obtained particle size was less than 400 nm with narrow size distribution and positive charge. In addition, the interaction between CH and CS was confirmed by FT-IR spectroscopy. The ability of these NCs to encapsulate curcumin was demonstrated and verified using UV-Vis and fluorescence spectrophotometer. However, the encapsulation efficiency (EE) of curcumin was moderate, at 56%. This might be due to the presence of free CS/CH and soluble complexes that competes with the NPs. In view of practical application, the water re-dispersibility of these curcumin-loaded CCNCs was tested using a lyophilized form with 5% trehalose as a cryoprotectant. We showed that CCNCs can enhance thermal and storage

stability as well as re-dispersibility of curcumin in water. Of interest, CH solubility in water was promoted after freeze-drying, which suggests favorable interactions between CH and trehalose.

In Chapter 3, we focused on enhancing the stability of CS/CH NPs (CCNPs) described in the previous chapter by a non-toxic cross-linker, genipin and evaluated the feasibility of genipin-crosslinked CCNPs (G-CCNPs) for curcumin delivery into the cells. DLS and TEM analysis revealed that G-CCNPs were more stable under acidic and neutral pH at physiological conditions as compared with NPs without cross-linking. The biocompatibility of G-CCNPs was evaluated on normal fibroblast cells (L929), and WST assay revealed that these NPs were non-toxic. Curcumin was delivered by G-CCNPs to both cancer (HeLa and A549) and normal cells (L929). Cytotoxicity *in vitro* of curcumin on cancer cells was improved by G-CCNPs. We found that this enhanced bioactivity of curcumin was not necessarily correlated with enhanced cellular internalization of NPs into the cells, as most G-CCNPs were located on the cell membrane. Rather, the stability of curcumin in the physiological condition was more important.

To eliminate the use of a cross-linker agent and overcome the limitation of CH, in Chapter 4, we fabricated NPs formed from the complexation between reduced bovine serum albumin (rBSA) and glycol chitosan (GC) (rBG NPs) and evaluated their feasibility as a nano-carrier for paclitaxel (PTX). We found that the degree of complexation between rBSA and GC was highly dependent on rBSA/GC mass ratio and pH. The optimum complexation was found to be at higher rBSA/GC mass ratio or at higher pH (6.5). Our results indicated that rBG NPs formation was governed by the initial rBSA aggregation in the solution, followed by the electrostatic complexation with GC to form NPs with core-shell structure. Moreover, rBG NPs had excellent stability without the help of external cross-linker agent. Hydrophobic and disulfide crosslinking are presumably responsible for stabilizing these NPs. We showed that

PTX can be efficiently encapsulated into these NPs. Unlike G-CCNPs, these NPs can be effectively internalized into the cells, which suggests that cross-linking reaction based on primary amines can affect colloidal stability and cellular internalization of NPs. Cytotoxicity *in vitro* revealed that PTX-loaded in rBG NPs had comparable anti-cancer activity compared with Taxol-like formulation at a longer time of incubation (48 h), suggesting that PTX was released slowly due to strong binding with these NPs, presumably via hydrophobic interactions.

5.2 Future work

Potential ideas that have not been carried out include *in vivo* studies for better evaluation of G-CCNPs and rBG NPs as nano-carrier for curcumin and PTX, respectively. It is suggested that hemolysis assay and immunogenicity testing should also be done for determining biocompatibility of these NPs. In terms of characterization of these NPs, advanced analytical techniques such as small-angle X-ray scattering (SAXS)/small-angle neutron scattering (SANS) may be of interest to get better understanding about the structure of these NPs. In terms of the formation of NPs, the use of defined structures of CH or GC, *i.e.*, molecular weight, polydispersity, chain arrangements, and degree of deacetylation is encouraged to rationally design NPs with desired properties. For CCNPs, the use of other stabilizers or CH derivatives should be explored to make NPs with better colloidal stability and effective cellular internalization. For rBG NPs, the formation of rBG NPs with redox-responsive ability should be explored. This might be possible through optimizing reducing conditions and chemical modification of BSA/GC.

ACKNOWLEDGEMENTS

I would like to express my utmost gratitude to Prof. Noriho Kamiya, for his guidance and support throughout PhD course in Kyushu University. It has been a great honor for having you as my academic advisor. Your insightful ideas and creative thinking have impressed me a lot and would be of help for me to become a better researcher. I am truly thankful for placing your trust and confidence in my abilities to carried out this research project. I would also like to thank Prof. Masahiro Goto, who served as my co-advisor and thesis committee, for his encouragement and continuous support throughout PhD course and for invaluable advice and suggestion during the lab meetings and on my PhD thesis. I am extremely proud and fortunate to become a member of the Goto-Kamiya Lab. I would like to express my sincere gratitude to Prof. Yoshiki Katayama for agreeing to be one of my PhD thesis committee. I really appreciate for his constructive comments and invaluable advice.

I would like to thank Assistant Prof. Rie Wakabayashi for helping me in many aspects of my research. I would also like to express my sincere gratitude to Assistant Profs. Fukiko Kubota, Yoshiro Tahara, and Kosuke Minamihata for their help and advice throughout my study in Kyushu University. Without their expertise and support, this work would not have been possible. I would also like to thank Dr. Momoko Kitaoka and staffs for their kindness and help in many occasions during my stay in Fukuoka.

I am grateful for all past and present members of the Goto-Kamiya Lab for their help, support, and friendship. In particular, I would like to appreciate Dr. Mari Takahara and Dr. Lili Jia for their useful advice and help in experiments and research. I would also like to thank Mr. Yuki Owada, Mr. Hiroki Kawashima, Mr. Ryuichiro Hashimoto, Mr. Mutsuhiro Katsuya, Mr. Naoki Fujimoto, Mr. Wataru Yoshida, Mr. Hiroki Obayashi, Ms. Czarina D.R. Rodriguez, and others for helping and teaching me doing some experiments. Special thank goes to Mr. Qingliang Kong for helping me a lot especially during my initial period in Japan and for our

friendship. I am grateful to Indonesian GK lab members (Tyas, Yovita, Lutfi, Kang Dani, Patma, Wahyu, Jessica, and Ghazy) for their help and support and our togetherness during my stay in Japan. I thank for all Japanese and international lab mates (Ms. Nguyen Minh Thi Hong, Mrs. Maha M. Sharaf, Mr. Md. Moshikur Rahman, Mr. C. Md Raihan, and others) for their help, friendship, and pleasant moments. I am fortunate to be a part of such conducive and supportive research environment in the lab.

I would like to appreciate PPIF, MUSFUK, and Imajuku Kaikan for their excellent support and togetherness. I also appreciate the support from the Support Center of Faculty of Engineering, particularly to Mrs. Yasura Oiwa. The financial support from the MEXT scholarship via the Embassy recommendation is also appreciated. Special thank goes to Prof. Uju, who is my former teacher at Bogor Agricultural University for introducing the GK lab and his support towards my academic career.

I would like to thank my family, especially my father and mother also my mother-in-law for their unconditional love and support. They have always been understanding, encouraging, and supportive in every decision I made. I dedicate this thesis to them. I am truly grateful to my wife, Istifa Rini and my son, Muhammad Daffa Wirakartakusumah for their utmost patience, unconditional love and support. They have always been my best supporters and partners in every aspects of my life. Thank you for bringing the joy and happiness in my life. I also dedicate this thesis to them. Lastly, but most importantly, I thank the almighty God Allah for what I am today and for guiding us to the right path. Without his blessings, this work would not have been possible.

Muhamad Alif Razi

Fukuoka, 17 July 2018